Bi-disperse Magnetorheological Fluids

by

Mona Nejatpour

A Dissertation Submitted to the
Graduate School of Sciences and Engineering
in Partial Fulfillment of the Requirements for
the Degree of

Doctor of Philosophy

in

Materials Science and Engineering

KOÇ ÜNİVERSİTESİ

September 24, 2020

Bi-disperse Magnetorheological Fluids

Koç University

Graduate School of Sciences and Engineering

This is to certify that I have examined this copy of a doctoral dissertation by

Mona Nejatpour

and have found that it is complete and satisfactory in all respects, and that any and all revisions required by the final examining committee have been made.

Committee Members:

Prof. Dr. Havva Yağcı Acar

Prof. Dr. İsmail Lazoğlu

Prof. Dr. Celaletdin Ergun

Assoc. Prof. Dr. Uğur Ünal

Asst. Prof. Dr. Mustafa Kemal Bayazıt

Date: 24/09/2020

Dedicated to my family

ABSTRACT

Bi-disperse Magnetorheological Fluids
Mona Nejatpour
Doctor of Philosophy in Materials Science and Engineering
September 24, 2020

Superparamagnetic iron oxide nanoparticles (SPION) are exploited in many different fields from automotive to medicine. In every field, there is always a need for better performance that exhibits new challenges to scientists. In this thesis work magnetorheological fluids and magnetic hydrogels are studied to solve the problems and improve the properties of these materials.

Magnetorheological Fluids (MRFs) are non-Brownian fluids that consist of micron-sized magnetic particles in carrier fluids, mostly different oils. The biggest challenge in MRFs is the prevention of sedimentation and enhancement of redispersibility to prolong shelf-life as well as life-in-use. This thesis work proposed and demonstrated a method to improve the stability and redisperability of MRFs with high particle loading while having good magnetorheological properties. Bidisperse MRFs composed of micron-sized magnetic particles and functional superparamagnetic nanoparticles which would interact with each other is proposed as the primary strategy. First, the idea was tested on a commercial MRF, 140-CG LORD® (with fatty-acid coated micron-sized particles in hydraulic oil). Poly(acrylic) acid and lauric-acid coated superparamagnetic iron oxide nanoparticles (SPION-PAA and SPION-LA) were synthesized and added in 5-20 weight percentages to 140-CG LORD® to understand the influence of surface coating and SPION content on the sedimentation and magnetorheological properties. Then, new bidisperse MRFs were prepared by adding commercial bare carbonyl iron (CI) and SPION-LA or SPION-PAA to different carrier fluids. Also, CI was coated with LA and bidisperse MRFs were prepared from CI-LA and SPION-LA or SPION-PAA in different carrier oils such as hydraulic oil, silicone oil, mineral oil and glycerol. Magnetorheological properties of prepared bidisperse MRFs were measured with Anton Paar 302 MCR rheometer in both rotational, and frequency modes and mechanical properties, as well as the sedimentation behavior of MRFs, were compared with 140-LORD MRF® as a

benchmark. SPION-PAA particles provided the best MRFs in both formulations with enhanced stability for months, better redispersibility and rheological properties at least as good as the commercial one. Selected bidisperse MRFs were used in washing machine MR dampers by the group of Prof. İsmail Lazoglu. This research was funded by TUBITAK and Arçelik (ID: 5150060).

ÖZETÇE

İki Dağılımlı Magnetoreolojik Akışkanlar
Mona Nejatpour
Malzeme Bilimi ve Mühendisliği, Doktora
24 Eylül 2020

Süperparamagnetik demir oksit nanoparçacıklarından otomotivden tıbba kadar pek çok farklı alanla yararlanılmaktadır. Her alanda daima, daha iyi performansa yönelik, bilim insanları için yeni zorluklar teşkil eden bir ihtiyaç söz konusudur. Bu tez çalışmasında bu malzemelere dair sorunları çözmek ve bu malzemelerin özelliklerini geliştirmek için magnetoreolojik akışkanlar ve magnetik hidrojeller çalışılmıştır.
Magnetoreolojik akışkanlar çoğunlukla çeşitli yağlardan oluşan taşıyıcı akışkanlar içerisindeki mikron boyutlu magnetik parçacıklardan meydana gelir. Magnetoreolojik akışkanlardaki en büyük zorluk raf ve kullanım ömürlerini arttırmak için çökelmelerini önlemek ve tekrar dağılabilirliğini geliştirmektir. Bu tez çalışması yüksek parçacık yüklü magnetoreolojik akışkanların iyi magnetoreolojik özelliklere sahip şekilde kararlılığını ve yeniden dağılabilirliğini arttırmak için bir yöntem önermekte ve sergilemektedir. Birbirleriyle etkileşimde olacak mikron boyutlu magnetik parçacıklar ve işlevsel süperparamagnetik nanoparçacıklardan oluşan iki dağılımlı magnetoreolojik ilk strateji olarak önerilmektedir. İlk olarak fikir ticari bir magnetoreolojik akışkan, 140-CG LORD® (hidrolik yağ içinde yağ aside kaplı mikron boyutlu parçacıklar içermektedir) üzerinde denenmiştir. Yüzey kaplamasının ve süperparamagnetik demir oksit nanoparçacık içeriğinin çökelme ve magnetoreolojik özellikler üzerine etkisini anlamak için poliakrilik asit ve lorik asit kaplı süperparamagnetik nanoparçacıklar sentezlenmiş ve 5-20 yüzde ağırlıklarda 140-CG LORD® 'a eklenmiştir. Ardından hidrolik yağ, silikon yağı, mineral yağ ve gliserol gibi çeşitli taşıyıcı yağlara ticari karbonil demir ve lorik asit kaplı süperparamagnetik nanoparçacık veya poliakrilik asit kaplı süperparamagnetik nanoparçacık eklenerek yeni iki dağılımlı magnetoreolojik akışkanlar hazırlanmıştır. Hazırlanan iki dağılımlı magnetoreolojik akışkanların magnetoreolojik özellikleri Anton Paar 302 MCR reometre ile hem rotasyonel hem de frekans modlarında ölçülmüş ve mekanik özellikleri ile çökelme davranışları referans olarak 140-CG LORD® iki dağılımlı magnetoreolojik akışkan ile karşılaştırılmıştır. Poliakrilik asit kaplı süperparamagnetik nanoparçacıklar aylarca kararlı kalabilmesi, daha iyi

yeniden dağılabilirlik ve en az ticari iki dağılımlı magnetoreolojik akışkan kadar iyi magnetoreolojik özelliklere sahip olmasıyla her iki fomülasyonda da en iyi magnetoreolojik akışkanları ortaya çıkarmıştır. Seçilen iki dağılımlı magnetoreolojik akışkanlar Prof. İsmail Lazoğlu'nun grubu tarafından çamaşır makinesi damperlerinde kullanılmıştır. Bu araştırma TÜBİTAK ve Arçelik tarafından finanse edilmiştir (ID: 5150060).

ACKNOWLEDGMENTS

At the outset, this is to extend my high appreciation and thanks to my advisor, Prof. Dr. Havva Funda Yağcı Acar for her guidance, great support, trust, patience and her friendly relationship with all members of the team while were very disciplined about our research and improvement. Her positive perspective and confidence in me persuaded me to proceed more productively. I feel deeply indebted to her.

I thank my MS thesis advisor Prof. Celaletdin Ergun for illuminating my academic path and helping me to discover what I like in the academic world.

I would like to thank Assoc. Prof. Dr. Uğur Ünal for his support, understanding, sincerity, friendly attitude and help in every issue, specifically in magnetorheological studies.

I would also wish to express my gratitude to my thesis committee members Assoc. Prof. Uğur Ünal and Prof. Çağatay Başdoğan, for their attention, suggestions, guidance and time that they devoted to the evaluation of my thesis progress.

I thank to all members of my PhD thesis committee Prof. Mustafa Kemal Beyazıt, Prof. Celaletdin Ergun, Prof. Çağatay Başdoğan, Prof. Uğur Unal and Prof. Havva Funda Yağcı Acar for their time, feedback, constructive critics and support.

I am thankful to Dr. Parviz Tarikhi for his guidance, help and support since my undergraduate study till now. I would like to thank Dr. Barış Yağcı for his support and help in characterization of my samples and his openness when I needed his help; Muharrem Güler for assisting me in the laboratory when I faced technical problems; Gizem Akay from Anton Paar for her help in understanding the science of rheological measurements; Gülçin Yılmaz for teaching me FTIR and XRF measurements; Prof. Dr. Numan Akdoğan and Dr. Mustafa Öztürk from Gebze Technical University for the VSM measurements.

I deeply appreciate the assistance, patience and friendliness of Koç University Surface Technology Research Center (KUYTAM) team, Dr. Barış Yağcı, Dr. Gülsu Şimsek, Dr. Işınsu Baylam, Rr. Hadi Jahangiri, Dr. Amir Motallebzadeh and Dr. Ceren

Yılmaz Akkaya.

I would like to thank Arçelik A.Ş. and Manufacturing and Automation Research Center under the supervision of Prof. Dr. İsmail Lazoğlu for the funding. Also, I am thankful to the members of Manufacturing and Automation Research Center for their kindness, effective teamwork, creative and stimulating collaboration during my PhD study.

I would like to express my sincere thanks to my former and present group members Dr. Ali Bayer, Dr. Özlem Ünal, Dr. Fatma Demir Duman, Dr. Emek Durmuşoğlu, Dr. Rouhullah Khodadust, Dr. Kübra Bilici, Dr. Özge Çavuşlar, Enes Buz, Pelin Turhan Buz, İrem Ülkü, Gözde Demirci, Mahshid Hashemkhani, Eda Aydındoğan, Mehmet Berk Bilgin, Pelda Akın, Kübra Nur Özvural and İrem Koç for their friendship and for their trainings in the labrotary.

I am grateful to my parents, my brother, my husband and to my cousin Dr. Parviz Tarikhi and all my relatives in Iran for their endless, unconditional support, trust, encouragement, guidance and love throughout my whole life.

TABLE OF CONTENTS

LIST OF TABLES

LIST OF FIGURES

ABBREVIATIONS

A	Area, exchange, Ampere
ACS	American Chemical Society
Ar	Argon
atm	Atmosphere
B	Boron, magnetic flux density
Ba	Barium
AFM	Atomic Force Microscopy
C	Coulomb, Celcius, Carbon
$C_{12}H_{24}O_2$	Lauric Acid
CI	Carbonyl Iron
cm	Centimeter
cm^3	Cubic centimeter
Co	Cobalt
CO_2	Carbon dioxide
COOH	Carboxylic acid
CNT	Carbon nanotubes
Cr	Chromium
Cu	Copper
CTAB	Cetyltrimethyl ammonium bromide
DEMAEMA	2-(Dimethylamino)ethyl methacrylate

DI	Deinoized
DLS	Dynamic light scattering
DNA	Deoxyribonucleic acid
DSC	Differential scanning calorimetry
Fe	Iron
$Fe_2CO_4{\cdot}2H_2O$	Iron(II) oxalate
Fe_2O_3	Iron(III) oxide
Fe_3O_4	Iron(II,III) oxide
$FeCl_2.4H_2O$	Iron(II) chloride tetrahydrate
$FeCl_3.6H_2O$	Iron(III) chloride hexahydrate
FTIR	Fourier-transform infrared spectroscopy
emu	Electromagnetic unit
g	Gram
G*	Complex modulus
G´	Storage modulus
G´´	Loss modulus
Gd	Gadolinium
GNP	Graphene nanoplatelet
h	Hour
H	Magnetic field, Hydrogen
H_2O	Water
H_c	Coercive field
HCl	Hydrochloric acid
HEMA	Hydroxyethylmethacrylate

I	Current
IL	Ionic liquid
IR	Infrared
K	Potassium, Kelvin
kA	Kiloampere
KBr	Potassium bromide
k_B	Boltzmann's constant
kDa	Kilodalton
K_u	Anisotropy constant
kV	Kilovolt
L	Liter
LA	Lauric acid
m	Magnetic moment, meter
M	Magnetic strength, mol
mbar	Milibar
MCA	Magnetocrystalline anisotropy
MFH	Magnetic fluid hyperthermia
min	Minute
ml	Mililiter
mm^2	Square milimeter
Mn	Manganese
MNP	Magnetic Nanoparticle
MPa	Megapascal
MR	Magnetorheological

MRF	Magnetorheological fluid
MRI	Magnetic resonance imaging
M_s	Saturation magnetization
mW	Miliwatt
M_w	Molecular weight
M_{xy}	Latitudinal magnetization
M_z	z-axis
N	Newton
Na_2CO_3	Sodium carbonate
Nd	Neodymium
NH_2	Amine
NH_4OH	Ammonium hydroxide
Ni	Nickel
NiO	Nickel(II) oxide
NIPA	Poly(N-isopropylacrylamide)
nm	Nanometer
NIR	Near-infrared
NP	Nanoparticle
O	Oxygen
OH	Hydroxyl
OPPI	[4-[(octyloxy)phenyl] phenyl] iodonium hexafluoro antimonate
p	Slope of the linear characteristic (shear stress vs flux density)
PAA	Poly(acrylic) acid
PAAm	Poly (acrylamide)

PDT	Photodynamic therapy
PEGDA	Poly (ethylene glycol) diacrylate
phr	Parts per hundred
PMMA	Poly (Methyl methacrylate)
PS	Photosensitizer
PTFE	Polytetrafluoroethylene
PTT	Photothermal therapy
PVA	Poly (vinylalcohol)
r_0	Critical radius for single domain to superparamagnetic
rad	Radian
r_c	Critical radius below which a particle acts as single domain
RF	Radiofrequency
rpm	Revolution per minute
RNA	Ribonucleic acid
ROS	Reactive oxygen specy
s	Second
SAR	Specific absorption rate
SEM	Scanning Electron Microscopy
Sm	Samarium
SPION	Superparamagnetic iron oxide nanoparticle
SQUID	Superconducting quantum interference device
Sr	Strontium
T	Temperature, Tesla
T_1	Spin-net relaxation time

T_2	Spin-spin relaxation time
T_b	Blocking temperature
T_c	Curie temperature
TEM	Transmission Electron Microscopy
TGA	Thermogravimetric analysis
UCST	Upper critical solution temperature
UV	Ultraviolet
V	Velocity
V_h	Hydraulic volume of the particle
V_m	Primary Volume
VSM	Vibrating-sample magnetometer
W	Watt
WLM	Worm-like micelle
vol%	Volume percent
wt%	Weight percent
YCo_5	An alloy of yttrium and cobalt
Zn	Zinc
ZnO	Zinc oxide
ZrO_2	Zirconium dioxide
γ^o	Shear rate
δ	Phase shift
η	Dynamic viscosity
η_p	Bingham plastic viscosity
μ_0	Vacuum permeability

μm	Micrometer
μ_B	Bohr magneton
υ	Kinematic viscosity
ρ	Density
τ	Shear stress
τ_0	Attempt time, dynamic shear stress
τ_B	Brownian relaxation time
τ_N	Néel relaxation time
τ_s	Steady-state shear stress
τ_y	Yield stress under magnetic fiels
ϕ	Volume fraction

Chapter 1

INTRODUCTION

1.1 Nanoparticles (NPs)

Nanoparticles are referred to as the materials with the size of 1-100 nm. Due to their nanoscale size, mechanical, chemical, electrical, optical, magnetic, electrooptical and magneto-optical properties of these particles are different from their bulk material. Therefore, in recent decades NPs have widespread applications in biotechnology, biomedicine, material science, engineering, catalysis and environmental areas [1,2,3]. Nano-sized crystals have reduced lattice constants, as a significant portion of the total number of atoms or ions is on the surface. Since the surface energy plays a significant role in thermal stability and reactivity, such properties are dramatically influenced at the nanoscale. Many of the bulk material property changes arise from a considerable increase in surface-to-volume ratio associated with the reduction in material size to the nanoscale. Bulk properties are no longer capable of predicting performance, when devices are manufactured below critical dimensions [4].

Superparamagnetic iron oxide nanoparticles (SPIONs) benefit from size-dependent unique properties and are at the center of this thesis work. This introductory part of the thesis will focus on the magnetic properties of SPIONs, their synthesis and applications with a basic introduction to magnetic materials in bulk and nanoscale.

1.1.1 Magnetic nanoparticles

The discovery of magnetism goes back to thousands of years ago that arises from our ancestor’s curiosity, followed by progress in science and technology. Magnetic

phenomena at the atomic scale were discovered in the first half of the last century and in recent decades it was discovered that magnetization in solid-state materials occurs at the nano scale. Magnetic nanoparticles attract tremendous since the discovery of the unmatched properties at the nanoscale and advent of new technologies enabled by MNPs[5]. Two main characteristics of nanoparticles are critical: (i) surface effects or size reduction effect (when particle size is reduced, a higher proportion of atoms are found at the surface); (ii) quantum confinement in electronic structure [6].

Naturally, magnetic nanoparticles can be found in bacteria and animals. Magneto-tatic bacteria live in dark environments and chains of 40-100 nm magnetite particles that they have, help them to navigate based on the earth`s magnetic field. It has been found that similar particles are available in the brains of bees, pigeons and tuna, but it is under investigation whether these particles serve for navigation. Magnetite and other oxide particles are also the reason for rock magnetism, and it is used in archaeological dating and monitoring the changes in the Earth's magnetic field. [5][7]

1.1.2 Properties of magnetic nanoparticles

Magnetic moment

The magnetic moment (m) of solids arises from the unpaired electrons with the orbital motion of electrons, the spin of the electrons and the spin of the protons which is the weakest due to the big mass of the proton in partially filled inner orbitals of transition-metal atoms. Hans Christian Oersted (1777-1851) in 1820 declared that electric current through a conductor develops a magnetic field around it or current through a coil of wire can act as a magnet. This informs that there is an intimate relationship between the electric current and magnetic field. At the atomic scale, the flow of electrons along a path initiates an electric current. In all atoms, electrons are revolving around the nucleus in different orbits. These revolving electrons initiate electrical currents in the orbits. These currents form a magnetic moment or dipole. The value of the moment in the atomic small current

loop is expressed by Equation 1.1, where I is the circulating current and A is the area of the loop. Electrons carry a negative electric charge of e = 1.602 x 10^{-19} C in perpetual motion according to the laws of quantum mechanics, so they behave as elementary current loops. [2,3]

$$m = IA \tag{1-1}$$

The iron series transition-metal or 3d elements Fe, Co and Ni and the rare-earth or 4f elements, such as Nd, Sm, Gd and Dy, Palladium series (4d), platinum series (5d) and actinide (5f) atoms have a magnetic moment in suitable crystalline environments. Two sources of the atomic magnetic moment are currents related to the orbital motion of the electrons and the electron spin. The spin is the main source of the magnetic moment of iron-series transition-metal atoms in metals (Fe, Co, Ni, YCo_5) and nonmetals (Fe_3O_4, NiO). The moment, measured in μ_B, is equal to the number of unpaired spins [5].

Magnetic moments are determined with a superconducting quantum interference device (SQUID) magnetometer and direct force measurements of the AFM, which allows measurements to be made at the nano level[8,9].

Anisotropy

Magnetic materials magnetize along a specific crystallographic direction. The preference of this direction is expressed quantitatively by the magnetocrystalline anisotropy, K. Although shape and stress can also lead to magnetic anisotropy, these effects are not significant for roughly spherical particles[10,11].

The electronic structure of the magnetic atoms or ions and the crystal structure of the materials govern the basic properties of magnetic materials. Both of these factors affect the strength of the magnetic coupling and, consequently, their saturation magnetization(M_s) and magnetocrystalline anisotropy (MCA). The M_s value is related to the magnitude of the atoms' or ions' magnetic moments, and the distance and angle between two adjacent magnetic atoms or ions. The magnetic moments can align along

one or more crystallographic directions, and this causes MCA. [10,11].

Classification of magnetic materials

Materials, in general, are classified as, diamagnetic, paramagnetic, ferromagnetic, ferrimagnetic and antiferromagnetic. In *diamagnetic materials (i.e. Au, Cu)*, a weak magnetic dipole appears under the external magnetic field and in the opposite direction to the applied magnetic field. Magnetic dipoles of *paramagnetic materials (i.e. Mn, Pt)* have random orientation but align with the field under the external magnetic field. *Ferromagnetic (i.e. Fe)* materials have aligned atomic magnetic dipoles within crystalline domains even in the absence of an external magnetic field, hence are the most widely known magnetic materials. The net direction of these domains may cancel each other but will align with the field if an external magnetic field is applied. *Ferrimagnetic (i.e. Ba ferrite)* and *antiferromagnetic (i.e. Cr)* materials consist of atomic dipole moments oppositely directed in sublattices of the crystals, where still a net moment was obtained in ferrimagnets but completely cancelled out in antiferromagnetic materials. Same classification is true for nanoparticles [12,13].

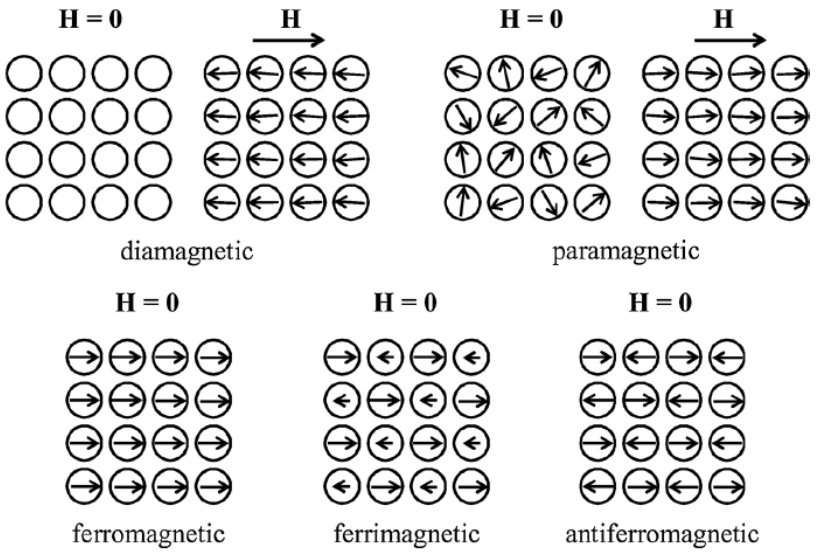

Figure 1.1: Arrangement of magnetic dipoles of different materials: diamagnetic, paramagnetic, ferromagnetic, ferrimagnetic, and antiferromagnetic materials in the absence and presence of external magnetic field (H)[14].

Hysteresis loop

The response of ferromagnetic materials to an applied field is well described by a hysteresis loop. If an external magnetic field of strength H is applied to a ferromagnet of magnetic strength M, the magnetization curve of Fig. 1.2 is observed and it is demonstrated that M increases with H until a saturation value (M_s). The magnetization curve displays a hysteresis loop, because all domains do not return to their original orientations when H is decreased after the saturation is reached. Accordingly, when H returns to zero, a *remnant magnetization* M_R lasts, and it can only be eliminated by applying a *coercive field* H_c in the opposite direction to the previously applied field. *A single domain magnetic material has no hysteresis loop and is called superparamagnetic*. At room temperature, iron oxide nanoparticles smaller than about 20 nm usually exhibit superparamagnetic behavior [2,5].

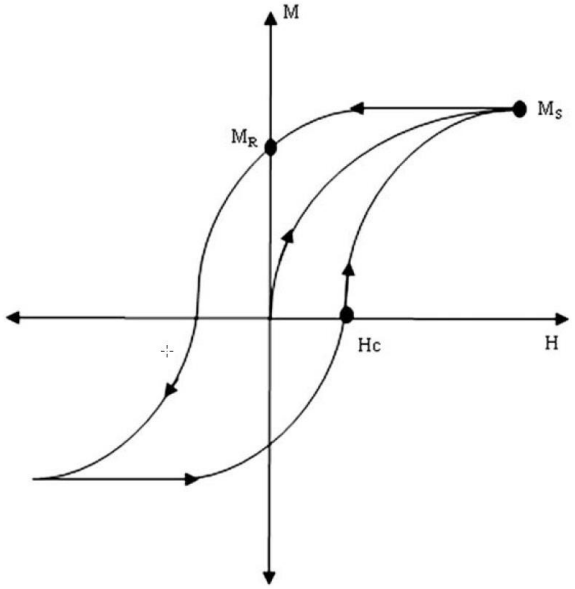

Figure 1.2: Magnetization M as a function of an applied magnetic field H[15].

Superparamagnetism

Ferromagnetic or *ferrimagnetic* materials with crystal sized below a critical diameter r_c (Equation 1.2) attain a single magnetic domain. As shown in Figure 1.3, if the size

continues to decrease to a value r_0 (Equation 1.3), the thermal energy and the energy required for a spin to change directions become comparable, and this causes the magnetic dipoles to be randomized in a short period of time. These kinds of small nanoparticles with no magnetic coercivity do not have permanent magnetic unless there is an external field. Under an applied external magnetic field, these particles can respond. Such particles are referred as *superparamagnetic nanoparticles*. [12,16,17,18]

$$r_c \approx 9\frac{(AK_u)^{1/2}}{\mu_0 M_s^2} \tag{1-2}$$

$$r_0 = \left(6\frac{k_B T_b}{K_u}\right)^{1/3} \tag{1-3}$$

In Equation 1-2, r_c is the critical radius below which a particle acts as a single domain particle, A is the exchange, K_u is the uniaxial anisotropy constant, μ_0 is the vacuum permeability, and M_s is the saturation magnetization. In Equation 1-3, r_0 is the transient point from a single domain to superparamagnetic, k_B is the Boltzmann constant, T_b is the blocking temperature and K_u is the anisotropy constant.

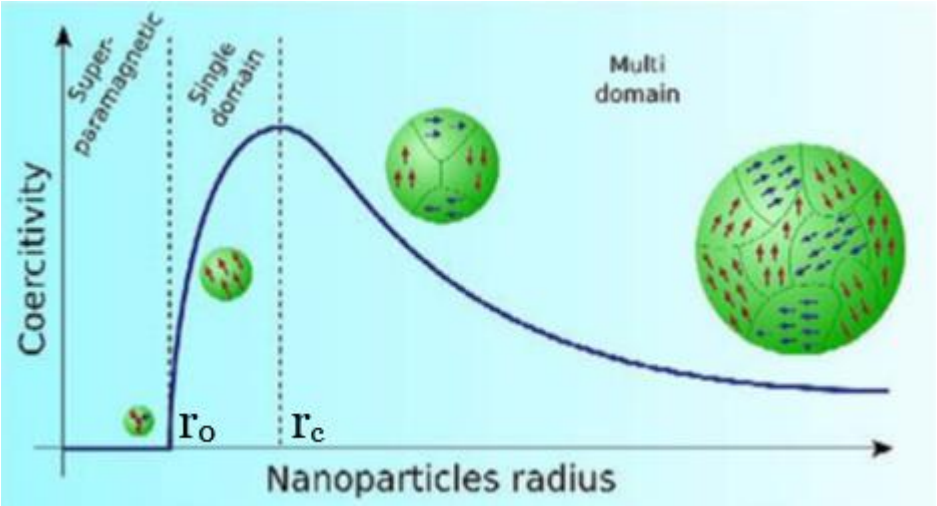

Figure 1.3: Schematic illustration of the coercivity-size relations of small particles [2]

Neel and Brownian Relaxation of Magnetic Nanoparticles

Two different mechanisms can occur during the stepped alignment of the magnetic moments in the same direction as the direction of the field. In the first mechanism the magnetic moments remain fixed regarding the single domain nanoparticle and the orientation of the magnetic moments approaches to the direction of the field with the rotation of the nanoparticles under the effect of the magnetic field. In the second mechanism, nanoparticles stay fixed and the magnetic moments rotate against them. The process which brings nanoparticles to the thermodynamic balance is referred as magnetic relaxation. Because of these magnetic moment rotation mechanisms, the Brown relaxation, related to the nanoparticle rotation, and the Neel relaxation related to the rotation of the magnetic moment inside the nanoparticle appear. In Neel rotation, organizing electronic states differently leads to magnetic moment internal rotation. Neel rotation arises under the influence of magnetic anisotropy of crystal structure and shape of the nanoparticles. In Brownian motion, all particles can rotate. Brownian and Neel rotations of nanoparticles have different relaxation time depending on different variables. The Brownian and Néel relaxation times τ_B and τ_N are given by

$$\tau_B = \frac{3\eta V_h}{k_B T} \tag{1-4}$$

$$\tau_N = \tau_0 exp\left(\frac{K_u V_M}{k_B T}\right) \tag{1-5}$$

where ferrofluid viscosity is η, the absolute temperature is T, and the hydrodynamic volume of the particle is V_h, Boltzmann's constant is k_B, attempt time is τ_0, anisotropy constant is K_u and MNP's primary volume is V_M[19,20,21,22,23,24].

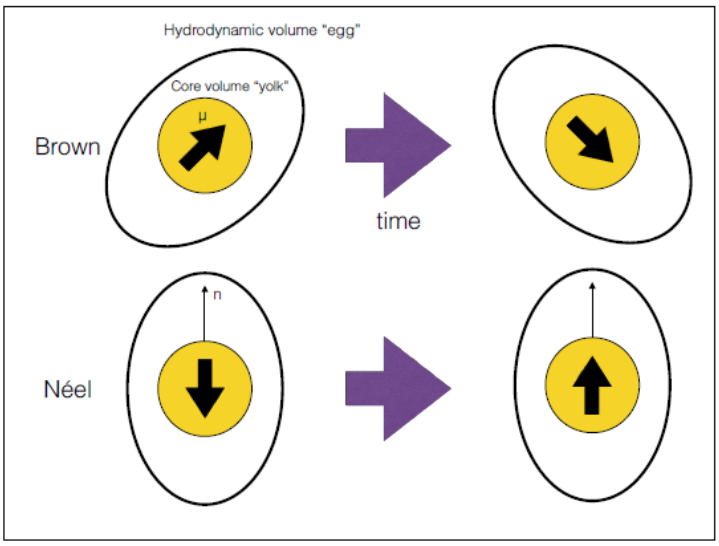

Figure 1.4: Néel and Brownian relaxation [19]

Since there has been no theoretical work that deals with Neel and Brownian relaxation simultaneously, it is simpler, when appropriate, to treat the relaxation as being pure Brownian or pure Néel. As the magnetic field increases the relaxation time of both Neel and Brownian motion decreases. Especially Neel relaxation time decreases in a faster rate than Brownian motion [19,20,21,22,23,24].

Also, the relaxation times caused by the Brownian or Néel mechanisms depend on the magnitude of the applied magnetic field. In particular, the Néel relaxation time is sensitive to the magnetic field strength and varies by many orders of magnitude for nanoparticle properties and magnetic field strengths [19,20,21,22,23,24].

Blocking Temperature and Curie Temperature

Particles, while they are superparamagnetic at a temperature, can show hysteresis at a lower temperature. If superparamagnetic particles are cooled, at some temperature called blocking temperature T_b the time required for complete magnetic relaxation will be infinite. At temperatures lower than the blocking temperature due to metastability rather than domain wall motion nanoparticles exhibit hysteresis. Thermal excitations orient the magnetic moments of different particles randomly at the blocking temperature, which is different from Curie temperature T_c where the spins within individual particles are

randomized by the thermal energy. This is shown in Figure 1.5. Generally, the blocking temperature is much lower than the Curie temperature [18].

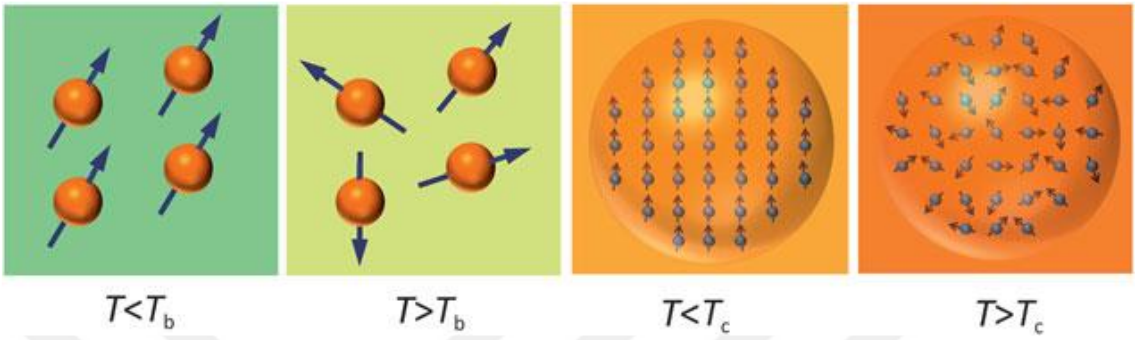

Figure 1.5: Alignment of SPION spins under the magnetic field at different temperatures in comparison with blocking temperature (T_b) and Curie temperature (T_c) [18].

The magnetic behavior of the particle is characterized by the blocking temperature, T_b, below which the particle moments appear frozen on the time scale of the measurement, τ_m (experimental measuring time τ_m.) Equation 1-6 is valid for single particles or a system of non-interacting particles with the same size and anisotropy. If the particles are not monodisperse, the distribution of particle sizes results in a distribution of blocking temperatures. In Equation 1-6 T_b is the blocking temperature, K_u is anisotropy constant, V_M is MNP's primary volume, k_B is Boltzmann's constant, τ_m is experimental measuring time, $_0$ is the inverse angular attempt frequency. [25]

$$T_b = \frac{K_u V_M}{k_B \ln(\tau_m/\tau_0)} \quad (1\text{-}6)$$

Hard and Soft Magnetic Materials

Magnetic materials are classified according to their magnetic coercivity. By descending order, the hardness of magnetic materials is classified as hard (permanent) and soft magnetic materials [11]. Materials that retain permanent magnetization in the absence of an applied field are known as hard magnets [12]. Hard magnetic materials or so-called permanent magnets have high coercivity, residual magnetization, and maximum energy product $(BH)_{max}$, which reflects the magnetic energy stored in the material and the Curie

temperature T_c, for which the ferromagnetic- paramagnetic transition. Therefore, these materials should have large magnetic anisotropy and magnetostriction, which requires excellent stability, including high mechanical strength, stability, and heat and corrosion resistance. [26,27]

Hard magnetic materials are categorized as metal magnets and oxide magnets. Metal magnets are divided into powerful rare earth magnets, such as Nd– Fe–B magnets, Sm–Co magnets, and alloy magnets, which have good temperature properties and are exemplified by alnico magnets and Fe–Cr–Co magnets. Oxide magnets use Fe oxides and are very inexpensive, and thus ferrite magnets (Ba- and Sr-based magneto plumbite ferrite magnets) are the magnets that people are most familiar with in daily life [27].

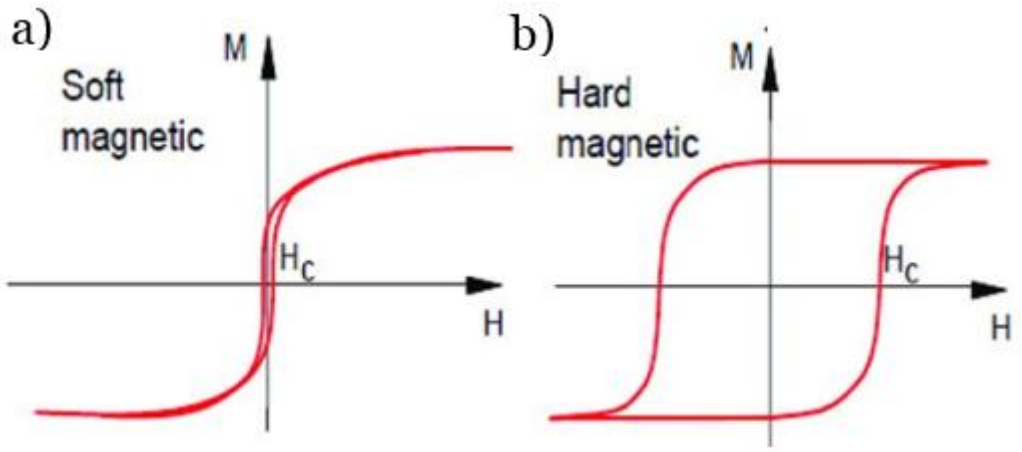

Figure 1.6: Hysteresis curve of a) soft and b) hard magnetic materials[27].

1.1.3 SPIONs

The main configurations of SPIONs are hematite, magnetite and maghemite. Hematite has a hard hexagonal crystal with a rhombohedral close-packed oxygen lattice system in which Fe(III) ions occupy two-thirds of the octahedral sites. Hematites (α-Fe_2O_3) are weak ferromagnets at room temperature, and by heating, meta-stable phase maghemite (γ-Fe_2O_3) can be achieved. Maghemite (γ-Fe_2O_3) is the second most common SPION in nature. γ-Fe_2O_3 has a cubic crystal structure. Like Fe_3O_4 (with cubic crystal structure), it

contains iron cations in tetrahedral and octahedral sites. Meghamite and magnetite are ferromagnetic. Synthesis of maghemite (γ-Fe_2O_3) can be achieved by oxidizing Fe_3O_4 at 300°C [28,29,30,31].

Magnetite (Fe_3O_4) has a close packed spinel crystale lattice formed by oxygen ions with iron ions located randomly between octahedral and tetrahedral sites. Magneteite has the highest saturation magnetization (300 times higher than hematite) for its unique electric and magnetic properties due to the transfer of electrons between Fe^{2+} and Fe^{3+} ions in the octahedral sites. A crystal of Fe_3O_4 has a spinel structure, space group Fd3m [32-34].

1.1.4 Methods of SPIONs Synthesis

Co-precipitation Method

MNPs in the co-precipitation method can be obtained by the reaction of iron salts and a base in aqueous solutions. The phase and size of the particles depend on the concentration of cations, the counter ions present, pH, temperature and stirring speed of the solution. By changing the synthesizing conditions mentioned above, the size of the particles can be controlled. It is mentioned that aggregation of the SPIONs during the synthesis by the coprecipitation method is probably because of their large ratio of surface area volume. Therefore, by adding anionic surfactants like proteins, starches, polymers, or polyelectrolytes for coating the particle surfaces, agglomeration of the particles can be minimized. [35].

Microemulsion,

Microemulsion is a synthesizing method that shape and size of SPIONs can be controlled by. In this method dispersal of a nonhomogenous mixture of water and oil phases at the presence of a surfactant is thermodynamically stable. At the interface of the oil and water the addition of surfactant material can form a monolayer by its hydrophilic head groups

in the aqueous phase and hydrophobic tail molecules can dissolve in the oil phase. Figure 1.7 illustrates the SPIONs synthesis by this method [36-42].

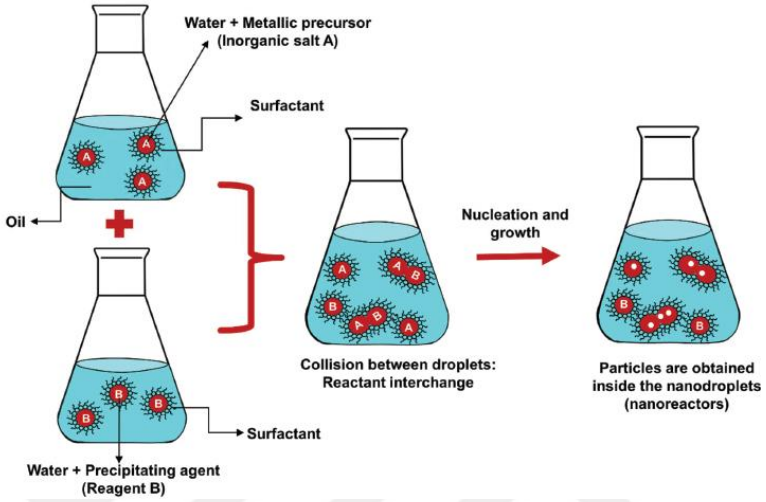

Figure 1.7: Schematic illustration of the microemulsion method (O/W reaction) for nanoparticle synthesis[36].

Thermal Decomposition

SPIONs in this method are synthesized in the presence of hot organic surfactants. By high-temperature decomposition of organometallic precursors, such as $[Fe^{n+}(acac)_n]$ (n = 2 or 3, acac = acetylacetonate), $Fe^{x}(cup)_x$ (cup = N-nitrosophenyl hydroxylamine) or carbonyls (such as $Fe(CO)_5$), using organic solvents and surfactants such as fatty acids, oleic acid, and hexadecylamine SPIONs with controlled size and size distribution can be synthesized. Disadvantages of using this method are high reaction temperatures, the use of toxic reagents, and SPIONs dispersing only in organic solvents. The microemulsion and thermal decomposition methods both, have a complicated process and need high temperatures. [28,29,36,37,43].

Hydrothermal and solvothermal

The hydrothermal method utilizes an aqueous solution to prepare SPIONs. This method

uses aqueous chemicals of iron salts, surfactants and precipitant solution in a sealed container at the high temperature range of 130°C to 250°C, and at high vapor pressure, generally in the range of 0.3 to 4 MPa [30, 36,37].

The synthesis process of the solvothermal method is the same as the hydrothermal synthetic method. Solvothermal method synthesis happens in an organic medium [36].

Mild reduction

The general principles for a mild reduction are: (1) Fe^{3+} is partially reduced to Fe^{2+} by sodium sulfate and (2) ammonium hydroxide is added to co-precipitate Fe^{3+}/Fe^{2+} salts to obtain nanoparticles [36].

Sonochemical method

High energy ultrasound is used for the synthesis of SPIONs. Ultrasound generates cavitation bubbles which can be used to transform the reactants into desired products at ambient temperature. The chemical effects of ultrasound are based on acoustic cavitation. Acoustic cavitation is defined as the formation, growth, and implosive collapse of bubbles in a liquid. The size and shape of the SPIONs can be controlled by regulating the refluxing temperature, power, and irradiation time. Temporary temperatures of 5000 K, pressures of 1800 atm and cooling rates higher than 10^{10} K/s are observed in the hotspots which are created by the collapse of the bubble [36,37,38].

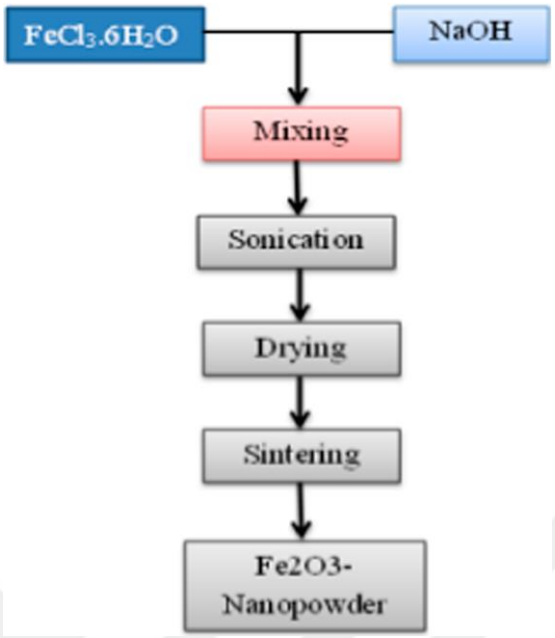

Figure 1.8: Flow chart of the sonochemical synthesis of iron oxide[35].

Microwave assisted synthesis

Microwaves from the electromagnetic spectrum can also be used for the synthesis of SPIONs consuming less energy and in a shorter time [36].

Polyol method

Polyol is a liquid-phase synthetic method in the presence of multivalent alcohols (alcohols with several OH groups) under high boiling conditions. Ethylene glycol is the simplest representative of the polyol family and, based on this, polyols comprise of a series of glycols diethylene glycol, triethylene glycol, tetraethylene glycol up to polyethylene glycol [40].

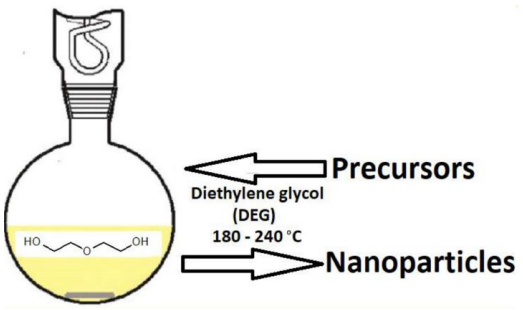

Figure 1.9: Polyol route for the synthesis of NPs [41].

1.1.5 Surface modification of SPIONs

SPIONs have an extensive application in biomedicine. Serious agglomeration in biological environments and fast recognition by the body immune system are the limitations in the usage of SPIONs in clinical applications. Therefore, biofunctionalizing SPIONs surface with organic coatings is the solution to overcome the barriers and making the application of SPIONs in diagnostics and therapeutics purposes possible. A medical SPION generally consists of three components: an iron oxide nanoparticle core that acts as a medicine carrier and contrast agent for MRI, a coating on the core that enhances favorable interactions between the SPION and the biological system, and a medical load that performs the designated function in the body [44,45].

The superparamagnetic property of SPIONs is not only dependent on the core size but also on its surface modifications. The graphical representation of multilayered SPIONs containing a nanoparticle core, coatings, and targeting moieties is shown in Fig. 1.10 [36].

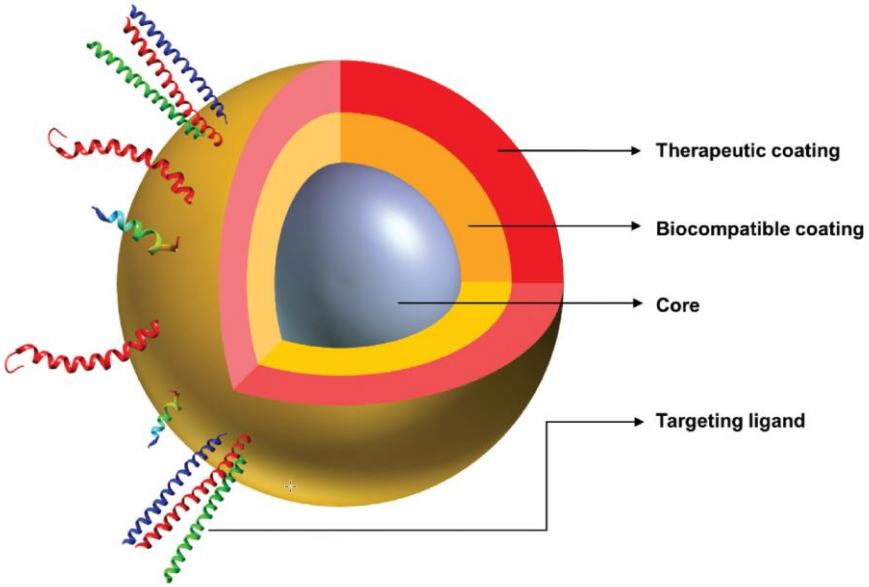

Figure 1.10: Graphical representation of multilayered SPIONs [36].

1.1.6 Application of SPIONs

Therapeutic SPIONs in Cancer Treatment

Cancer related deaths is the second reason for human death in the world after heart diseases. Because of the uncontrolled growth of tumor cells, cancer spread to other organs and cause death in humans. Conventional methods in cancer treatment include surgical removal of the cancerous tumor, radiation therapy, chemotherapy, or a combination of them. However, these methods have some drawbacks including the toxicity of the conventional methods to the surrounding healthy cells, drug resistance of cancers because of low dosage of the drugs, ineffectiveness because of cancer cells spreading to nearby lymphs and organs (stage IV), difficulty in overcoming the biological barriers, and tumor reoccurrence after a period of improvement. Therefore, new cancer treatment techniques are desirable and using SPIONs with their unique properties to replace or partner conventional cancer treatment methods is demanded. SPIONs in various new techniques can be used with reduced side effects, cytotoxicity, targeted therapy and using high drug

dosage. These methods include MRI, targeted drug delivery, photothermal therapy, gene therapy, immunotherapy, protein therapy, photodynamic therapy and magnetic hyperthermia. [14,46].

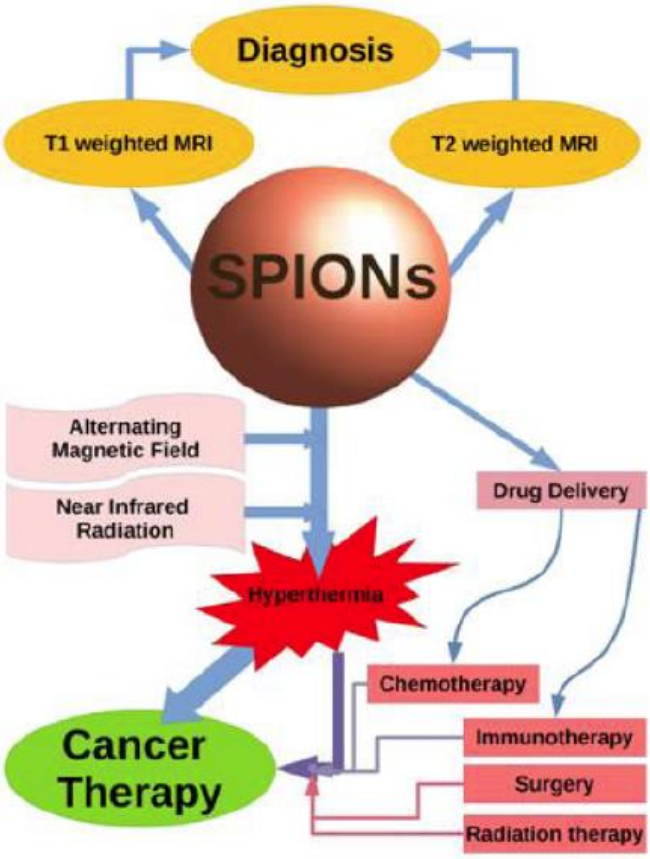

Figure 1.11: Overview of the multiple functions of SPIONs and the potential for synergy with other methods of cancer therapy [46].

Magnetic resonance imaging (MRI)

In MRI as a result of applied magnetic field magnetic moment of protons in a sample line up along the z-axis (M_z) with a magnitude of M_0. The time needed for the magnetic moments to reach the stable state is called the relaxation time. The reasons for MRI contrast in soft tissue are the differences in the proton density, spin-net relaxation time (T_1) and spin-spin relaxation time (T_2) of the protons. T_1 is the time constant of the exponential recovery of M_0 along the z-axis after an RF pulse. For protons that relax more slowly (extended T_1), full magnetization does not happen before the following RF pulses,

and as a result they produce less signal and cause the saturation effect. T_2 is the time constant of the exponential decline of the latitudinal magnetization (M_{xy}) after an RF pulse. Intrinsic variances of T_1 and T_2 are minor and mostly special materials are used clinically to improve the contrast between the tissue and the surrounding tissue [21,47,48].

SPIONs are the best candidates for MRI contrast due to their superparamagnetic behavior [49,50]. SPIONs improve contrast by decreasing the T_2 relaxation time of water protons near the NPs and producing visible signal voids (negative contrast) – seen as dark spots - on T_2-weighted images. This is different from commercial contrast agents, such as gadolinium chelates, which reduce the T_1 relaxation times, producing positive contrast, or bright spots, on the image [21].

MRI imaging should be exact for biomedical detection and treatment of diseases, especially internal pathologies like cancerous tumors. Advantages of SPIONs over traditional MRI contrast are relatively high and long-lasting signal, as well as the insensitivity of their contrast enhancement effect to the difficult molecular water-coordination dependence of Gd chelates as a contrast agent. Furthermore, SPIONs can be designed to be targeted to specific biological tissues or cancerous tumors, results in localized contrast at the biological location of interest [21].

Drug delivery

In drug delivery no drug is free from side effects, and these side effects usually arise from non-specificity in drug action. The concept of magnetic targeting starts with attaching drug molecules to magnetic nanomaterials followed by the injection and guidance of these particles to a site of action under the influence of localized magnetic field-gradients and holding there at the site till the completion of therapy and final removal. SPIONs high surface area for surface modification with biocompatible polymers and drug loading, controlling their size within the desirable range result, controllable magnetization in the specific site of the targeted organ as mentioned, can yield powerful targeted delivery vehicles which can deal with this issue [36,51].

In designing SPIONs for drug delivery there are some physicochemical characteristics that effects the drug delivery efficiency including shape, size and surface properties of SPIONs. Rod-shaped and non-spherical nanoparticles show a longer blood circulation time compared to spherical particles. Huang *et al.* found that the shape of the nanoparticles could affect their biodistribution, clearance, and biocompatibility in vivo [51,52]. The size of the nanoparticles is a critical issue since in the body SPIONs smaller than 10 nm can be removed by renal clearance and SPIONs with a size larger than 200 nm are agglomerated in the spleen or are taken up by phagocytic cells of the body. However, SPIONs with the size of 10-100 nm circulate longer in the body since they can avoid being caught by the reticuloendothelial system easily. They can also penetrate through very small capillaries [53,54]. The surface charge of SPIONs also determines their distribution in the body and affects internalization in their target cells [51].

Chemotherapy is an old method used for cancer treatments. Conventional chemotherapy methods use circulatory unite for drug delivery into tumor sites so it is not specific and high dosages of drugs against tumor cells can damage healthy tissues.

Targeting drug delivery into the tumor site has been gained specific attention as a replacing method for chemotherapy. Biocompatible, surface functionalized SPIONs are under great attention for drug delivery applications. High dosage drug loaded SPIONs by magnetically targeted drug delivery are directed to the tumor sites under the applied magnetic field and enhance the aggregation of nano-drugs at the target area and perform cancer treatment [36,55].

SPIONs act in cancer gene therapy by magnetofection. Magnetofection is based on the application of functionalized SPIONs loaded with nucleic acids. The nucleic acids loaded to SPIONs are transported to the target cells with an applied external magnetic field and these nucleic acids are introduced into the cells [36,56].

In protein therapy, protein drugs are being sent into the cancer cells. This method is a safe and direct method in cancer treatment. SPIONs are able to protect these proteins and improve the protein transfer to the tumor site by acting as an intracellular access vehicle [36].

Hyperthermia

Another way of using SPIONs in biomedicine is magnetic hyperthermia. Cancerous cells are more sensitive to temperature than normal cells. SPIONs are the best candidates for hyperthermia since they have a high specific absorption rate (SAR). The heating efficiency of SPIONs is measured using the SAR that helps to convert the magnetic field into heat, based on Neel and Brownian relaxations of SPIONs involved [14,57,58].

Magnetic fluid hyperthermia (MFH) can achieve localized, controlled heating in deep tissue and SPIONs can achieve high cellular selectivity via surface modification [59].

There are two general ways to administer SPIONs to induce hyperthermia. The first approach is to inject SPIONs directly in the tumor area. The second is to introduce SPIONs by infusing them into the veins, which enables a more homogenous distribution in the circulatory system. Cancer cells are affected more than healthy cells by temperature increase and they are mainly eliminated at higher temperatures than 46 °C by cell necrosis in temperature dependent thermal therapies. In moderate hyperthermia cancer treatment temperature range is between 41-46 °C [57,58,59].

Photothermal therapy (PTT)

Absorption of laser energy by magnetic nanoparticles results in photothermal responses including temperature rise, refractive index change and thermoelastic expansion, which is a diagnostic tool for biomedical applications. In addition, short-pulsed laser irradiation of nanoparticles results in a rapid temperature rise that is utilized therapeutically to kill surrounding malignant cells [60]

In recent years, near-infrared (NIR) laser-induced photothermal therapy (PTT), an application of the nanotechnology has become a minimally invasive treatment option for cancer. In this therapy the tumor site can be exposed to a specific amount of photoenergy directly. This increases the efficiency of the therapy as minimizing the damage to the healthy cells.SPIONs have a photothermal effect and as they are non-toxic, magnetic,

chemically stable, and biocompatible, could be used as an alternative PTT material [49,61]

Photodynamic therapy (PDT)

PDT is a promising treatment against several types of cancers. Photodynamic therapy (PDT) uses light irradiation in combination with chemical photosensitizers (PS) to destroy target tumor tissues [62].

Drug loaded magnetic nanomaterials in the target environment require a relatively lower dose to achieve therapeutic action. The most common nanomaterials used in PDT are functionalized SPIONs [63].

Wastewater treatment

Contaminants in wastewater are heavy metals, inorganic and organic pollutants, and many other complex compounds that put human lives and the ecological environment in danger, hence have to be removed. Applications of SPIONs in contaminated water treatment can be categorized under two groups: (a) technologies which use SPIONs as a kind of nano-sorbent or immobilization device for effective removal of the contaminant and (b) those which use SPIONs as photocatalysts to break down or to make contaminants less toxic [64,65].

1.2 Magnetorheological Fluids (MRFs)

Magneto-rheological fluids (MRF) are suspensions of magnetizable particles in a low viscosity Newtonian non-magnetic liquid called carrier fluid such as hydraulic oil, silicon oil, mineral oil, glycerol and paraffin oil and show non-Newtonian behaviour in an

external magnetic field. Under the application of an external magnetic field, magnetic particles align anisotropically in the direction of the magnetic field lines and form string-like structures parallel to the applied magnetic field lines, resulting in high yield stress in the system and form aggregates in which MR fluid change to a semi-solid structure. Some of the outstanding features of MRFs are adjustable apparent viscosity, quick response time and high dynamic flow strength. [66-74]

Jacob Rabinow at the US National Bureau of Standards discovered and prepared MRF and MR devices [75]. Because of the increasing demand for magnetorheological fluids in today's modern industries, there is a growing need for stable MRFs with good magnetorheological effect [76].

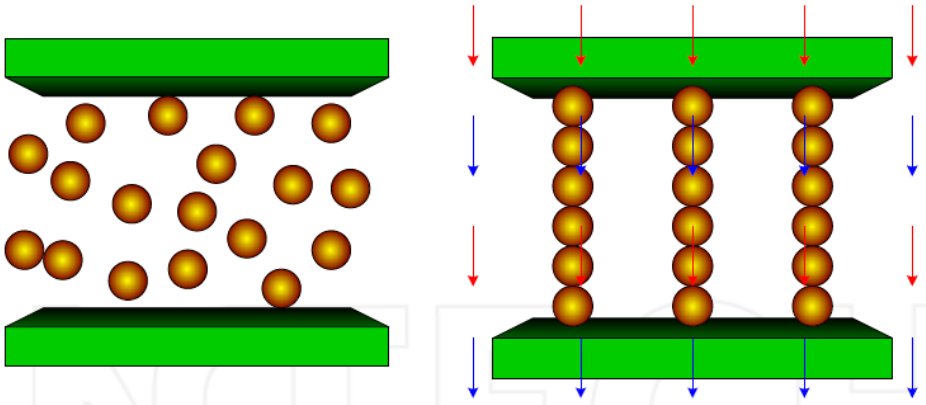

Figure 1.12: MRF particle structures a) with no applied magnetic field b) under applied magnetic field [77].

1.2.1 Components of magnetorheological fluids

MRFs are prepared by mixing all the components (base fluid, magnetizable particles, and stabilizer additives) together. The important issue is the type and fraction of used components for achieving MRF with high magnetorheological properties and stability for an acceptable period [76].

Continuous phase

Rheological properties, tribological properties and temperature stability are the main factors for carrier liquid selection. The viscosity of the continuous phase in MRF is one of the most important criteria to be considered since low viscosity of the carrier fluid can lead to instability and sedimentation of particles and high viscosity may increase the viscosity of MRF when there is no applied magnetic field which is not favorable. In general, oils with low viscosity are preferred for MRFs. Typically, petroleum-based oils (like hydraulic oil), silicone oils, mineral oils, polyesters, polyethers, water, synthetic hydrocarbon oils and ionic liquids (IL) are being used [76,78].

Dispersed phase

Magnetorheological behavior of MRFs depends on the strength of a magnetic field and the magnetizability or the saturation magnetization of the magnetic particles. Conventional MRFs are two-phase fluids consist of a non-magnetizable carrier fluid and large amounts of highly magnetizable micron-sized particles dispersed in the carrier fluid. As the particles in an MRF many metals (i.e. carbonyl iron), alloys (i. e. iron-cobalt alloy) and ceramic compositions (i. e. nickel-zinc ferrites) can be used. Iron particles produced by the thermal decomposition of iron pentacarbonyl are commonly used because of their large saturation magnetization ($\mu_0 M_s$ = 2.1 T). Some iron alloys have higher saturation magnetization than pure iron and can offer high magnetorheological properties for the MRFs, but many of the alloying elements, like cobalt, have a high price and would make the MRF too expensive for many applications [69,70,71,72,74].

In recent decades, a combination of magnetic or non-magnetic particles in different sizes or shapes is being used as well especially to improve the stability of the conventional MRFs that will be discussed later [79,80].

1.2.2 Magnetorheological properties of MRFs

Magnetorheology is one of the topics under the science of rheology that study the flow and deformation of the materials like MRFs, magnetic gels, magnetic foams and magnetic elastomers, under applied magnetic field. MRFs are the most magnetorheologically studied materials because of their wide application in mechanical devices MRFs have a low viscosity when they are not under an external magnetic field. Under applied magnetic field magnetic particles in carrier fluid become magnetized and align along the field lines and form anisometric aggregates that extend across the system. The material comes to exist (MRF) with this process has a large yield stress. Also, the apparent viscosity of these MRFs highly depends on the shear rate and their viscoelasticity is higher under the applied magnetic field [70,71].

Shear stress

Studying the relation between shear stress and shear strain of MRFs is important for designing MR devices and predict how they work. MRFs behave similar to carrier fluids, the difference is that MRFs are more concentrated because of the metallic particles in them. In simple shear of the MRF at a constant shear rate γ^{o}, the resulting shear stress τ will depend on the absolute value of the magnetic flux density B. To simplify the correlation mathematically, the steady-state shear stress τ_s is assumed to be proportional to the absolute value of the imposed flux density. The proportion (p) in this formulation is the slope of the linear characteristics in shear stress-flux density [68,76]:

$$\tau_s = p|B| \tag{1-7}$$

Yielding

There are three yield stresses measured through shearing flow experiments (Fig. 1-13): the elastic-limit yield stress, the static yield stress and the dynamic yield stress. The elastic-limit yield stress is the maximum shear stress that can be applied while the material is still able to recover completely when the stress is removed. The static (or frictional) yield stress is the minimum stress the fluid starts to flow. Finally, the dynamic yield stress is the stress required to continuously break the aggregates which reform when there are magnetostatic forces present once the stress is higher than the static yield stress. Yield stress can be calculated by fitting a viscoplastic constitutive model, such as the Bingham (Equation 1-8), Herschel–Bulkley (Equation 1-9) or Casson (Equation 1-10) equations to experimental data at nonzero shear rates. The dynamic yield stress is usually higher than the static yield stress. Even though this is undoubtedly the most widely used yield stress estimator, the determination of the dynamic yield stress is controversial and always involves the use of indirect methods. [70,72,81,82,83,84]

$$\tau = \tau_0 + \eta\dot{\gamma} \tag{1-8}$$

$$\tau = \tau_0 + \eta\dot{\gamma}^n \tag{1-9}$$

$$\tau^{0.5} = {\tau_0}^{0.5} + \eta^{0.5}\dot{\gamma}^{0.5} \tag{1-10}$$

where τ is shear stress, τ_0 is dynamic yield stress, η is viscosity, $\dot{\gamma}$ is shear rate and n is power-law exponent.

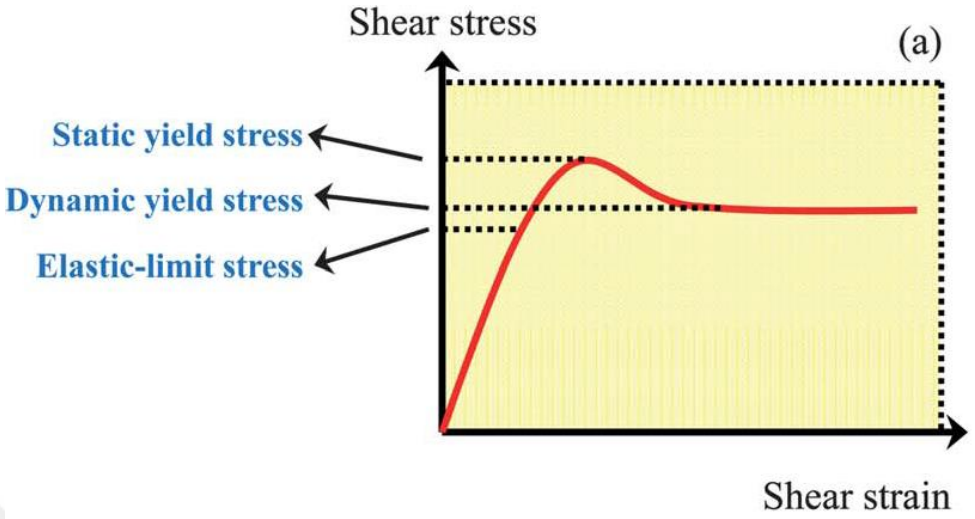

Figure 1.13: Hypothetical stress-strain curve for a quasistatic shear deformation illustrating the elastic limit yield stress, static yield stress and the dynamic yield stress. [70,82]

Viscosity

The viscosity can be expressed in two ways. One definition of viscosity is called dynamic viscosity as the other one is called kinematic viscosity. Dynamic viscosity η is defined as [71]:

$$\eta = \frac{\tau}{\gamma^o} \tag{1-11}$$

where τ is shear stress and γ^o is shear rate.

Kinematic viscosity υ is defined as [71]:

$$\upsilon = \frac{\eta}{\rho} \tag{1-12}$$

where η is dynamic viscosity and ρ is density.

Complex modulus

Complex shear modulus G*

Law of elasticity for oscillatory shear tests are given as:

$$G^* = \tau_A \gamma_A \tag{1-13}$$

where G* is complex shear modulus, τ_A is shear-stress amplitude and γ_A is strain amplitude G* describes the entire viscoelastic behavior of a sample [83]

Storage modulus G' and loss modulus G"

The phase shift δ, which is always less than 90° represents the time lag between the preset and the resulting sinusoidal oscillation and is determined for each measuring point. This angle is shown below under the G* vector (Figure 1.14) [75].

The x-axis is drawn from the other end of the phase shift to the right ant the y-axis is drawn perpendicular to the x-axis in the upward direction. The x component of the G* vector is the elastic portions of the viscoelastic behavior and represented as storage modulus, G'. The y component of the G* vector is the viscous portion of the viscoelastic behavior and represented as loss modulus, G". To be able to draw the complete vector diagram G* and δ are sufficient, G' and G" can be derived from these parameters. (Figure 1.15) [75].

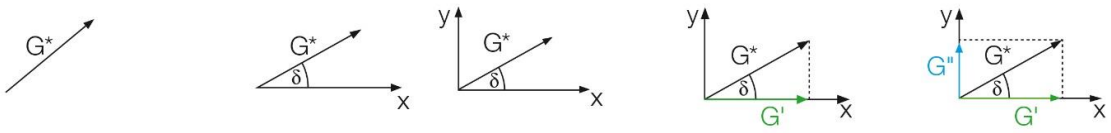

Figure 1.14: Development of a vector diagram: (1) Vector is drawn as it length to be as the total amount of the complex shear modulus G*, (2) x-axis is drawn using the G* vector and phase-shift angle δ (3) y-axis is drawn perpendicular to the x-axis, (4) G' is the x component of the G* vector (5) G" is the y component of the G* vector [75].

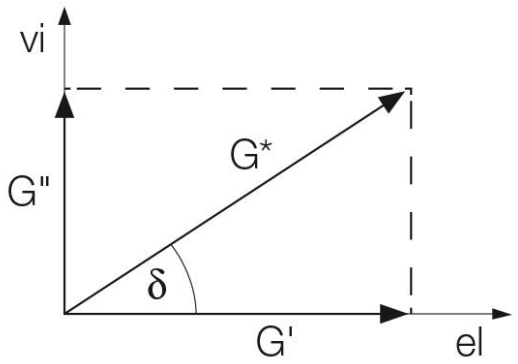

Figure 1.15: Vector diagram illustrating the relationship between complex shear modulus G*, storage modulus G' and loss modulus G" [75].

The storage modulus G' quasi describes the solid-state behavior of the sample as the loss modulus G" can be considered as the liquid-state behavior of the sample.

Sedimentation

Sedimentation is mainly caused by the large density difference between the dispersed particles and carrier fluid according to the sedimentation law that has been presented in Equation. 1-14

$$V(\phi, d) = \frac{|\rho p - \rho c| g d^2}{18 \upsilon \rho c} \frac{[1-\phi]}{\left[1 + \frac{4.6\phi}{(1-\phi)^3}\right]} \qquad (1\text{-}14)$$

where V is the particle migration velocity (m/s), ρp is the particle density (kg/m^3), ρc indicates the density of the liquid medium (kg/m^3), υ is the kinematic viscosity of the liquid medium, d is the particle diameter, and ϕ represents the volume fraction [85,86].

Another formula for sedimentation ratio calculation has been given by Equation 1-15 [87].

$$Sedimentation\ ratio\ (\%) = \frac{height\ of\ the\ particle\ rich\ phase}{height\ of\ the\ entire\ fluid} \times 100 \qquad (1\text{-}15)$$

1.2.3 Rheometry

Modern rheometers can be used for shear tests and torsional tests. They operate with continuous rotation and rotational oscillation shown in Figure 1.16. A rotational rheometer is a device that is used to study the flow and deformation behaviour of materials. The material is generally measured under shear load that is formed by placing the sample between the two surfaces of the measuring geometry, one surface remains stationary and the other rotates dragging the specimen along. The device is generally supplied with plate-plate, cone-plate or concentric cylinder geometries shown in Figure 1.17. The most used geometry used in measuring magnetorheological properties of MRFs is parallel plates geometry. [74, 75]

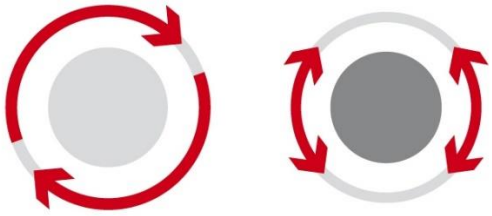

Figure 1.16: Measuring principle of a typical rheometer for rotational tests with continuous rotation (left) or rotational oscillation (right) [75]

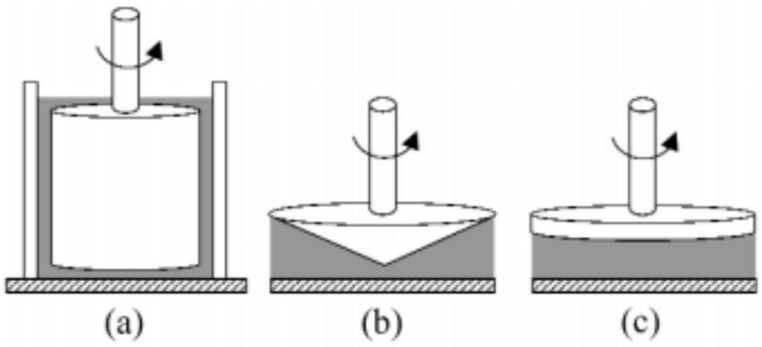

Figure 1.17: a) Concentric cylinder geometry, b) cone and plate, c) parallel plate geometry [74]

1.2.4 Applications of MRFs

MRFs are preferable for damping and dissipative devices because of the sudden change (few milliseconds) in its behavior under the magnetic field. They can be integrated into mechanical systems for silent and quick responses [87].

Three major operational modes are be described for MRFs [88]: *The valve mode* refers to the fluid flowing because of a pressure gradient between two stationary plates, which is used in hydraulic controls, servo valves, dampers, shock absorbers and actuators and has broad application in automobile industry [88]. *The direct shear mode* refers to the fluid located between two plates those move with a relative velocity in regards to each other, which is used in clutches, brakes, chucking and locking devices, dampers, breakaway devices, and structural composites. *The squeeze mode* refers to the fluid running between two plates moving perpendicular to the magnetic field, which finds less application areas and is mostly used in small-amplitude vibration and impact dampers. [88].

Besides, multiple fluid modes or mixed-mode MRF devices that simultaneously employ at least two basic operational modes have alternatively been developed to enlarge the efficiency of MR devices. Operational modes of MRFs have been illustrated in Fig. 1.18 [80,88,89].

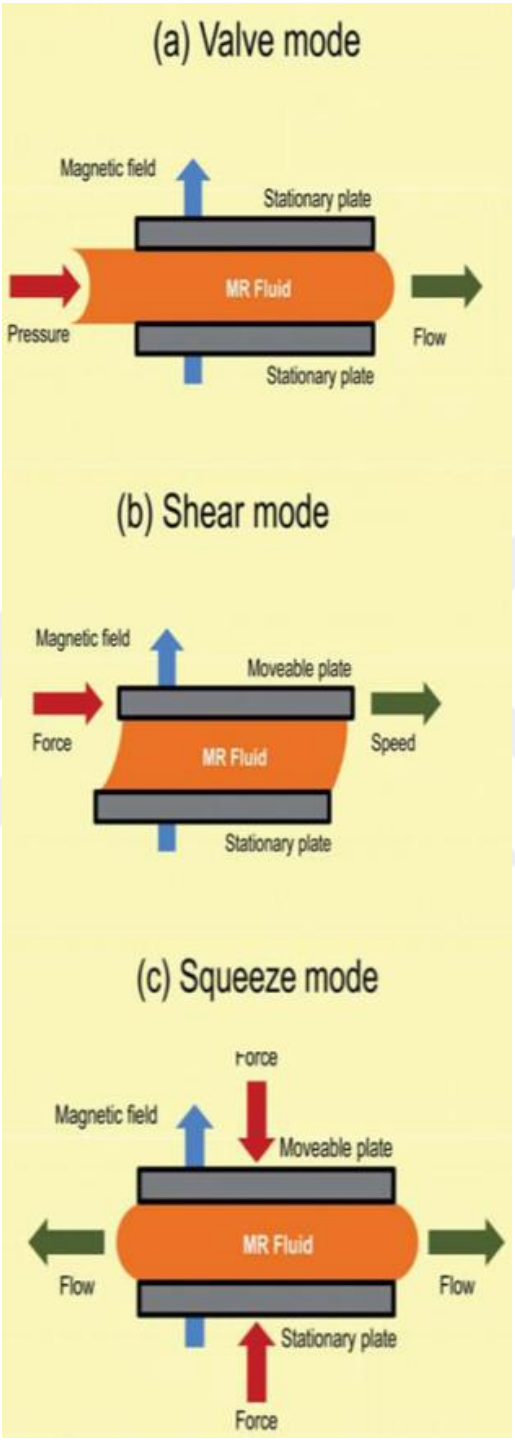

Figure 1.18: Basic operational modes for controllable MRF devices: (a) pressure driven flow mode, (b) direct shear mode, and (c) biaxial elongational flow mode. [80]

In mechanical structure and magnetic circuit applications, the basic assembly components in the design of an MRF damper involve the MRF cylinder and MRF control valve. The

MRF cylinder is filled with MRFs and separated by a moveable piston for outputting mechanical motion. The MRF control valve is employed to produce the damping effect under the controllable applied magnetic fields [88,90].

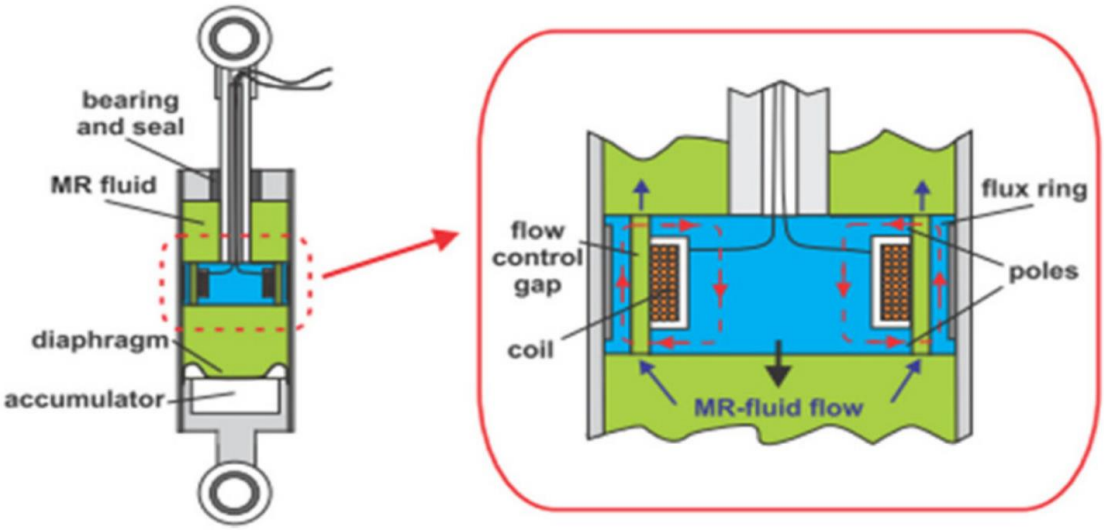

Figure 1.19: prototypical MR damper [90].

As a new technology MR dampers and MR brakes have been used in orthopedic knee applications (Figure1.20 a, b) [90].

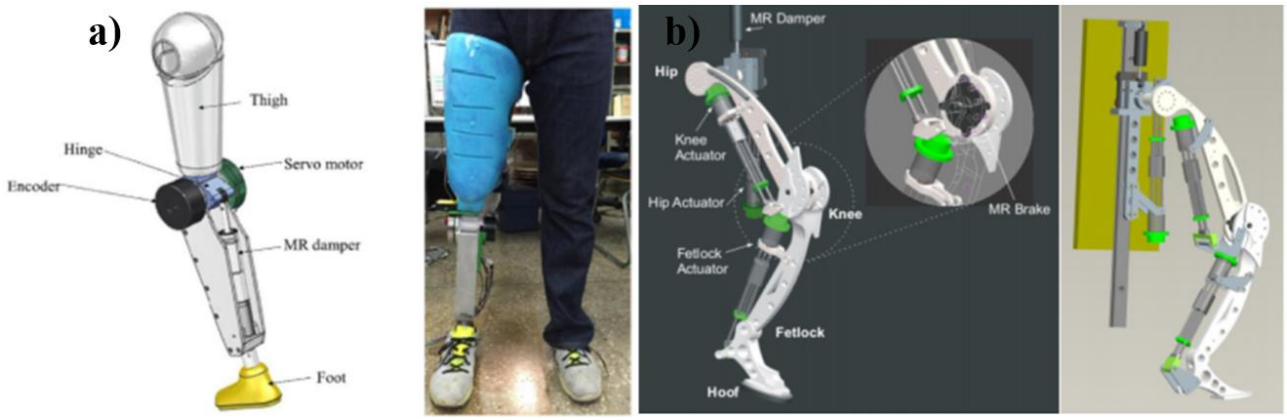

Figure 1.20: Orthopedic artificial knee using a) MR damper and b) MR damper and MR brake [90].

MR brakes and clutches are easy to control in smaller volume in compare to the conventional devices. In these MR devices a low power supply and a small size controller are being used in creating a current source in a magnetic coil. The working principles of

MR dampers and clutches are based on MRF viscosity increase under applied magnetic field strength, which results in resistance to motion between two disks and quick energy transmission (Figure 1.21 a,b)[91,92,93].

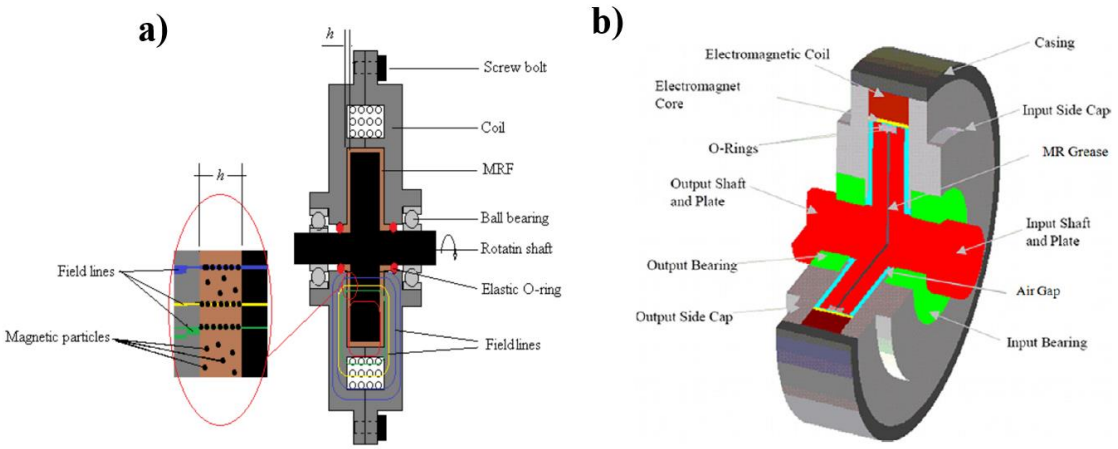

Figure 1.21: The schematic image of a) MR brake and b) MR clutch [91, 92].

MRFs also have a wide application as a vibration absorber for example in vehicle suspension systems, as a vibration absorber in buildings and bridges as an earthquake precaution [90,94]. MRFs are being used in surface polishing machines to improve surface smoothness and to minimize the damage of the polished surfaces [94,95]. Figure 1.22 and Figure 1.23 present some of the examples of the forementioned MR applications.

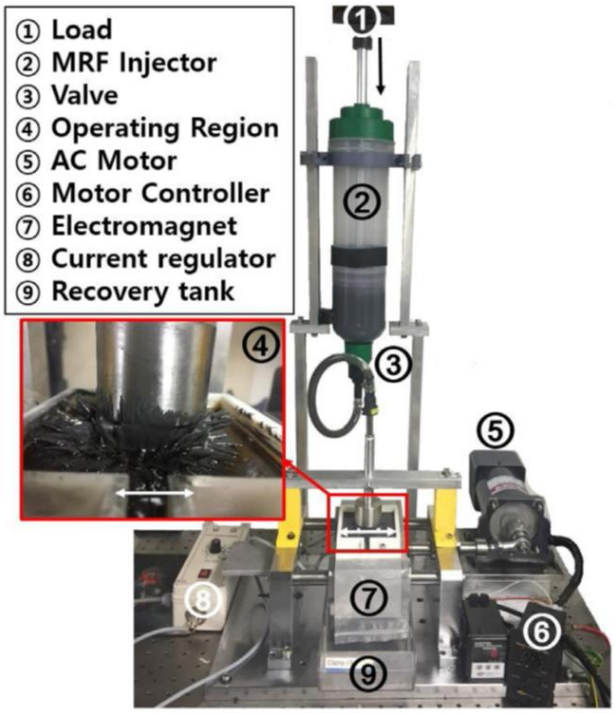

Figure 1.22: image of MR polishing device;

Figure 1.23: MR dampers in infrastructures for vibration absorber during earthquakes [90,95]

1.2.5 An overview on MRFs stabilization techniques

Major problems in using MRFs are particle sedimentation and re-dispersibility of particles because of density difference between heavy micron-sized particles and carrier fluid and favored interparticle aggregation due to the large surface area to- volume ratios that tend to reduce the surface energy resulting in some cases in severe re-dispersibility problems. Also, oxidation of magnetic particles by the pass of time weakens the magnetization saturation and MR [67,76,96]. Different methods have been suggested to solve these problems:: (i) addition of thixotropic agents like silica nanoparticles [97-109]; (ii) surface coating of micron sized magnetic particles with fatty acids, polymers of silica [110-117], (iii) using additives like thixotropic agents or polymers [66,80,118-123]; (iv) use of viscoplastic media or water-in-oil emulsions as continuous phases [124-129]. Although some of these procedures have been effective in reducing the aggregation and precipitation, it also has been proved that the magnetic chaining responsible for the magneto-viscous effect can be weakened, as the concentration of stabilizing agents increase [71]. Also, redispersion of the sediment is usually difficult due to remnant magnetization and such solutions fail to improve redispersion significantly. Yet, the settling problem of MRFs has not been completely solved from the practical point of view. Actually, a way to bypass this sedimentation problem was to sell the solid components of the commercial MRFs to be mixed with the carrier liquid at the site of use [130].

The idea of combining particles of two different sizes, namely “bidisperse” MRFs and surface coating of both micron and nano-size magnetic in bidisperse MRFs have been tested to provide an enhancement in the stability. Colloidal nanoparticles thermodynamically favor dispersion and hence, replacement of part of the micron sized particles with the nanosized ones enhances stability under gravitational force [131]. Sedlacik *et al.* prepared dimorphic MRF from spherical carbonyl iron (CI) (35 wt%, 0.75 ± 0.56 μm) and Fe rod-like particles (5 wt%, length = 590 ± 185 nm, diameter = 135 ± 42 nm) in silicon oil 92]. Dimorphic MRF showed better resistance to sedimentation but there was about 30% sedimentation even after 2.5 h. Silica coating of the particles

enhanced the wettability of particles in silicon oil, but the incorporation of such a non-magnetic component reduced the magnetization response. The use of lower density nanoparticles seems to offer better performance. Incorporation of non-magnetic particles usually enhanced stability yet, reduced magnetorheological properties [104]. The combination of magnetic particles provided a better solution in general. Plachy *et al.* prepared MRFs by adding non-magnetic rod-like ferrous oxalate dihydrate ($Fe_2CO_4 \cdot 2H_2O$) particles and iron oxide (Fe_3O_4) magnetic rod-like particles to CI (60 wt%) in silicon oil [132]. Authors have reported that replacing 5 wt% of CI with magnetic or non-magnetic rod like particles improved the stability due to lower density and physical prevention of dense CI agglomeration. But, significant sedimentation was still observed after 30 h in 10 wt% dimorphic MRFs (sedimentation ratio was about 0.2). Magnetorheological properties of these dimorphic MRFs were improved over pure CI based one since non-magnetic rods cause stronger viscous dissipation, and the magnetic rods assume chain like structures at lower magnetic fields. Cvek *et al.* studied the influence of the morphology effect further and added carbon allotropes (1 wt%), fullerene (C60) powder, carbon nanotubes (CNTs), and graphene nanoplatelets (GNPs) into the carbonyl iron-based magnetorheological fluids (60 wt%) [133]. They have reported that although magnetorheological behaviour was weakened due to disruption of CI chaining, the stability was enhanced (tested up to 100 h) due to low density and increased friction force when CNT was used. C60 acted as a gap filler and aided the chaining of the CI so offered a better magnetorheological response. but did not provide an advantage in sedimentation or redispersibility of the sediment. GNP did not either improve the stability significantly. Ashtiani *et al.* compared the influence of magnetite (13 wt%, 12 nm) versus fumed silica (3 wt%, 12 nm) addition to CI (62 wt%, 3 μm) in silicon oil. Magnetite addition improved magnetorheological properties and improved the stability over only CI based MRF however 25-30% very quick precipitation was recorded [104]. On the other hand, silica nanoparticles improved stability up to 2000 h with poorer magnetic properties compared to magnetite added MRF. Lopez-Lopez *et al.* dispersed CI (10 vol%) in oleic acid stabilized iron oxide nanoparticles (12 vol%) in kerosene [6]. They hypothesized that the remnant magnetization around CI attracted the magnetite and significantly

lowered sedimentation rate due to repulsion of oleic acid coating of magnetite nanoparticles, which was reported for 25 min only. Iglesias *et al.* claimed that CI dispersed in ferrofluid resists sedimentation better based on MRFs prepared with more than 30 vol% CI and about 1.55-8 vol% oleic acid coated magnetite (6 days analysis) [102]. They also report increasing yield stress with increasing magnetic nanoparticle content but not beyond 3 vol%. Wereley *et al.* prepared a bidisperse MRF from 30 nm and 30 μ iron particles with 60 wt% particle loading and 2 wt% lecithin in hydraulic oil [103]. Up to 30 wt% loading of nanoparticles a clear tradeoff between the sedimentation and yield stress was demonstrated. Overall, they have reported that at 20 wt% nano-loading, an order of magnitude improvement in sedimentation was achieved with 15% increase in yield stress. Leong *et al.* added 1 wt % nano sized oleic acid coated magnetite (about 8nm) to CI in hydraulic oil at 80.98 wt% particle concentration and reduced the sedimentation slightly without reducing yield stress [106]. However, after 200h almost 50 % of particles were sedimented. It was also suggested that the nanoparticles fill the space between the micron sized CI while forming a chain under a magnetic field hence provided a slightly higher viscosity and yield stress under applied magnetic field.

Anupama et al. have prepared bidisperse MRFs using Mn-Zn particles (mean diameter of 220 nm) with 10, 20, 40 wt% in silicon oil [134]. They have studied the effect of saturation magnetization, particle size, size-distribution, and concentration of the particles on the magnetorheological properties of MRFs. This study has mentioned that the stability of MRFs was enhanced but with no presented stability results. Also results show that magnetorheological values of the prepared bidisperse MRFs are low which is related to using just nanosized magnetic particles mostly in the range of 20-400 nm.

Susan-Regia *et al.* prepared different bidisperse MRFs by adding oleic-acid coated magnetite nanoparticles (250 nm) in 5, 10, 40 wt % to ferrofluid (NPs with the size of 7.5 nm in transformer oil) with different saturation magnetization values of ferrofluid and in another sample added micron-sized Fe particles (10 μm, 40wt%) to ferrofluid with the highest saturation magnetization [135]. Due to achieved magnetorheological results they reported that the bidisperse MRF with micron-sized Fe particles have the highest magnetorheological values but there was no report about the stability of the prepared

bidisperse MRFs. This research reported that before putting samples in the rheometer they were redispersed the MRF sample by sonication which can be due to bidisperse MRFs instability.

Zhang *et al.* prepared 4 different MRF samples by using uncoated CI particles (67.5-75 wt%), nanomagnetic particles (0 or 7.5 wt%), Polyoxyalkylene modified fatty acid ester (0 or 25 wt%) and Polyoxyalkylene-modified fatty acid amide (0 or 25 wt%) and compared their stability with commercial MRF-122EG and they used MRFs in MR damper with an evaluation equipment used as a robot mechanism [136]. Results show that the stability of bidisperse MRF using CI, nanomagnetic particles and Polyoxyalkylene-modified fatty acid amide was much better than the MRF-122EG after 30 days and in MR damper its damping force was higher than the commercial MRF-122EG but still sedimentation of the bidisperse MRFs was observed.

As an example, Guerrero-Sanchez *et al.* [125] used different ionic liquids (ILs) as the carrier fluid with 25 wt% magnetite micron-sized particle loadings. As a result, MRF with 1-ethyl-3-methylimidazolium diethyl phosphate had 95 % sedimentation ratio after 1680 h but with low VSM magnetization value and weak magnetorheological properties. Ashtiani *et al.* [123] used series of acids with the same carboxyl group but different carbon chain lengths (C12, C14, C16, and C18) as an additive in synthesizing MRFs with CIs (≤ 5μm,52-72 wt%) in silicon oil. 90 % sedimentation ratio reported for the most stable MRF (62 wt% CIs and 3% stearic acid) after 2000 h but with weak magnetorheological properties especially with serious low yield stress value. Zhang *et al.* [126] used Polytetrafluoroethylene (PTFE) micro powders dispersed in methyl silicon oil to fabricate PTFE-oil organogel. CIs (8.5 μm, 10 vol%) were dispersed in thixotropic organogel (10.1 vol% PTFE) to prepare MRFs. As a result, the sedimentation ratio of the MRF was 98 % after 7 days but its magnetorheological properties were too weak due to a large amount of non-magnetic additive.

Surface coating magnetic particles and adding nanosized particles as a second phase called bidisperse MRFs as another solution for solving the sedimentation problem of the MRFs have been suggested in previous works. Mirlik *et al.* [96] prepared MRFs with surface functionalized CIs with silane and cholesterol. 95% sedimentation ratio for MRF

with 15 vol% particle loading was reported but because of the surface functionalization of CIs weak magnetorheological properties were observed. Jun *et al.* [97] used iron oxide coated polymeric micron-sized (9 μm) particles for preparing MRFs with weak magnetization power of particles and as a sequence low magnetorheological properties with 95 % sedimentation ratio after 100 h. Zhang *et al.* [98] used commercial coated CIs with two layers of silica nanoparticles and phosphate (1-3 μm- 30 vol%) for preparing MRF and 88% sedimentation ratio reported after 16 days and has reported that using surface coated CI improves the stability of the MRFs in comparison MRF with unmodified CIs but with lower magnetorheological values than available commercial MRFs like 140-CG LORD. Liu *et al.* [117] prepared MRFs by using oleic acid-coated CIs (1.0-2.5 μm, 20-30 wt %) and strontium hexaferrite nanoparticles (0.11 μm, 0-10 wt%) as an additive. Results show that an MRF with 20 wt% CI and 10 wt% strontium hexaferrite nanoparticles had an 88% sedimentation ratio after 22 days. Weak magnetorheological properties especially at high temperatures were reported. Ngatu *et al.* [137] prepared dimorphic MR fluid with iron loading (8±2 μm, 50-80wt%) and nanowires (230nm diameter and 7.6±5.1 μm length, 2-8wt%). The most stable MRF with 76 wt% iron and 4 wt% nano wires had 94.3% sedimentation ratio without reporting the duration of the sedimentation and also results showed a weak magnetorheological property of bidisperse MRFs. Jönkkäri *et al.* [124] prepared different bidisperse MRFs by adding a total of 15 vol% magnetic CIs (2 μm, 90-100 wt%) and iron nanoparticles coated with double shell $FeO–Fe_3O_4$ (50 nm, 0-5-10 wt%) into silicon oil and 1-ethyl-3-methylimidazolium diethyl phosphate ionic liquid (IL). The sedimentation ratio of the bidisperse MRF with 90 wt% CI and 10 wt% nano-sized magnetic particles loading in IL was reported 91% after 100h with weak magnetorheological properties result. Zhu *et al.* [138] synthesized functionalized iron nanoparticles (30-50 nm) with a layer of oxide on the surface of the NPs. MRFs were prepared using just coated iron nanoparticles or commercial CI (1-5 μm), each MRF with 40 vol% particle loading. Also, for sedimentation control magnetic particle loading of each two MRF was reduced to 10 vol%. Results showed instability of MRFs with 57.2 % sedimentation ratio of MRF with just NPs and 7.2 % for the MRF with CI after 10 days. Zhu *et al.* [139] synthesized iron

nanoparticles (30-50 nm) and prepared bimodal MRFs by mixing CI particles (2-4 μm) and iron nanoparticles and dispersed in the silicon oil. The particle ratios in MRFs were as follows: the mass of NPs accounts for 0%, 25%, 50%, 75%, and 100% of the total particle mass, respectively. For rheological measurement, the total particle concentration of the five kinds of MR fluids was 40 wt%, while for the sedimentation test, the particle concentration was 10 wt%. Results show that after 10 days of stability control there is a noticeable sedimentation of all prepared bimodal MRFs. Dorosti *et al.* [140] prepared MRF by adding worm-like micelles (WLMs) to CI particles (60 wt%) in water based MRFs, using Cetyltrimethyl ammonium bromide (CTAB) as a dispersant in the presence of KBr. Sedimentation results showed 85 % ratio of sedimentation after 50h for the MRF with the highest concentration of CTAB (0.2 M).

1.3 The research proposal

Sedimentation of magnetorheological fluids (MRFs) with high magnetic loading in industrial applications is one of their main drawbacks which has been a subject of many research activities in the field. All proposed solutions provide still limited self-life or life-in-use with reduced magnetorheological quality in many cases as described in detail in section 1.2.

The main focus of this thesis is to improve the stability and redispersibility of MRFs with high particle loading without sacrificing the magneto-viscous effect for long-term use (for months) of such fluids. To achieve this, the use of small superparamagnetic iron oxide nanoparticles (SPION) with an appropriate surface coating that would provide a favorable interaction between the micron-sized Fe-particles and SPIONs is suggested in this thesis. Such MRFs are considered as bidisperse MRFs and mostly studied at low particle loading, with two different sizes of micron-scale magnetic particles or with the combination of magnetic and non-magnetic particles as described in section 1.2. Here, providing an attractive interaction between SPION and micron-sized magnetic particles is suggested as a favorable approach to maintain good magnetorheological properties and to provide enhanced stability to MRFs. In Chapter 2, improvement of the sedimentation of a commercial MRF, 140-CG LORD®, composed of fatty acid coated, micron-sized Fe-

particles suspended in oil is described by the addition of poly(acrylic)acid (PAA) or lauric acid (LA) coated SPIONs, forming all magnetic bidisperse MRFs with particle loading above 80 weight %.

The idea behind using LA and PAA coating is to test the impact of two different types of interaction, hydrophobic interaction (weak van-der-Waals) and electrostatic interaction between micron-sized and nano-sized magnetic particles on MRF properties. Magnetorheological properties, stability and redispersibility of bidisperse MRFs were studied as a function of SPION coating and content. The stability of bidisperse MRFs has been significantly improved with both SPIONs.

In Chapter 3, a new bidisperse MRF was developed in house from the mixture of the functional SPIONs developed in Chapter 2 and the most widely used, micron-sized carbonyl iron (CI). CI is usually used as bare particles, yet to enhance nano and micron-sized particle interactions as well as to improve the stability and dispersibility of CI in a carrier fluid, CI was also coated with LA. The influence of different carrier fluids, particle loading, CI coating, SPION type and amount and addition of polyvinylalcohol (PVA) on the stability and magnetorheological properties of these bidisperse MRFs is described in Chapter 3. Besides, concerning the high temperature applications, magnetorheological properties of bidisperse MRFs were also studied at different temperatures.

Finally, the superiority of these bidisperse MRFs was demonstrated in vibration damping of a home-made damper in washing machines by the group of Prof. İsmail lazoğlu.

Chapter 2

BIDISPERSE MRFs: FUNCTIONAL SPIONS ADDED TO COMMERCIAL MRF

The aim of this phase of the thesis work is to improve the stability and redispersibility of commercial MRFs with high particle loading without sacrificing the magneto-viscous effect for better and long-term use of such fluids. Commercial MRFs usually contain micron-sized Fe particles, mostly called as carbonyl iron. In order to achieve this, we suggest the use of small superparamagnetic iron oxide nanoparticles (SPION) with an appropriate surface coating that would provide a favorable interaction between the micron-sized Fe-particles and SPIONs in order to enhance the stability of MRFs with high particle loading over a period of months and maintain good magnetorheological properties. Although non-magnetic content is usually shown to reduce the magnetic response, enhancing interaction between SPION and micron sized magnetic particles may impact both magnetorheological properties and stability of bidisperse MRFs positively. To test this idea, we have prepared poly(acrylic) acid (PAA) or lauric acid (LA) coated SPIONs as an additive for the commercial MRF, 140-CG LORD®, producing bidisperse MRFs, comprising magnetizable micron sized fatty acid coated Fe-particles and nanosized functional SPIONs. The idea behind using LA and PAA coating is to test the impact of two different types of interaction, hydrophobic interaction (weak van der Waals) and electrostatic interaction between micron-sized and nano-sized magnetic particles on MRF properties. Magnetorheological properties, stability and redispersibility of bidisperse MRFs were studied as a function of SPION coating and content. The stability of bidisperse MRFs has been significantly improved with both SPIONs.

2.1 Experimental

2.1.1 Materials

140-CG LORD® (average particle (fatty acid coated Fe) diameter 1-10 μm, density 3.54-3.74 g/cm^3, 85.44 wt% particle concentration) was purchased from LORD® Inc. Hydraulic oil (Mobil DTE 27, kinetic viscosity 95.3 mm^2/s at 40 °C) was used as a diluent. $FeCl_3.6H_2O$ (ACS reagent, 97%), $FeCl_2.4H_2O$ (reagent plus, 98 %), ammonium hydroxide (25 %, super pure) and lauric acid (for synthesis, purity ≥ 99.0 %) were purchased from MERK (Germany). Poly(acrylic acid) (M_w 2100 kDa) was purchased from Sigma (USA). All reagents were used without further purification.

2.1.2 Synthesis of lauric acid coated SPIONs (SPION-LA)

Lauric acid (LA) coated SPIONs were prepared according to the published procedure [141]. As an example; 500 ml deionized water was degassed with Ar in a 1 L 3-neck round bottomed flask for 45 min and then 0.044 mol $FeCl_2.4H_2O$ and 0.088 mol $FeCl_3.6H_2O$ were added to the flask and stirred at 400 rpm with an overhead stirrer under Ar. The solution was heated up to 80°C, 0.072 mol lauric acid ($C_{12}H_{24}O_2$) was added to the solution and then 78ml NH_4OH was added to the mixture under vigorous stirring. The brown/black solution was stirred for 30 min at 700 rpm at 80°C under Ar. The solution was then cooled down to room temperature and placed on a hand-held magnet overnight. If any precipitate formed, it was removed by magnetic decantation. Next, LA coated SPIONs were precipitated in isopropanol twice, dried and stored as powder at room temperature.

2.1.3 Synthesis of poly(acrylic acid) coated SPIONs (SPION-PAA)

Poly(acrylic acid) coated SPIONs were synthesized according to the published procedure [142]. Briefly; 500 ml de-ionized (DI) water was degassed in a 1 L 3-neck round bottom flask under Ar flow for 45 minutes and then 0.496 mol $FeCl_2.4H_2O$ and 0.993 mol $FeCl_3.6H_2O$ were added to the flask and stirred at 400 rpm. The solution was heated up to 80°C and 0.0038 mol (7.98 g) PAA was added to the solution. Then, 0.55 mol NH_4OH

was added to the reaction mixture and the brown solution was stirred for 30 min at 700 rpm at 80°C under Ar atmosphere. The reaction solution was cooled down to room temperature, left on a hand held magnet overnight to remove any precipitate if exits and then washed with DI water using 30kDa sartorius centrifugal filters. The total volume was changed four times with DI water. Aqueous SPION-PAA was stored at room temperature. Dried samples were prepared by evaporating water via a rotary-evaporator at 60°C.

2.1.4 Preparation of bidisperse MRFs

Commercial 140-CG LORD® was first diluted from reported 85.4 wt% to 80 and 83 wt% with hydraulic oil. This was necessary for the efficient mixing of SPIONs with the commercial MRF. Dried SPION-LA and SPION-PAA in 6 and 12 wt% with respect to the weight of micron sized Fe-particles were added to diluted 140-CG LORD®. Mixtures were homogenized with a light duty homogenizer (ISOLAB) at 12000 rpm for 2 minutes. Table 2.1 presents the list of all MRFs prepared and used in this study. For example, MRF-2 has 80 wt% micron size Fe particles and 6wt% SPION-LA.

Table 2.1: Composition and code of MRFs.

MRFs	**Code**
85.4 wt% 140-CG LORD® (original composition)	140-CG
80 wt% 140-CG LORD® (diluted with hydraulic oil)	MRF-1
MRF-1 + 6 wt% SPION-LA	MRF-2*
MRF-1 + 6 wt% SPION-PAA	MRF-3*
MRF-1 + 12 wt% SPION-LA	MRF-4*
MRF-1 + 12 wt% SPION-PAA	MRF-5*
83 wt% 140-CG LORD® + 12 wt% SPION-PAA	MRF-6*

*amount of SPIONs are based on the wt% of micron size Fe-particles in the bidisperse MRFs.

2.1.5 Characterization methods

The hydrodynamic size of SPIONs were determined using Malvern Zetasizer dynamic light scattering instrument. Crystal sizes of magnetic particles and morphology were analyzed using Tecnai G2 F30 bright field high resolution (HR) (acceleration voltage = 200 kV) transmittance electron microscopy and ZEISS Ultra plus Scanning Electron Microscopy (SEM). For taking SEM of commercial MRF and bidisperse MRFs samples were washed with methanol and dried at 60°C. SPIONs were drop cast on C-coated Cu-grids for the TEM analysis.

Quantum Design PPMS9T VSM was used to determine the magnetic properties of the particles at 305 Kelvin. The organic content of SPIONs was determined from the dried samples using TA Q500 thermogravimetric analysis (TGA) under Ar by heating samples between room temperature and 900 °C at a heating speed of 10 °C/min. Functional group analysis was performed using Thermo Scientific Nikolet iS 10 FTIR instrument.

A 302 MCR Anton Paar rheometer was used for the magnetorheological characterization of MRFs. Measurements were done in both steady shear mode and frequency sweep mode in tween-gap parallel plate (MRF covers the top and bottom of the plate) condition. In all measurements the diameter of the plate was 10 mm and the gap between the two plates was 0.339mm.

The values of yield stress as a function of magnetic field strength were calculated from shear stress-shear rate curves using the Bingham model since it was the recommended model by the Lord Corporation for 140-CG LORD. Bingham model is one of the most widely used models for MRFs [143-145]. According to the Bingham model, the shear stress is given by

$$\tau = \tau_y + \eta_p \dot{\gamma}, \qquad \tau \geq \tau_y \tag{2-1}$$

$$\dot{\gamma} = 0 \quad \tau < \tau_y \tag{2-2}$$

where τ is shear stress, τ_y is the yield stress under magnetic field, η_p is the Bingham plastic viscosity defined as the slope of the flow curve and $\dot{\gamma}$ is the shear rate.

The sedimentation ratio was calculated using Eq. 1-14 [146].

2.2 Results and Discussion

2.2.1 Synthesis and characterization of SPIONs

SPIONs with PAA or LA coating were prepared in aqueous solutions. PAA coating provided a hydrophilic coating with carboxylate functional groups on the nanoparticle surface. LA molecules form a bilayer around the SPION core providing an aqueous suspension of SPIONs. Hydrophobic, LA monolayer coated SPIONs were isolated upon precipitation of aqueous colloidal solution in isopropanol. SPIONs with average crystal sizes of 5 (SPION-LA) and 3 nm (SPION-PAA) (Fig. 2.1) and average hydrodynamic sizes of 90 nm (SPION-LA) and 120 nm (SPION-PAA) were obtained (Fig. 2.2). Hydrodynamic size indicates the formation of small clusters as usually expected [147]. Organic contents of SPION-LA and SPION-PAA were determined as 33 and 27 wt%, respectively, by TGA (Fig. 2.3). FTIR analysis of both SPION-LA and SPION-PAA has a band at ca 535-580cm^{-1} corresponding to Fe-O bond vibration and peaks at ca 1570cm^{-1} for the carboxylate groups adsorbed on SPION crystals. C-H stretching bands were around 2800-3000 cm^{-1} and were stronger for LA, while overlapping OH stretching bands (3200-3400 cm^{-1}) were more pronounced for PAA coated SPIONs (Fig 2.4).

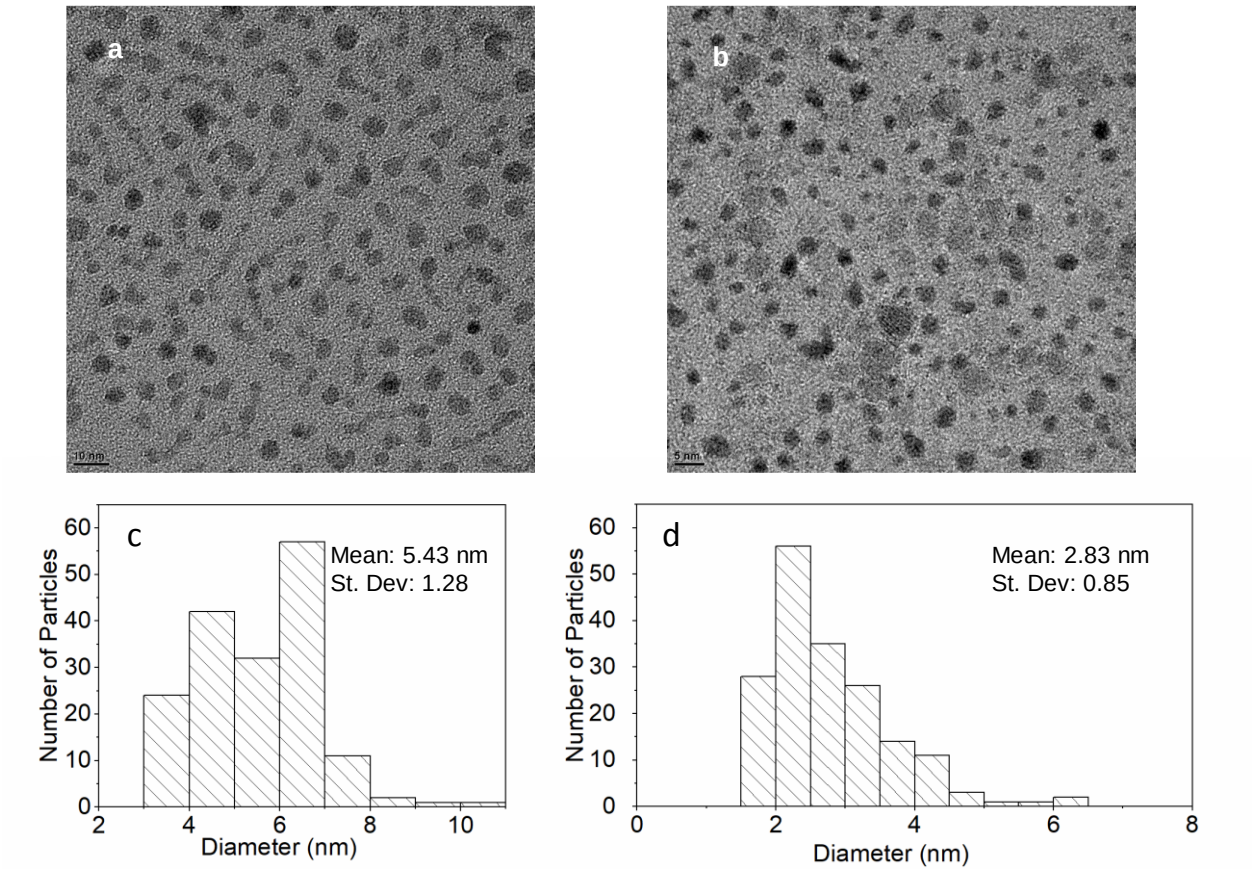

Figure 2.1: TEM images of a) SPION-LA (scale bar:10 nm) and b) SPION-PAA (scale bar:5 nm). The average size of the c) SPION-LA (170 particles were counted) and d) SPION-PAA (177 particles were counted) nanoparticles calculated by image analysis (Image J software).

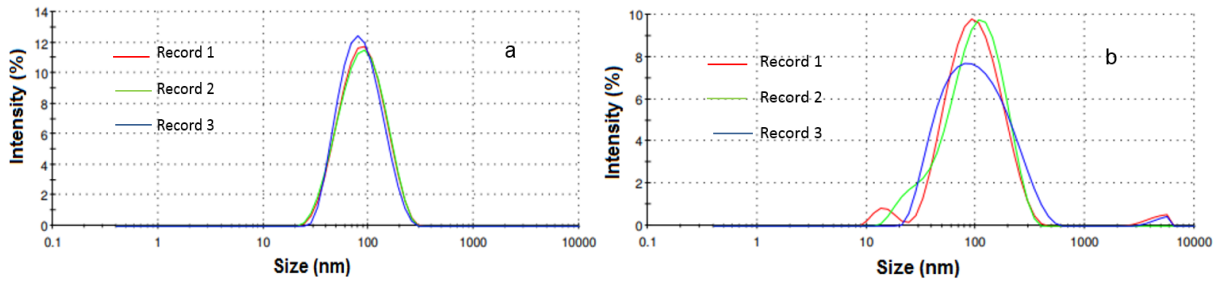

Figure 2.2: Hydrodynamic sizes of a) SPION-LA and b) SPION-PAA measured by DLS and reported based on the scattered light intensity. Each trace represents a different run.

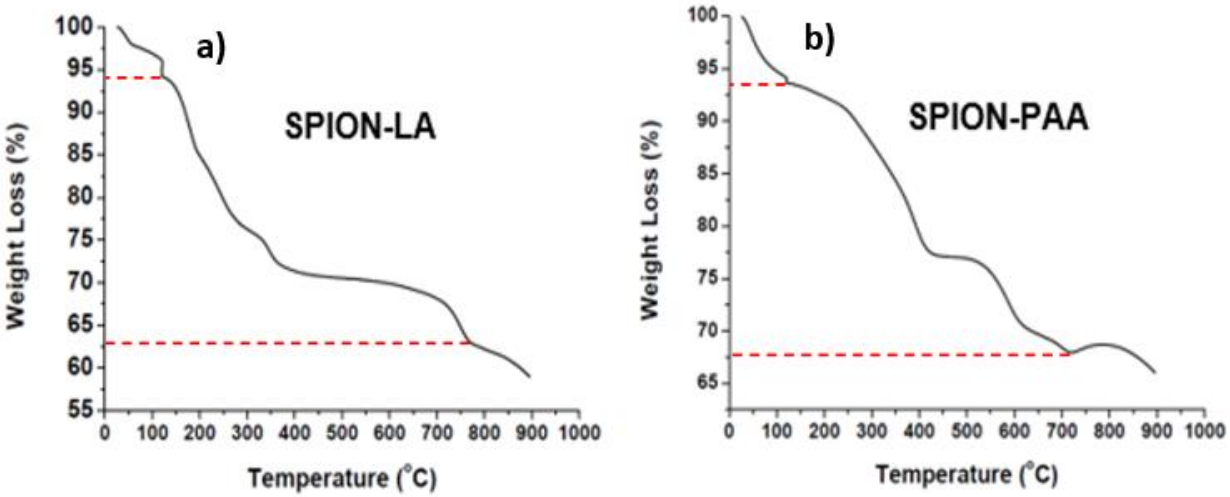

Figure 2.3: TGA result of a) lauric-acid coated SPIONs and b) polyacrylic-acid coated SPIONs. Samples were kept at 120 ºC for 10 min to lose the bound water.

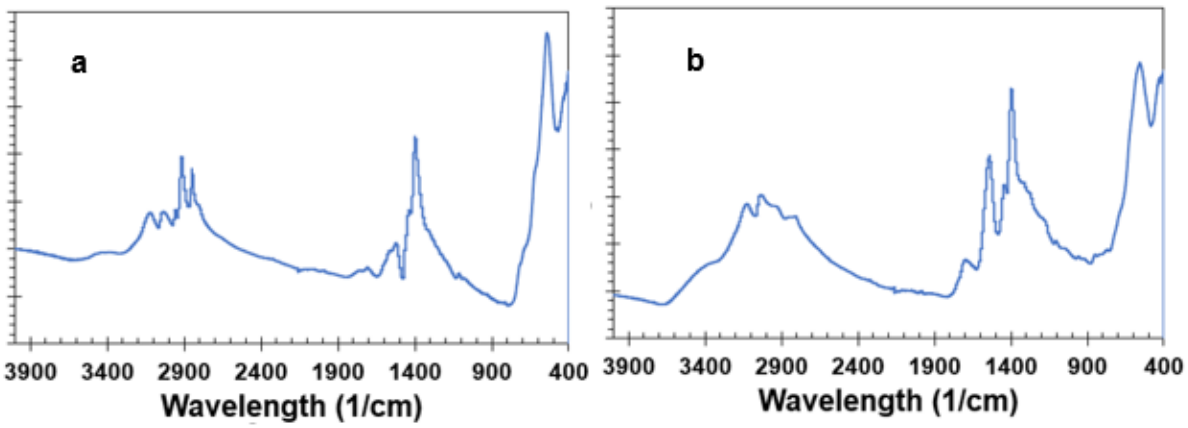

Figure 2.4: FTIR result of a) SPION-LA and b) of SPION-PAA

Bidisperse MRFs were prepared from the diluted 140-CG LORD® to 80 and 83 wt% by addition of hydraulic oil in order to provide a homogenous mixing of nanoparticles with the commercial MRF. SPIONs were added in powder form to the diluted MRFs in 6 and 12 wt% with respect to the magnetic particle content of the diluted commercial fluid. Higher nanoparticle loadings (such as 20 wt%) cause a tremendous increase in the apparent viscosity hence, they are not reported in this study. 140-CG LORD® and its diluted forms are used as benchmark and control.

SEM images of 140-CG LORD® show 1-6 µm size particles (Fig. 2.5a). Adsorption of SPIONs on micron sized Fe-particles in case of both SPION-LA (MRF-4) (Fig. 2.5b) and SPION-PAA (MRF-5) (Fig. 2.5c) is clearly seen in their SEM images. This suggests

that both LA and PAA coating on SPIONs provided a favorable interaction between the nanoparticles and micron sized ones of the commercial MRF. LA coating of SPIONs probably interacted with the fatty acid coating of Fe-particles via hydrophobic interactions [141,148]. PAA coating may provide a binding between the Fe-particles and SPIONs, possibly due to partial displacement of fatty acid from the Fe-particle surface via carboxylates of the SPION-PAA providing a simultaneous electrostatic binding on SPION and CI [149].

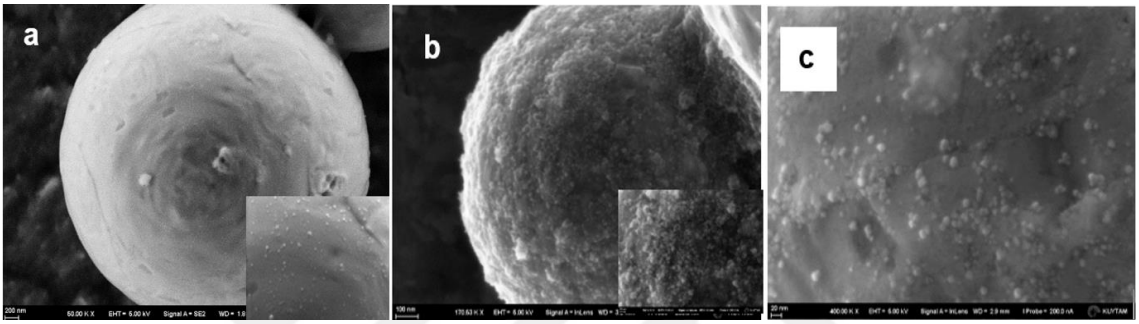

Figure 2.5: SEM images of a) commercial140-CG LORD® MRF, b) MRF-4 composed of SPION-LA/140-CG LORD®, c) MRF-5 composed of SPION-PAA/140-CG LORD®.

VSM measurements were performed at 305 K to evaluate the magnetic behavior of the SPIONs, 140-CG LORD® and MRF-5 (Fig 2.6. a, b). SPIONs showed no coercivity, remnant magnetization or hysteresis loop, indicating superparamagnetic nature. The saturation magnetization of SPION-PAA and SPION-LA are 22 and 40 emu/g. The difference between the two particles may arise from many reasons including size, surface defects which becomes more important with decreasing size, aggregation, and organic content difference, but values are within different M_s values reported for such nanoparticles [147, 150].

The commercial 140-CG LORD® with micron sized Fe-particles has a saturation magnetization of 200 emu/g. Bidisperse MRF-5 with 80 wt% Fe-particles and SPION-PAA (12 wt% with respect to Fe-particles) has a lower saturation magnetization, 175 emu/g, than 140-CG LORD® as expected, yet this is quite a high magnetization value.

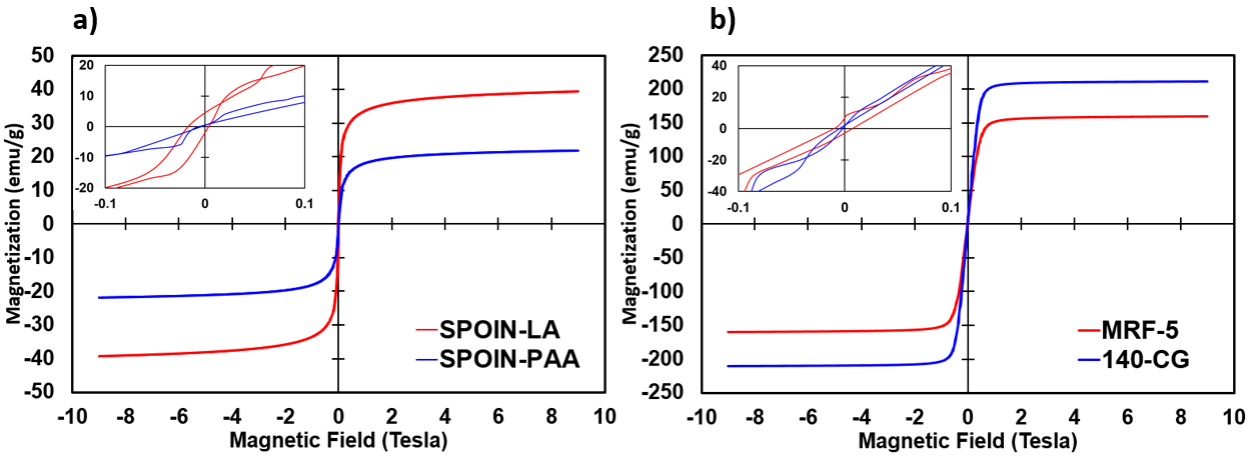

Figure 2.6: Field dependent magnetization of a) SPION-PAA and SPION-LA, b) 140-CG LORD® and MRF-5.

2.2.2 Rheological properties under steady shear mode

First, the apparent shear viscosity of 140-CG LORD® and the bidisperse MRFs were measured as a function of shear rate at four different magnetic field strength (33, 80, 120 and 141 kA/m) (Fig. 2.7). Here, we also used 140-CG LORD® diluted with hydraulic oil (MRF-1) since new bidisperse MRFs has lower micron sized Fe-particle content and we want to determine the improvement that can be achieved by the addition of nanoparticles to an MRF with similar content of micron-sized particles. As can be seen in Fig. 2.7, dilution of particle concentration from 85.4 to 80 wt% reduced the apparent viscosity of the 140-CG LORD®. Apparent viscosity decreases as shear rate increases at all applied magnetic field strength for all MRFs, as expected. An abrupt drop in the apparent shear viscosity at a low shear rate region indicates a shear thinning behavior. As would be expected from MRFs, apparent viscosity increases with the increasing magnetic field strength and MRF-5 showed the highest apparent viscosity among all bidisperse MRFs and has the closest value to 140-CG LORD® and slightly better than MRF-1 at all magnetic field strength. At all applied magnetic field strength and at a low shear rate, 140-CG LORD® has the highest apparent viscosity but as the shear rate increases apparent viscosity difference between bidisperse MRFs and 140-CG decreases. In addition, bidisperse MRFs with 12 wt% loading of SPIONs resulted in a higher apparent viscosity than those containing 6 wt % SPIONs.

At 33 ±1 kA/m, MRF-5 has the highest apparent viscosity of all the MRFs including the 140-CG LORD®. At other field strength, although like each other, MRF-5 has slightly higher apparent viscosity than MRF-1, and MRF-5 and MRF-6 are like each other with lower apparent viscosity than MRF-5.

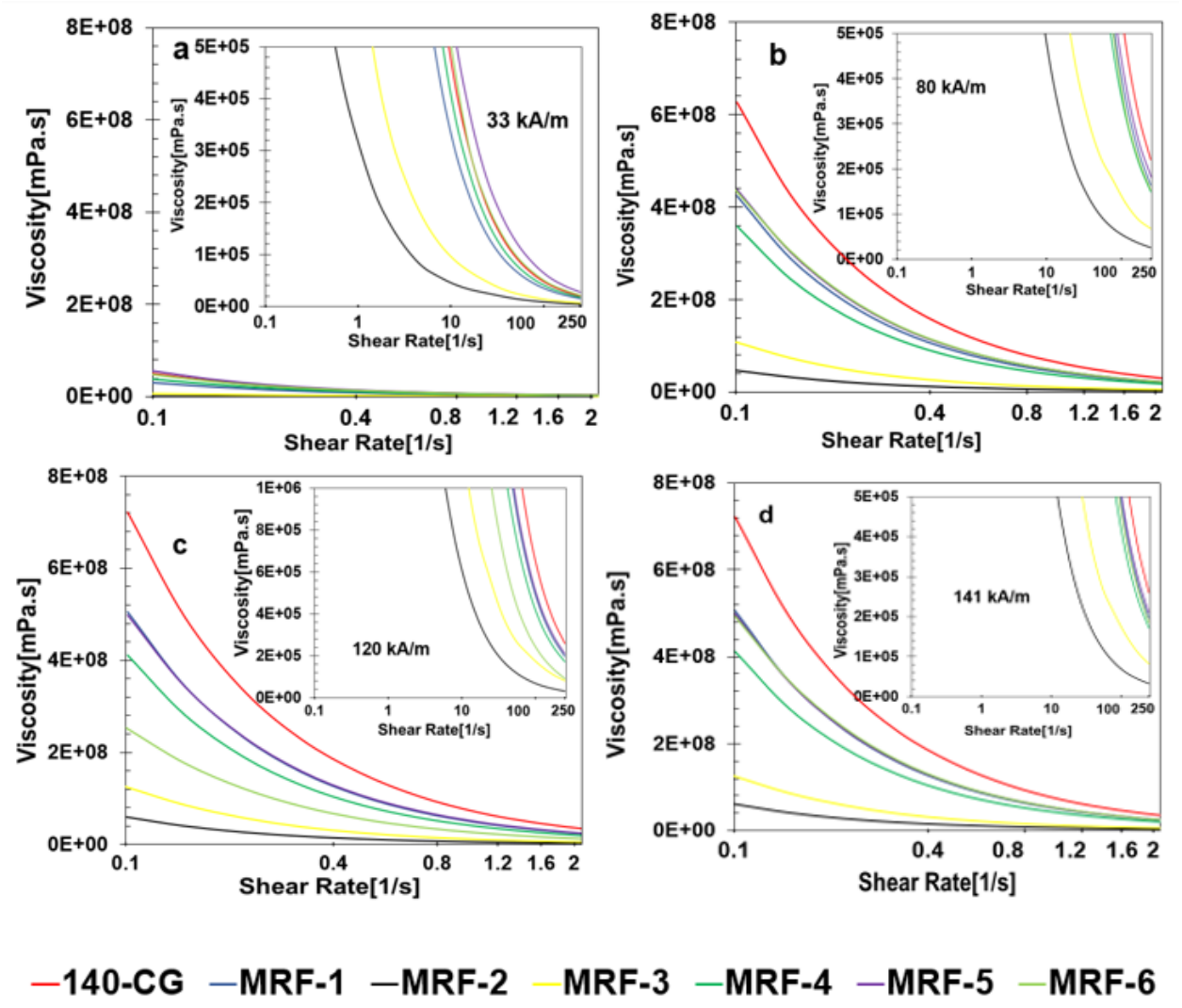

Figure 2.7: Viscosity vs. shear rate of 140-CG LORD® MRF and bidisperse MRFsunder a) 33 kA/m, b) 80 kA/m, c) 120 kA/m, d) 141 kA/m, applied magnetic field strength.

Shear stress of all synthesized bidisperse MRFs at 0-250 s^{-1} shear rate was measured at different applied magnetic field strengths, as well. Fig. 2.8 shows the region of 100-250 s^{-1} shear rate for a better comparison of MRFs and shear stress at 0-250 s^{-1} has been presented in Fig. 2.9. Again, MRF-1 shows a significant drop in the shear stress compared to the commercial one. For all MRFs, as the magnetic field strength increases the shear stress increases and for the bidisperse MRFs, shear stress increases with the SPION

loading. This is in line with our expectation: As the magnetic field strength and/or magnetic nanoparticle content increases, micro-nano particles magnetize and form strong chain like structures. SPION-PAA loaded MRFs show higher shear stress than SPION-LA loaded ones. Indeed, MRFs with SPION-LA showed the lowest shear stress values at all magnetic field strengths. This suggests that the interaction of the SPION-LA with micron sized particles are weaker than SPION-PAA. At low field strength (33 ± 1 kA/m), all bidisperse MRFs with SPION-PAA perform better than MRF-1, and MRF-5 has the highest shear stress (Fig. 2.8. a). At higher field strength, 140-CG LORD® has the highest shear stress among all these fluids and MRF-5 has higher shear stress than MRF-1 and the other bidisperse MRFs. The difference between MRF-5 and 140-CG LORD® increases with increasing field strength. One should not forget that the micron sized Fe-particles are less in bidisperse MRFs, but the presence of SPIONs differentiates MRF-5 and MRF-1 which has similar amounts of micron sized particles, in favour of the bidisperse MRF.

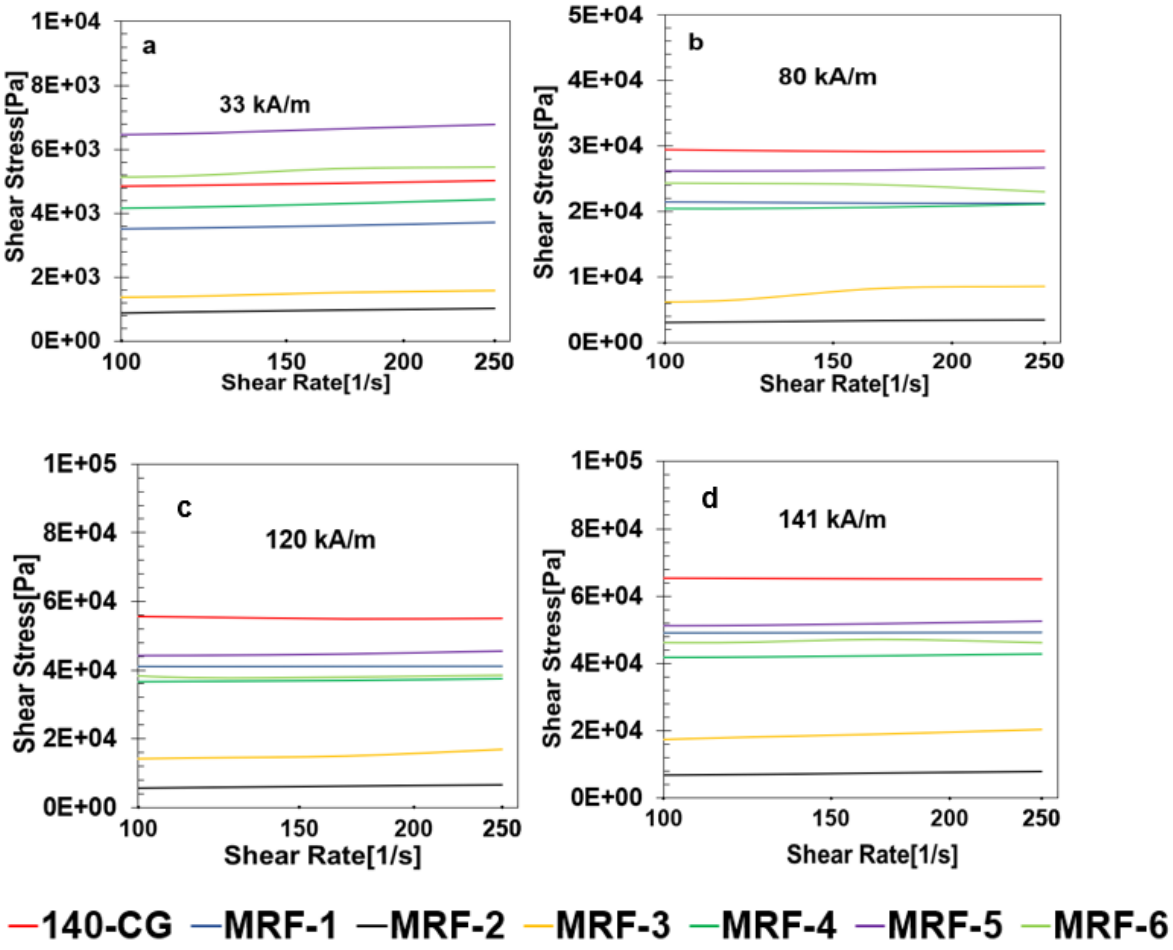

Figure 2.8: Shear stress vs. shear rate of MRFs under a) 33 kA/m, b) 80 kA/m, c) 120 kA/m, d) 14 kA/m, applied magnetic field strength.

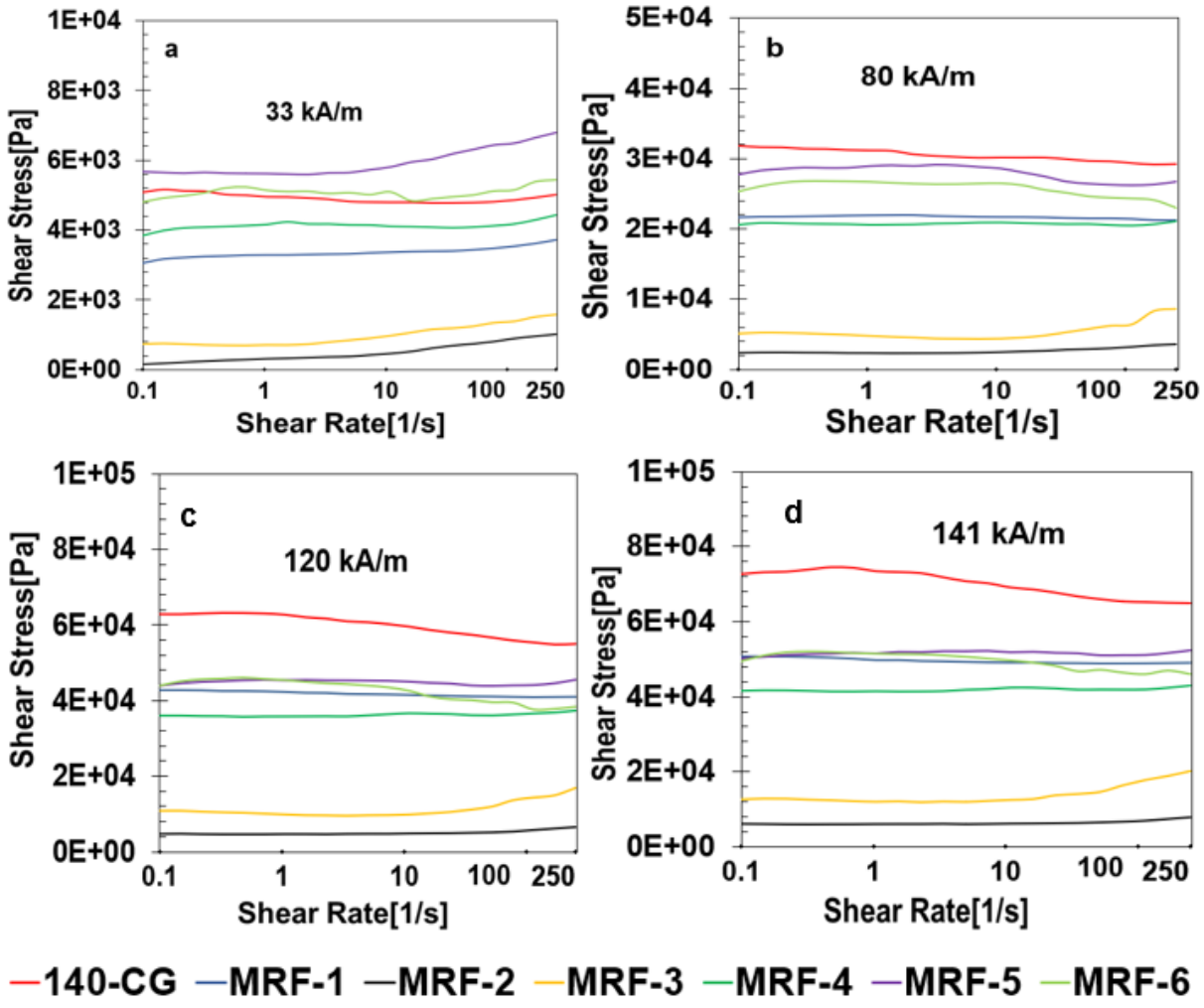

Figure 2.9: Shear stress vs. shear rate of MRFs under a) 33 kA/m, b) 80 kA/m, c) 120 kA/m, d) 141 kA/m, applied magnetic field strength.

Yield stress is the minimum stress needed for the transformation from solid-like to fluid-like states, which gives a quantitative idea of the point where all internal structures are broken. The value of yield stress as a function of magnetic field strength in Fig. 2.10 was calculated from shear stress-shear rate curves using the Bingham-plastic model. MRF-1 with 80 wt% micron sized Fe-particles have lower yield stress values than the 140-CG LORD® as expected due to lower particle loading. Bidisperse MRFs with 12 wt% SPION-PAA showed similar yield stress to 140-CG LORD® up to 120kA/m, but at higher magnetic field strength the yield stress of MRF-5 and MRF-6 were like MRF-1. MRF-4 with 6% SPION-PAA showed a similar behavior to MRF-1 up to 100 kA/m but then fall

below MRF-1. At around 170 kA/m MRF-5 had a higher yield stress than MRF-1: 60kPa versus 50kPa. Here, MRF-2 and MRF-3 with SPION-LA nanoparticles showed much lower yield stress than all other fluids. Rheometer stopped measuring the yield stress of 140-CG LORD® after 160 kA/m applied magnetic field strength since the rheometer stops at around 80 kPa shear stress due to torque limitation of the rheometer. As the viscosity of 140-CG LORD is higher than the bidisperse MRFs at a given magnetic field strength, it reaches the limiting shear stress at a lower applied magnetic field strength than others. We were able to collect yield stress data for bidisperse MRFs at higher applied magnetic field strength. This data clearly indicates that the use of SPION-PAA provides a stronger interaction between Fe-particles and SPIONs enhancing better packing/chaining under magnetic field than SPION-LA.

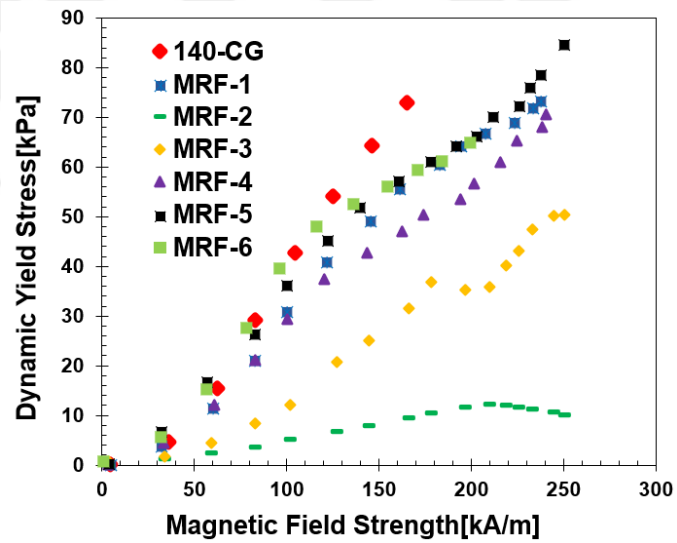

Figure 2.10: Dynamic yield stress vs. magnetic field strength for 140-CG LORD®, diluted commercial MRF (MRF-1) and bidisperse MRFs at 250 s^{-1} shear rates.

2.2.3 Rheological properties in oscillatory mode

Oscillatory experiments give information on the viscoelastic properties of the proposed MRFs. Here, loss modulus and storage modulus versus angular frequency under different (0.01%, 10% and 100%) strain were measured. Fig. 2.11 represents storage modulus and loss modulus of 140-CG MRF, MRF-1 and two of the best bidisperse MRFs (MRF-5 and

MRF-6) at 10 and 100% strain and at three different magnetic field strengths. In general, after applying a magnetic field, fluids show viscoelastic behavior and their storage modulus are greater than their loss modulus. A significant drop in the storage modulus with increasing shear and enhancement with the increasing magnetic field strength was observed. At 10% strain, MRF-5 and MRF-6 have comparable storage modulus which is between 140-CG and MRF-1. This is in agreement with the previous data. At 100% strain though, these bidisperse MRFs behave like 140-CG, while MRF-1 had a poorer performance. Yet, this difference is reduced at high magnetic field strength. MRF-1 with low micron-size particle content forms weaker chains, while the addition of nanoparticles that are interacting with the micron-sized particles, aid the formation of strong solid like chains of magnetic particles, almost as good as the original 140-CG LORD. The yield points for these four MRFs were calculated from the intersection of storage and loss modulus curves at 100% at each magnetic field strength (Table 2.2). Results show that at all magnetic field strengths, MRF-5 and MRF-6 have higher yield point than commercial 140-CG LORD®, suggesting stronger interaction of all magnetic particles and resistance to deformation, which has critical importance in practical applications.

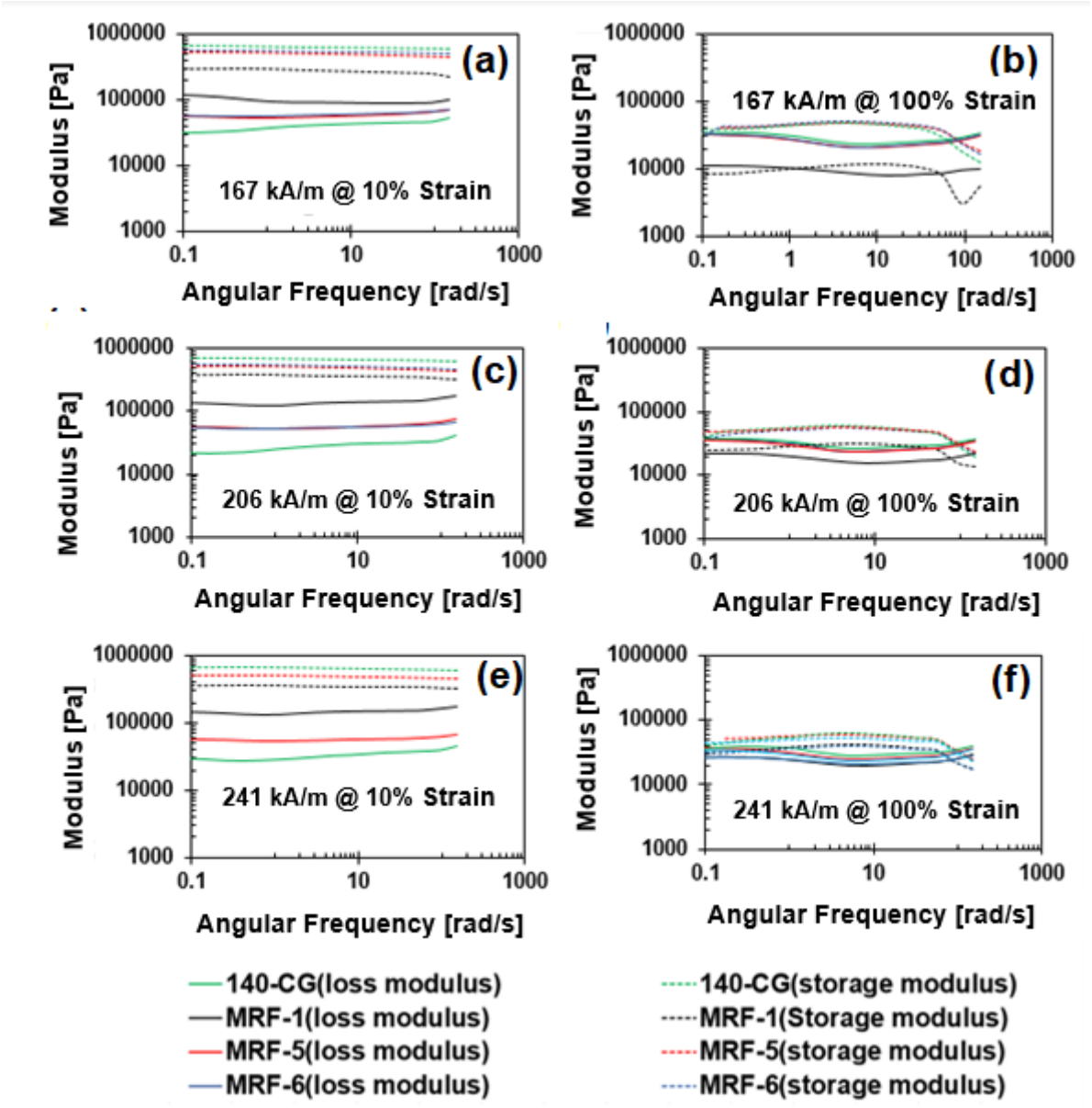

Figure 2.11: Storage (dashed lines) modulus and loss (solid lines) modulus versus applied angular frequency under different magnetic field strength: a) 167 kA/m and 10 % strain, b) 167 kA/m and 100 % strain, c) 206 kA/m and 10 % strain, d) 206 kA/m and 100 % strain, e) 241 kA/m and 10% strain and 241 kA/m and 100 % strain.

Table 2.2: Angular frequency at yield point rad/s under 100% strain.

Magnetic Field Strength [kA/m]	140-CG LORD®	MRF-1	MRF-5	MRF-6
92	38	8	55	54
167	60	55	82	83
206	90	76	100	95
241	90	82	105	96

2.2.4 Stability of bidisperse MRFs

Stability, hence, the sedimentation behavior of 140-CG LORD® and MRF-6 were monitored for 4 months at rest (Fig. 2.12). All vials were fully filled with the MRFs. Notable sedimentation was observed as early as 20 days and increased over the period of 4 months in the case of commercial MRF (Fig. 2.12a-c). However, bidisperse MRF-6 started to sediment much slower and in smaller extent (Fig. 2.12a-c). The difference between the sedimentation of the two MRFs is quite significant after 4 months at rest. Re-shaking of these partially sedimented MRFs to redisperse its micron sized, and nano-sized magnetic particles is one of the most practical and standard procedure. Hence, both MRFs were shaken after 4 months and their re-sedimentation was monitored for 20 days. Resuspension of MRF-6 was much easier, and sedimentation was again less and slower than the commercial MRF (Fig. 2.12d-e). Sedimentation ratios calculated for 140-CG and MRF-6 (Fig. 10) show a dramatic difference between the two. While 140-CG LORD® had about 5% sedimentation on day 10, MRF-6 showed no sedimentation.

Here, it is also very important to point out that the sedimentation behavior of the commercial MRF heavily depends on its freshness. 140-CG LORD® tested in Fig. 2.12 and MRF-6 compared with it were prepared from fresh 140-CG LORD®. When such bidisperse MRFs were prepared with a relatively old 140-CG LORD® (6-12 months old), the sedimentation of commercial MRF and the improvement in stabilization achieved by bidisperse MRFs are much more dramatic (Fig. 2.14). This also indicates that fatty acid coating on CI in monodisperse MRF is not providing enough steric stabilization to prevent aggregation. On the other hand, the mixture of fatty acid coated Fe-particles and fatty acid

coated SPIONs provides a better stability to commercial MRF which consists of only the former particles.

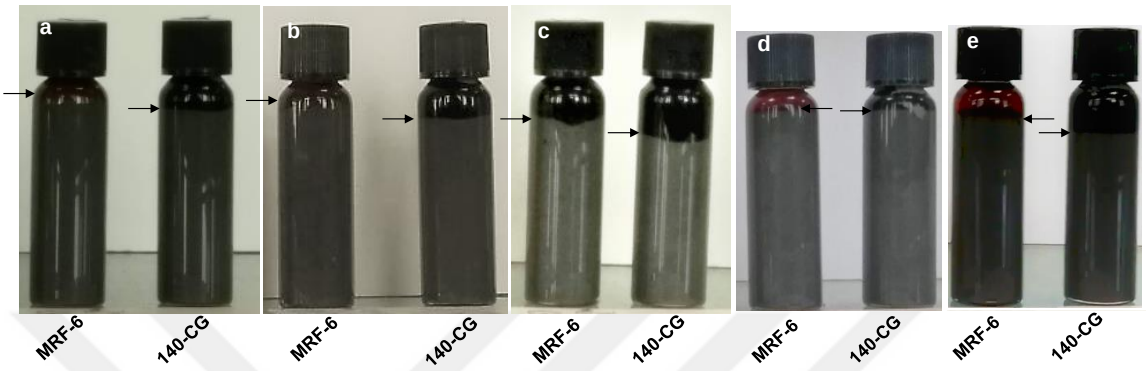

Figure 2.12: Sedimentation of bidisperse MRF-6 and 140-CG MRF LORD a) after 20 days, b) after 30 days, c) after 4 months. Sedimentation of re-shaken MRF-6 and 140-CG MRF LORD after 4 months at rest: d) 5 days and e) 19 days after re-shake.

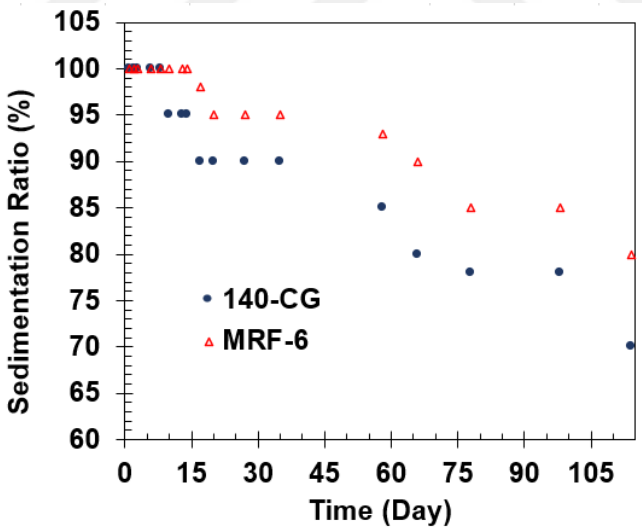

Figure 2.13: Sedimentation of bidisperse MRF-6 and 140-CG MRF LORD.

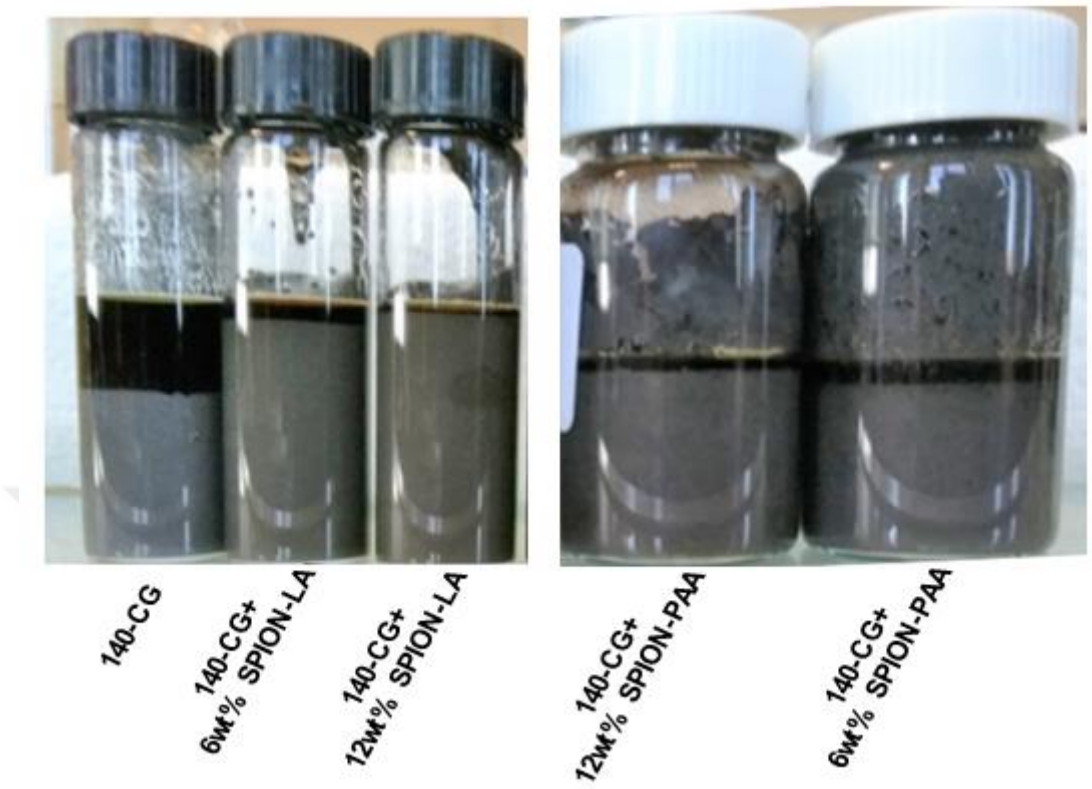

Figure 2.14: Sedimentation of 140-CG MRF and prepared bidisperse MRFs after 2 days.

2.3 Conclusion

Novel bidisperse MRFs were prepared, by adding either LA or PAA coated SPIONs to the diluted commercial 140-CG LORD® MRF, using MOBIL 27 hydraulic oil at different amounts to improve the stability of commercial MRFs without sacrificing the magnetorheological properties. Interestingly, both nanoparticles adsorb on the surface of fatty acid coated micron sized Fe-particles of the commercial MRF. We suggest that the hydrophobic interaction between the fatty acid coatings of SPION-LA and Fe-particles, and carboxylic acid binding to Fe-particle`s surface is responsible for such interaction.

Bidisperse MRFs have 175 emu/g saturation magnetization, which is slightly lower than 140-CG LORD®. Rheological properties of commercial MRF and prepared bidisperse MRFs were measured in both rotational and frequency modes. Shear stress of 140-CG LORD® under high magnetic field strength was higher than bidisperse MRFs with 12 wt% SPION-PAA. In addition, under low shear rates (0.01-2 s^{-1}) 140-CG LORD® had a higher viscosity than the bidisperse MRFs. But under higher shear rates than 2 s^{-1}

there was no viscosity difference between the commercial and bidisperse MRFs with 12wt% SPION loading. Also, increasing the NPs loading improved the magnetorheological response of the MRFs and the addition of SPION-PAA showed better results than SPION-LA. Yield stress of MRF-5 and MRF-6 were similar to commercial MRF up to 110 kA/m magnetic field strength. At higher magnetic field strengths 140-CG reaches its yield point sooner with a higher yield stress value than the MRF-5 and MRF-6. In frequency sweep mode, selected bidisperse MRFs with 12 wt% loaded SPION-PAA reached their yield point at a higher angular frequency than the commercial MRF.

The addition of nanoparticles to the commercial MRF with particle loading above 80 wt%, improved the stability of dispersions and ability to re-suspend. This was better with 12 wt% nanoparticle loading. Considering the magnetorheological performance and resistance to sedimentation and re-suspension efficiency, 12 wt % SPION-PAA loaded bidisperse MRFs are quite promising.

Here, it is important to draw one`s attention to the fact that all bidisperse MRFs that were cited from the literature have used bare CI or Fe-particles, yet the commercial MRF that we have used here consists of fatty acid coated Fe-particles, and hence has much higher particle loading. Overall, at even quite high particle loadings, the addition of SPION-PAA, which is suggested to interact with micron sized particles electrostatically, provide a better chaining property and resistance to agglomeration and sedimentation, and improve re-suspension by preventing hard sediments.

Chapter 3

BIDISPERSE MRFS BASED ON FUNCTINOLIZED SPION AND CARBONYL IRON

The main focus of this study is to develop new MRFs with high particle loading (at and above 80 weight percent) with long term stability and good magneto-viscous properties to be used in industrial MR machines. In order to achieve this, bidisperse MRFs composed of highly magnetizable micron sized particles with surface functional SPIONs are suggested as in the case of MRFs discussed in Chapter 2. Here, micron-sized CI was used as the main component. CI does not have a surface coating. In order to enhance its dispersibility in a hydrophobic carrier fluid, it was also coated with lauric acid. As the minor component, SPIONs synthesized in Chapter 2 was used in 6-12 wt-%. In addition, a small amount of PVA was added to the formulation to enhance the stability, which is commonly used in the MRF formulations [101]. The idea behind LA coating on CI was two fold: To enhance its dispersibility in a hydrophobic carrier fluid and to enhance the interaction of CI with the SPIONs. Here, the impact of different carrier fluids on the stability and magnetorheological properties of bidisperse MRFs were also tested. As the carrier fluid mineral oil, paraffin oil, silicon oil and hydraulic oil were tested. Magnetorheological properties and stability of bidisperse MRFs were studied as a function of SPION coating and content. Commercial 140-CG LORD® was used as a benchmark. The stability of bidisperse MRFs has been significantly improved with SPION-PAAs.

The stability of MRFs for high-temperature use is also a concern. Few studies have been done on the magnetorheological behavior of MRFs at different temperatures [151,152,153]. Magnetorheological properties of bidisperse MRFs were also measured at different temperatures and results showed that temperature increase, slightly influences the yield stress of bidisperse MRFs under different magnetic field strength. Some of these bidisperse MRFs were tested on an MR damper developed by Prof. İsmail Lazoğlu. Measured axial force on the MR damper at different currents showed that the axial force of the most stable bidisperse MRF produced here has performed as good as the

commercial one with an advantage of enhanced stability that would extend the lifetime of the damper.

3.1 Experimental

3.1.1 Materials

Commercial carbonyl iron (≥ 97% Fe basis) was purchased from Sigma Aldrich. Mineral oil 330760-1L (Lot # MKBZ8254V) and paraffin oil 18512-1L (Lot # STBG7873) from Sigma Aldrich, silicon oil 1000 VCS from ChemBio and hydraulic oil (Mobil DTE 27, kinetic viscosity 95.3 mm^2/s at 40 °C) were tested as carrier fluids. Polyvinyl alcohol (PVA, mwt:13000), lauric acid [$CH_3(CH_2)_{10}COOH$] and poly(acrylic acid) (Mw 2100 kDa) from Sigma Aldrich. $FeCl_3.6H_2O$ (ACS reagent, 97%), $FeCl_2.4H_2O$ (reagent plus, 98 %) and ammonium hydroxide (25 %, super pure) were purchased from MERK (Germany). All reagents were used without further purification.

3.1.2 Synthesis of Functional SPIONs

SPION-LA and SPION-PAA synthesized in Chapter 2 were used.

3.1.3 Synthesis of Lauric Acid Coated Carbonyl Iron (CI-LA)

Firstly, 200 g of commercial carbonyl iron was placed into a 1-L round bottomed flask and treated with 500 ml of 0.5 M HCl for 10 minutes to attain reactive hydroxyl groups on the surface of CI particles. Then acid-treated CI powder was washed with distilled water for 5 times (600 ml each time), ethanol for 3 times (250 ml each time), and acetone for 3 times (200 ml each time) using a decantation method. Finally, the powder was dried for 3 h at 60°C with a rotary evaporator (Heidolph) to remove the residual acetone [110]. Surface-activated dry CI powder (190 g) was put into 1-L three-neck round bottomed flask equipped with a mechanical stirrer and a reflux condenser and 600 ml ethanol was added to the flask. . Then the mixture was heated in an oil bath at 110°C. 25 g Lauric acid was added to the flask when the temperature of the mixture reached 80°C, and the mixture

was stirred at 600 rpm for 6 hours. Then, the solution was cooled down to room temperature and the particles were removed and washed with deionized water three times with the decantation method. Finally, LA coated CI particles were dried at 60°C using a rotary evaporator.

3.1.4 Preparation of bidisperse MRFs

To prepare uncoated CI-based MRFs, CI was added to the carrier fluid at different wt% and stirred with homogenizer-light duty (ISOLAB) at 12000 rpm for 1 minute and then SPION-LA or SPION-PAA was added to the mixture at different wt% and homogenized for 1 minute. In preparing CI-LA based bidisperse MRFs, firstly, PVA (3wt% with respect to carrier fluid) was added to the carrier fluid and homogenized 1 minute and then SPIONs were added and homogenized another 1 minute Table 3.1. summarizes all formulated MRFs.

Table 3.1: Synthesized bidisperse MRFs and commercial LORD® as a benchmark

Bidisperse MRFs	**Code**
140-CG MRF LORD®	140-CG
85wt% CI in HO	MRF-1
80wt% CI in HO	MRF-2
80wt% (68wt%CI+12wt%SPION-PAA) in HO	MRF-3
83wt% (71wt%CI-LA+12wt%SPION-PAA+3wt%PVA of the oil) in HO	MRF-4
84wt% (72wt%CI-LA+9wt%SPION-PAA) in hydraulic oil	MRF-5
84wt% (72wt%CI-LA+12wt%SPION-PAA+3wt%PVA of the oil in HO	MRF-6
83wt% (71wt%CI-LA+12wt%SPION-PAA+3wt%PVA of the oil) in MO	MRF-7
83wt% (71wt%CI-LA+12wt%SPION-PAA+3wt%PVA of the oil) in paraffin	MRF-8
80wt% CI in MO	MRF-9
75wt% CI in SO	MRF-10
75wt% CI in glycerol	MRF-11

HO: Hydraulic oil, MO: mineral oil, SO: silicon oil

3.1.5 Characterization methods

The hydrodynamic size of SPIONs was determined using Malvern Zetasizer dynamic light scattering instrument. Crystal sizes of magnetic particles and morphology were analyzed using Tecnai G2 F30 bright field high resolution (HR) (acceleration voltage = 200 kV) transmittance electron microscopy and ZEISS Ultra plus Scanning Electron Microscopy (SEM). For taking SEM of commercial MRF and bidisperse MRFs samples were washed with methanol and dried at 60°C. SPIONs were dropped cast on C-coated Cu-grids for the TEM analysis.

Quantum Design PPMS9T VSM was used to determine the magnetic properties of the particles at 305 Kelvin. The organic content of SPIONs was determined from the dried samples using TA Q500 thermogravimetric analysis (TGA) under Ar by heating samples between room temperature and 900 °C at a heating speed of 10 °C/min. Functional group analysis was performed using Thermo Scientific Nikolet iS 10 FTIR instrument.

A 302 MCR Anton Paar rheometer was used for the magnetorheological characterization of MRFs. Measurements were done in both steady shear mode and frequency sweep mode in tween-gap parallel plate (MRF covers the top and bottom of the plate) condition. In all measurements, the diameter of the plate was 10 mm and the gap between the two plates was 0.339 mm.

The values of yield stress as a function of magnetic field strength were calculated from shear stress-shear rate curves using the Bingham model since it was the recommended model by the Lord Corporation for 140-CG LORD. The Bingham model is one of the most widely used models for MRFs [139,140,141]. According to the Bingham model, the shear stress is given in Equation 2-1 and Equation 2-2

The sedimentation ratio was calculated using Eq. 1-14 [146].

3.2 Results and Discussion

3.2.1 Synthesis and Characterization of Magnetic Particles

SPION-LA and SPION-PAA synthesis and characterization was detailed in Chapter 2. LA coating of CI was confirmed with FTIR (Figure 3.1). The sharp peak at 680-740 cm^{-1} shows C=C stretching bond vibration. The peak at 445-475 cm^{-1} indicates Fe-O

stretching. Broad absorption at 2800-3000 cm^{-1} is assigned to O–H stretching vibration of LA and peaks at 1650-1740 cm^{-1} arises from C=O bond of LA. Binding of carboxylate to crystal surface causes a shift in the peak position [117, 154, 155, 156].

SEM images of CI show 1-6 µm size particles (Figure 3.2a,). Adsorption of SPION-PAA on micron-sized CI-LA particles (MRF-4) (Fig. 3.2c) is clearly seen in their SEM images. PAA coating may provide a binding between the CI-particles and SPIONs, possibly due to partial displacement of LA from the CI-particle surface via carboxylates of the SPION-PAA providing a simultaneous electrostatic binding on SPION and CI [149].

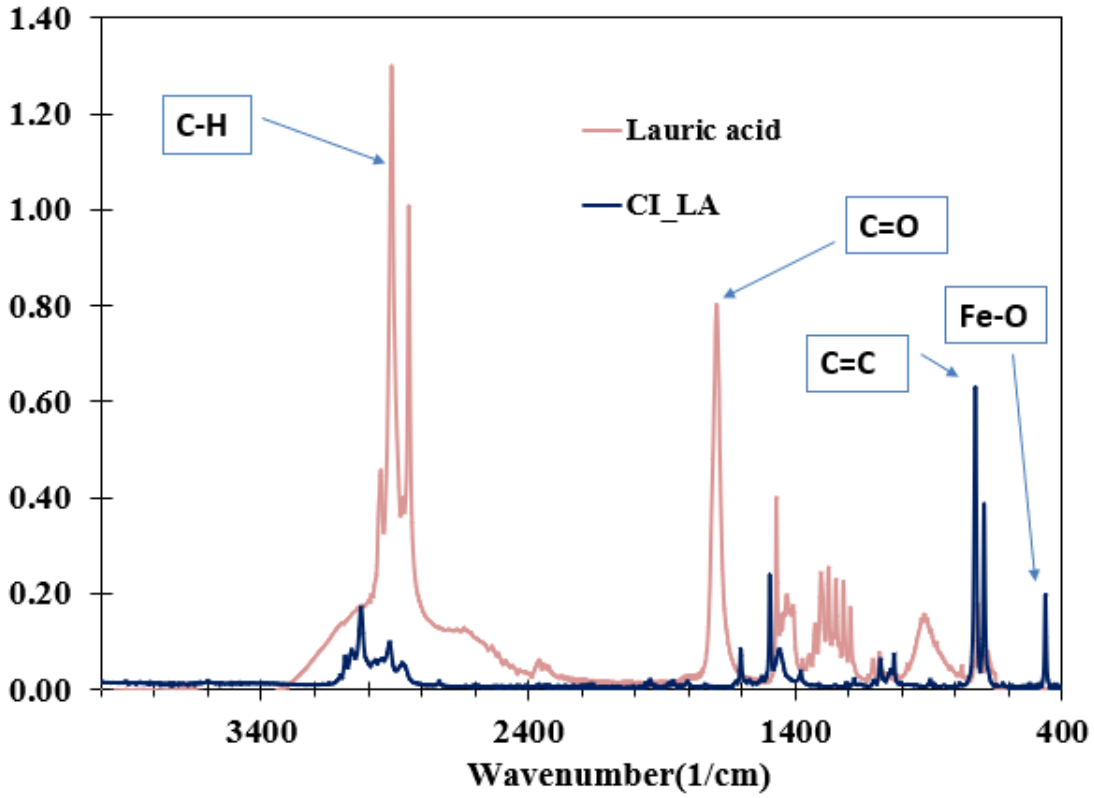

Figure 3.1: FTIR spectra of LA and CI-LA.

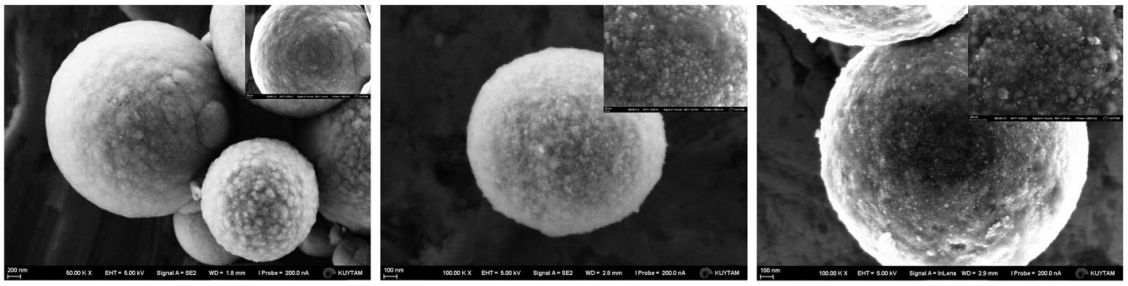

Figure 3.2: a) Bare carbonyl iron, b) CI-LA, c) MRF-4

VSM measurements were performed at 305 K to evaluate the magnetic behavior of the CI, CI-LA, and MRF-4 (Figure 3.3). It can be found that both micron-sized magnetic particles in 140-CG, CI, and CI-LA possess 205 emu/g saturation magnetization so it can be understood that LA coating of CI did not hamper the magnetic properties of the CI. The saturation magnetization of bidisperse MRF-4 is 171.5 emu/g which is slightly lower than CI and CI-LA due to lower intrinsic saturation magnetization of the SPION content (Fig 3.3).

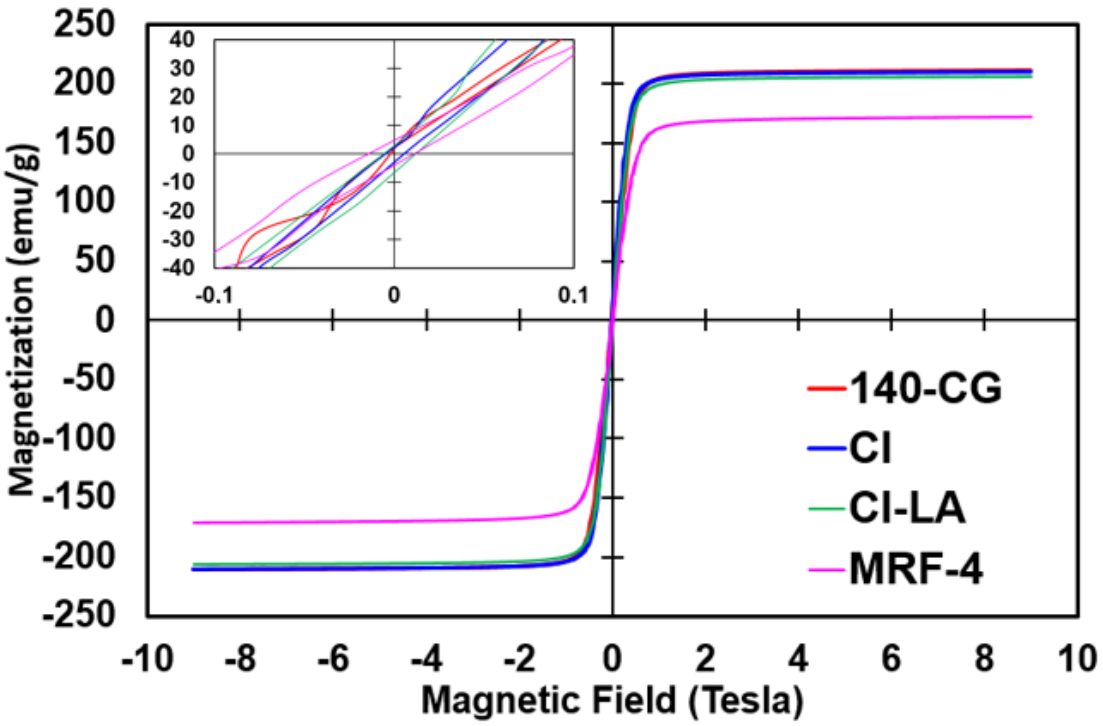

Figure 3.3: VSM results for 140-CG, CI, CI-LA and MRF-5

3.2.2 Stability of MRFs

Initially, CI was dispersed in different carrier fluids, namely, hydraulic oil, mineral oil, silicon oil and paraffin at 75-85 wt% particle loading. Sedimentation of particles was monitored for 48 days (Figure 3.4).

MRF-1 and MRF-2 which has 85 and 80 wt% CI in hydraulic oil showed significant sedimentation which decreased dramatically when 80 wt% CI was dispersed in mineral oil (MRF-9). Dispersion of 75 wt% CI in silicon oil (MRF-10) and in glycerol (MRF-11) showed improved stability over the dispersions obtained in hydraulic oil, with more resistance to sedimentation in silicon oil. Hydraulic oil was successfully used in Chapter 2 for the development of stable bidisperse MRFs in Chapter 2 from 140-CG. Hence, 12wt% SPION-PAA (MRF-3) was added to CI (68 wt%) in hydraulic oil. MRF-3 showed dramatic enhancement in stability which resulted in about 5% sedimentation after 28 days and stayed stable for the rest of the tested time (Figure 3.4Then, in order to enhance the dispersibility to CI in carrier fluids, bidisperse MRFs from CI-LA were produced. MRF-4-7-8 have the same particle composition, 71 wt% CI-LA, 12 wt% SPION-PAAand 3 wt% PVA in hydrolytic oil, mineral oil and paraffin, respectively. After four months at rest, no sedimentation in MRF-4 was observed, while MRF 7 and 8 showed clear sedimentation starting at 1st week and after 10 days, respectively (Figure 3. 5). Hence, it can be concluded that hydraulic oil has a positive role as a carrier fluid in the stability of the bidisperse MRF using functionalized SPION-PAA and CI-LA. Comparison of MRF-3 and MRF-4 shows improved stability of the latter which not only has PVA but also uses CI-LA instead of CI at even higher loading. This suggests the positive impact of LA coating on CI on the stability of bidisperse MRFs. MRF-5 had a composition similar to MRF-5 but no PVA and did not show the same stability as MRF-4, indicating the necessity of PVA in long term stability of the bidisperse MRFs. However, MRF-5 stayed stable for 10 days and then about 5% sedimentation was observed (Figure 3.5).

Based on these results best candidates for further studies are MRF-3-4-5-10-11. MRF-6 was produced as a replica of MRF-4 but it had 72 wt% CI-LA instead of 71 wt%.

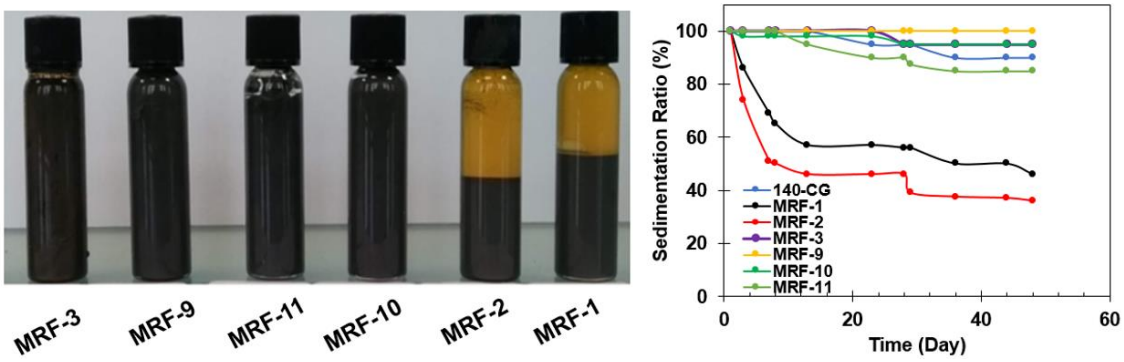

Figure 3.4: Stability of MRFs and bidisperse MRFs using bare CI after 48 days.

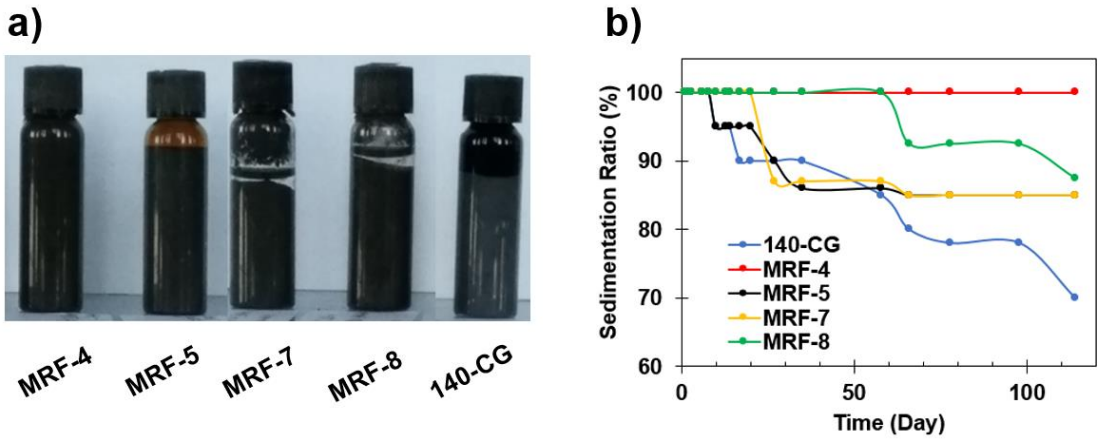

Figure 3.5: Stability of 140-CG LORD® MRF and bidisperse MRFs using CI-LA after 4 months.

3.2.3 Rheological Properties

Magnetorheological performances of MRFs were investigated under various magnetic fields. Shear stress as a function of shear rate at various magnetic field strengths was measured.

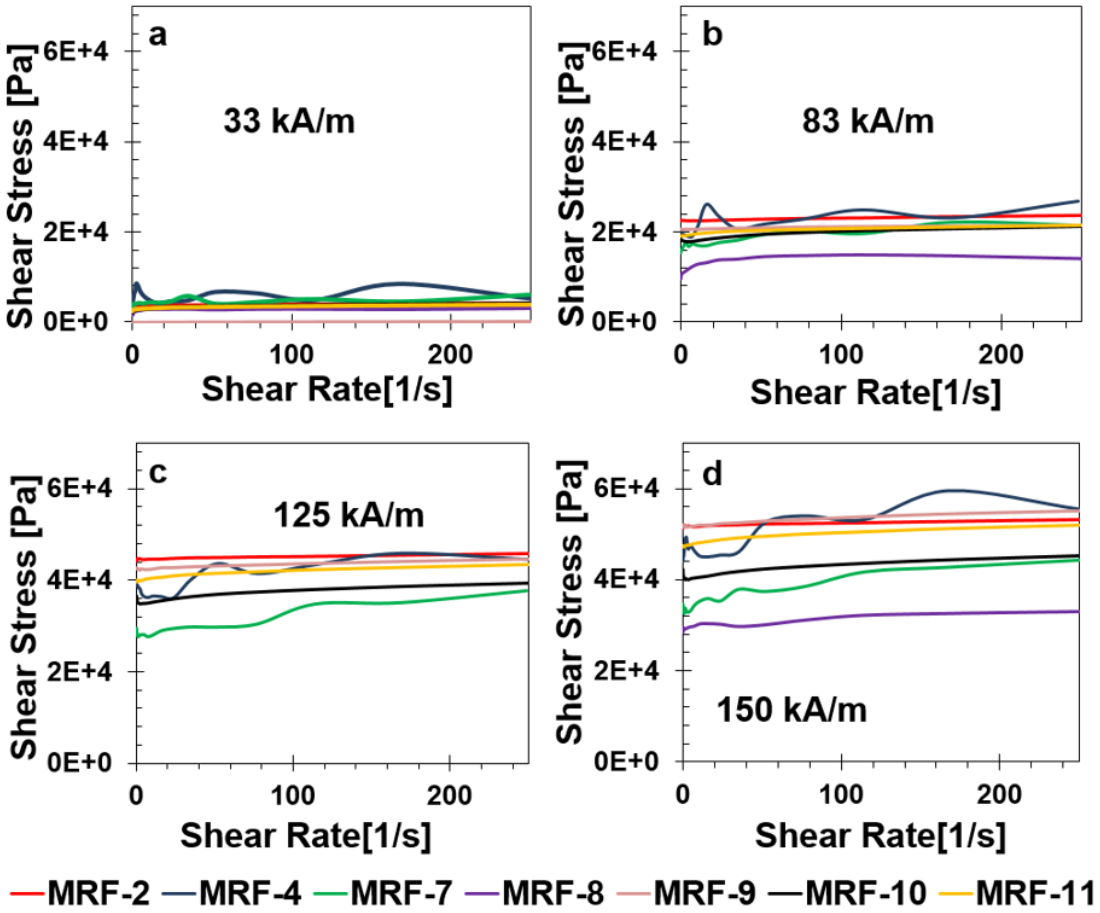

Figure 3.6: Shear stress under shear rate for MRFs using under; a) 33 kA/m, b) 83 kA/m, c) 125 kA/m, d) 150 kA/m magnetic field strength.

All samples show a linear behavior over the entire range of the shear rate (Figures 3.6 and 3.7). All MRFs studied here show typical magnetorheological behavior. Shear stress at a given shear rate rises with the applied magnetic field for all samples, which is due to the formation of chains of particles as a result of strong dipole-dipole interaction under the magnetic field. In Figure 3.6 MRFs with different carrier fluids are compared. An appreciable difference between MRFs is observed only at and above 125 kA/m. Between MRF-2-9-10-11 which contains only CI as the magnetic content, the lowest shear stress was seen with MRF-10 which has only 75 wt% CI in silicon oil. MRF-11 with the same CI content but in glycerol has higher shear stress. As expected MRF-2 with 85 wt% CI in hydraulic oil has the highest shear stress followed by MRF-9 with 80 wt% CI in mineral oil. At 150 kA/m the difference between the two became insignificant. MRF-4-7-8

represent another set where MRFs differ only in the carrier fluid. In that case, the shear stress decreased in the order of hydraulic oil, mineral oil and paraffin. Overall, it was observed that hydraulic oil gives the best magnetorheological response so far accompanied with enhanced stability. It is also valuable to compare the shear stress of 140-CG and MRF-1-2 which are not bidisperse and wherein the homemade MRFs have uncoated CI. As can be seen in Figure 3.7, shear stress decreases with the decreasing content of the CI. Comparison of MRF-2 with MRF-3 wherein the total magnetic content is 80 wt% but MRF-3 has only 68 wt% CI, indicates that the content of micron-sized magnetizable particles is critical for high shear stress. Therefore, all other bidisperse MRFs were prepared in hydraulic oil with CI-LA (MRF-4-5-6) at above 80wt% magnetic content with 71-72 wt% CI-LA, and the MR behavior of those MRFs is discussed in detail through the entire chapter. Shear stresses of these bidisperse MRFs, namely MRF-4-5-6 are comparable to each other and to MRF-2 with 80 wt% CI at all magnetic field strengths (Figure 3.7).

Overall, decreasing shear stress with decreasing CI content of the fluid could be explained with weaker chain formation between the particles in a diluted solution. . On the other hand, the addition of SPIONs to CI alters the shear stress-shear rate behavior as well as stability. Evaluation of the data together shows that at total 80 wt% magnetic particle loading (MRF-2 and MRF-3), when this is distributed as 68% CI and 12% SPION-PAA, stability is enhanced dramatically but shear stress decreased significantly. Increasing the CI content by using CI-LA to 71-72 wt% along with SPION-PAA and 3 wt% PVA (MRF-4-5-6) increased the shear stress again to the level of MRF-2 with 80 wt% CI only, but more importantly provided dramatically improved stability compared to poor stability of MRF-2. Among these three bidisperse MRFs, the best stability was observed with MRF-4 and MRF-6 which may be related to higher SPION content which is 12 wt% while MRF-5 has 8 wt% SPION. An increase in the shear stress with additives was reported in several publications, and the increase in shear stress was assigned to friction or flocculation induced enhanced interaction between particles [157]. In our samples, PAA coating on SPION may strengthen the interaction between particles as described in Chapter 2, which results in higher shear stress, there may be a critical amount needed for such favorable interaction.

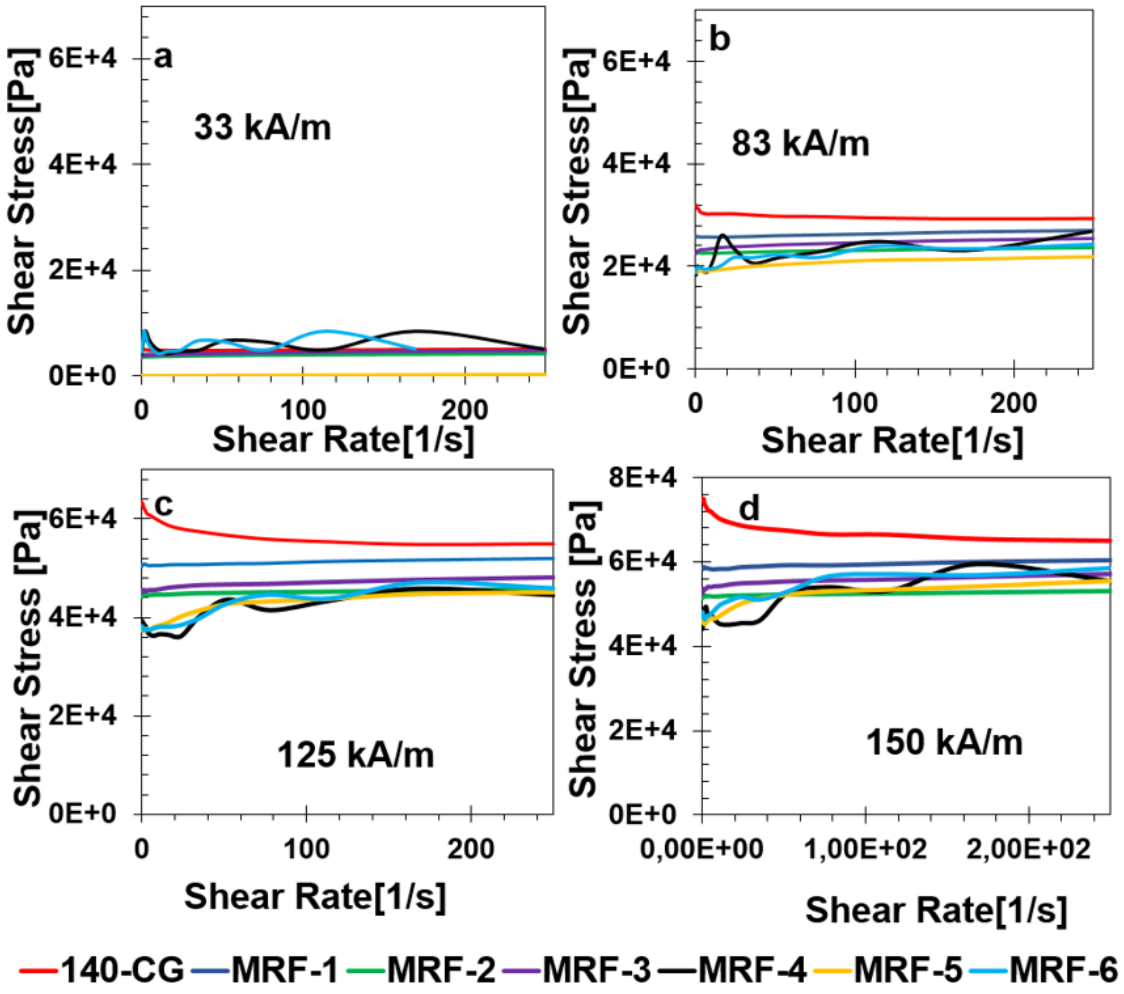

Figure 3.7: Shear stress under shear rate for MRFs using under; a) 33 kA/m, b) 83 kA/m, c) 125 kA/m, d) 150 kA/m magnetic field strength.

Apparent viscosity vs shear rate curves are given in Figure 3.8 and Figure 3.9. The apparent viscosity increases at a given shear rate with the magnetic field, as expected. All samples are showing shear thinning behavior. Among all samples, the highest viscosity is observed for commercial 140-CG MRF. The samples with no coating (MRF 1-2-9-10-11) have higher viscosities than those with modified surfaces. The trend is similar to the shear stress-shear rate behavior. Modification of CI with SPION nanoparticles decreases the viscosity of the fluid, but the further modification of the surface of CI with LA and the addition of PVA did not affect the viscosity. Only noticeable difference was observed between bidisperse MRF-4-7-8 which has the same composition but differ in the nature

of the carrier fluid and at all magnetic field strengths the viscosity decreased in the order of MRF-4, MRF-7 and MRF-8, indicating one more that bidisperse MRF in hydrolytic oil is not only better for stability but for magnetorheological properties, as well.

Apparent viscosity vs. magnetic field strength are given in Figure 3.10 and Figure 3.11. Apparent viscosity of all MRFs increases as the applied magnetic field strength increases, as expected. Magnetization of the particles increases with an increasing strength of the applied magnetic field which in turn causes stronger alignment of the particles in the direction of the applied field and as a result viscosity of the MRFs increases [158].

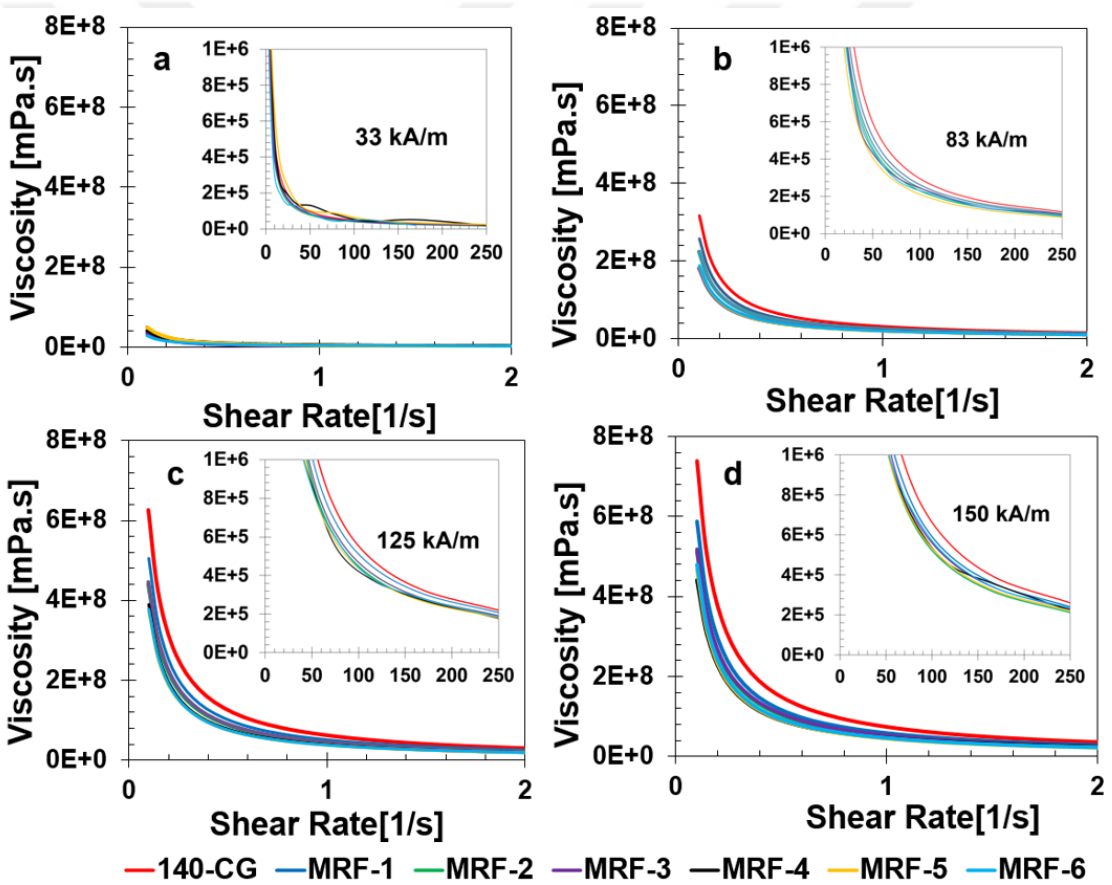

Figure 3.8: Apparent viscosity under the shear rate for MRFs under; a) 33 kA/m, b) 83 kA/m, c) 125 kA/m, d) 150 kA/m magnetic field strength.

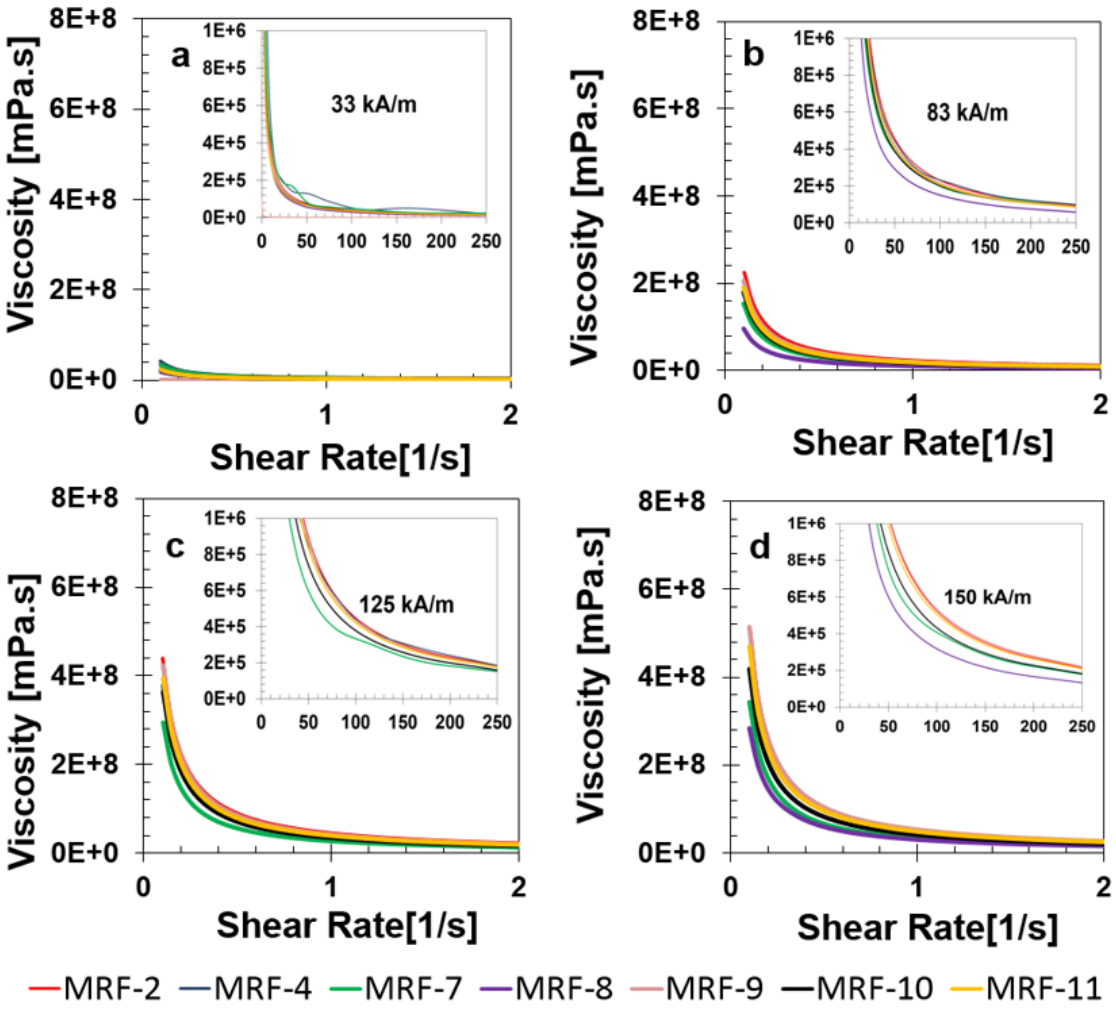

Figure 3.9: Apparent viscosity under the shear rate for MRFs under; a) 33 kA/m, b) 83 kA/m, c) 125 kA/m, d) 150 kA/m magnetic field strength.

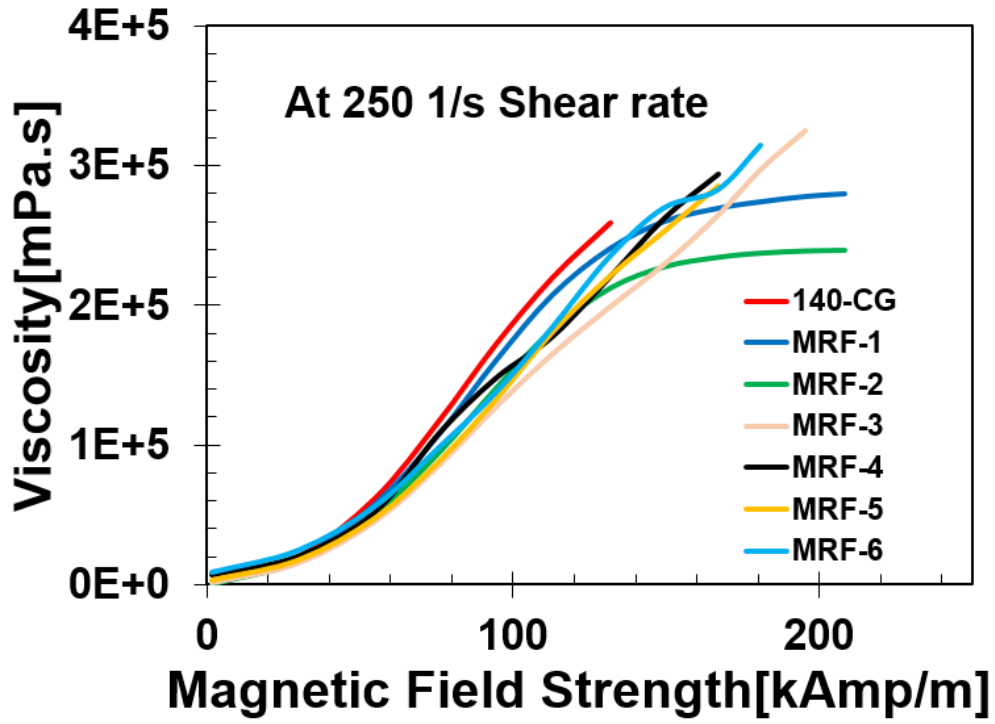

Figure 3.10: Apparent viscosity versus magnetic field strength.

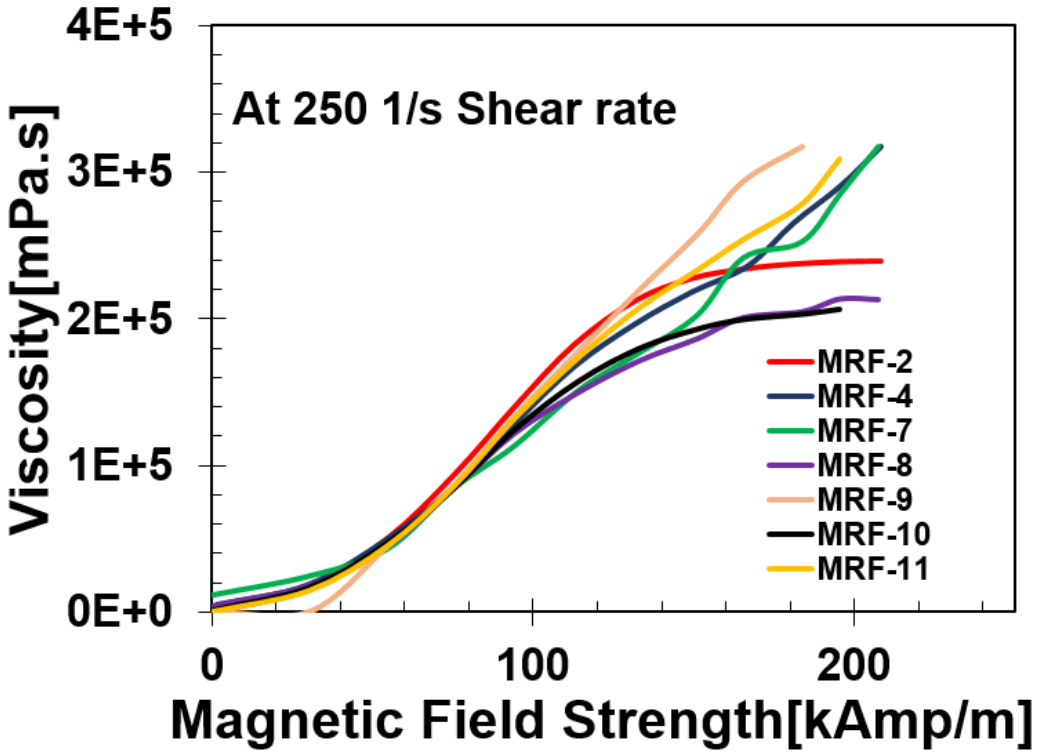

Figure 3.11: Apparent viscosity versus magnetic field strength.

Yield stress is the minimum stress required for the transformation from the solid-like behavior to the fluid-like behavior. At the yield stress, the internal structure is broken. The yield stress was calculated by using the Bingham model, and its dependence on the magnetic field is given in Figure 3.12 and Figure 3.13. Bidisperse MRFs from CI-LA shows higher yield stress values than bare CI loaded MRF. PAA coated SPION increases the yield stress, which could be assigned also to the stronger interaction between particles as well.

The effect of temperature on the MR properties of CI-LA based bidisperse MRFs (MRF 4-5-6) was also investigated. Yield stress measurements were performed at three different temperatures: 20-45-60 ºC (Figure 3.14). The performance of commercial MRF, 140-CG is similar at all temperatures. Bidisperse MRFs, show a decrease in the yield stress with increasing temperature, particularly at higher magnetic fields. Still, MRF fluids are durable at such temperatures, which allows MRFs to be used in relatively high temperatures.

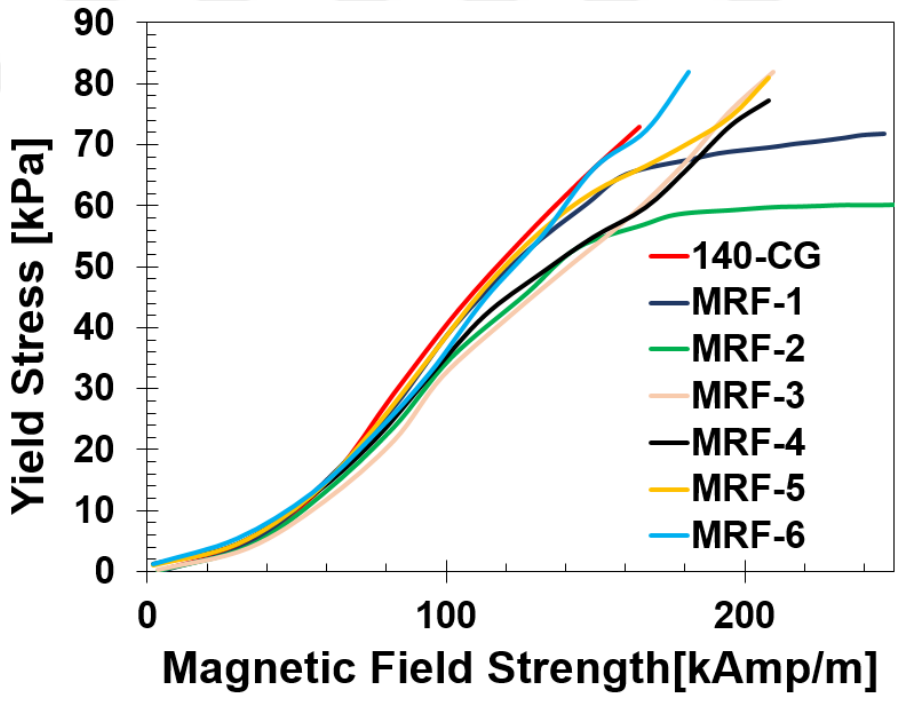

Figure 3.12: Dynamic yield stress versus magnetic field strength.

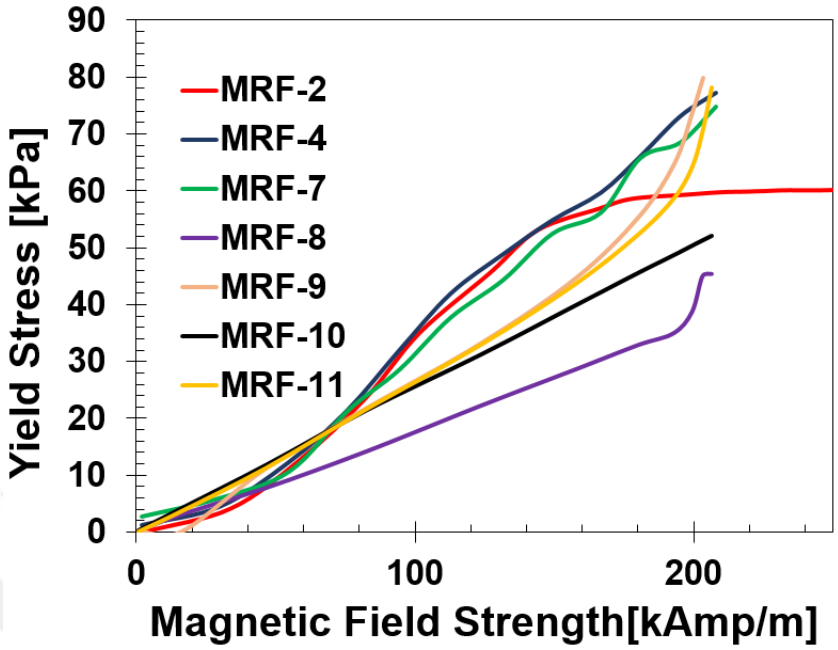

Figure 3.13: Dynamic yield stress versus magnetic field strength.

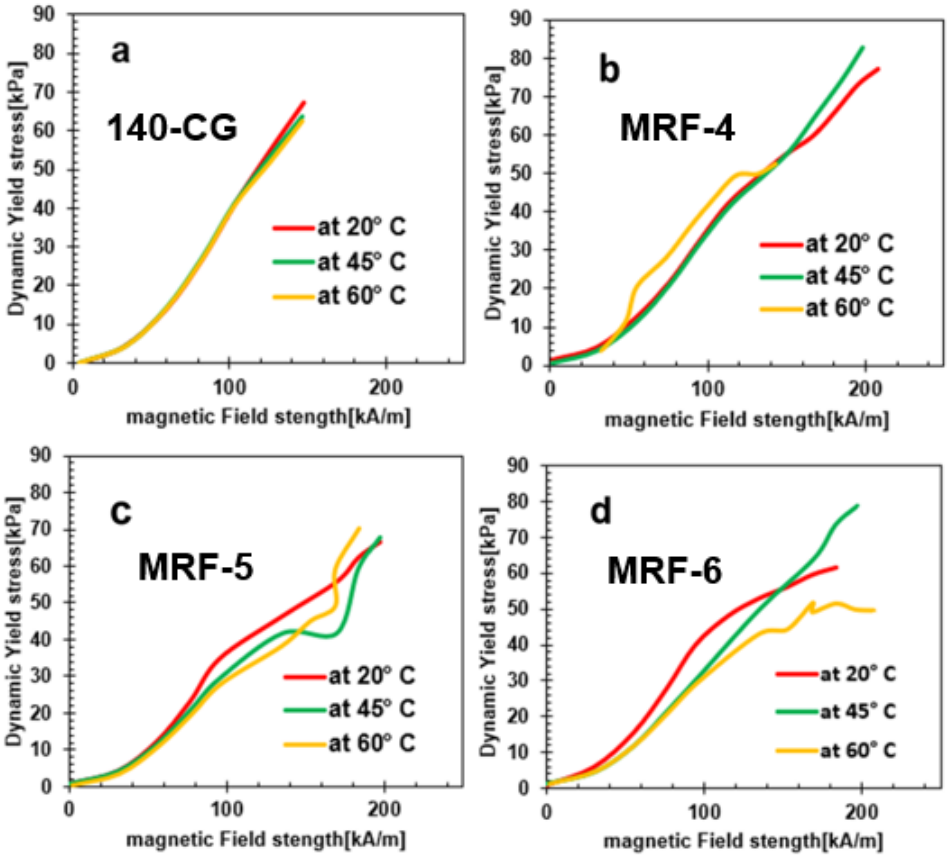

Figure 3.14: Dynamic yield stress versus magnetic field strength at 20°C, 45°C and 60°C for a) 140-CG, b) MRF-4, c) MRF- 5 and d) MRF-6.

3.2.4 Rheological Properties in Oscillatory Mode

Oscillatory experiments give information on the viscoelastic properties of the proposed MRFs. Here loss modulus and storage modulus versus angular frequency under 10wt%, and 100wt% strains were measured. Figure 3.15. a-f represents storage modulus and loss modulus of modified CI-LA based bidisperse magnetorheological MRFs (MRF-4-5-6). Under low strains, there is no structural change in MRFs. As the magnetic field was applied the fluids had viscoelastic behavior and their storage modulus had a higher value than loss modulus. In Figure 3.15. a,c,e under 10% strain, there is no intersection between storage modulus and loss modulus. But in all applied magnetic fields at 100% strain, loss and storage modulus intersect each other at a specific applied frequency which means after that point MRF loses its structure and solid-phase turns to liquid phase and the value of loss modulus becomes higher than storage modulus. Table 3.2 summarizes the dynamic yield points of MRFs based on applied frequency under 100% strain and different applied magnetic field strengths. Results show that synthesized bidisperse MRFs have a higher yield point than 140-CG commercial LORD®. It proves that synthesized samples in this research are more stable than the commercial 140-CG MRF LORD® under dynamic loading.

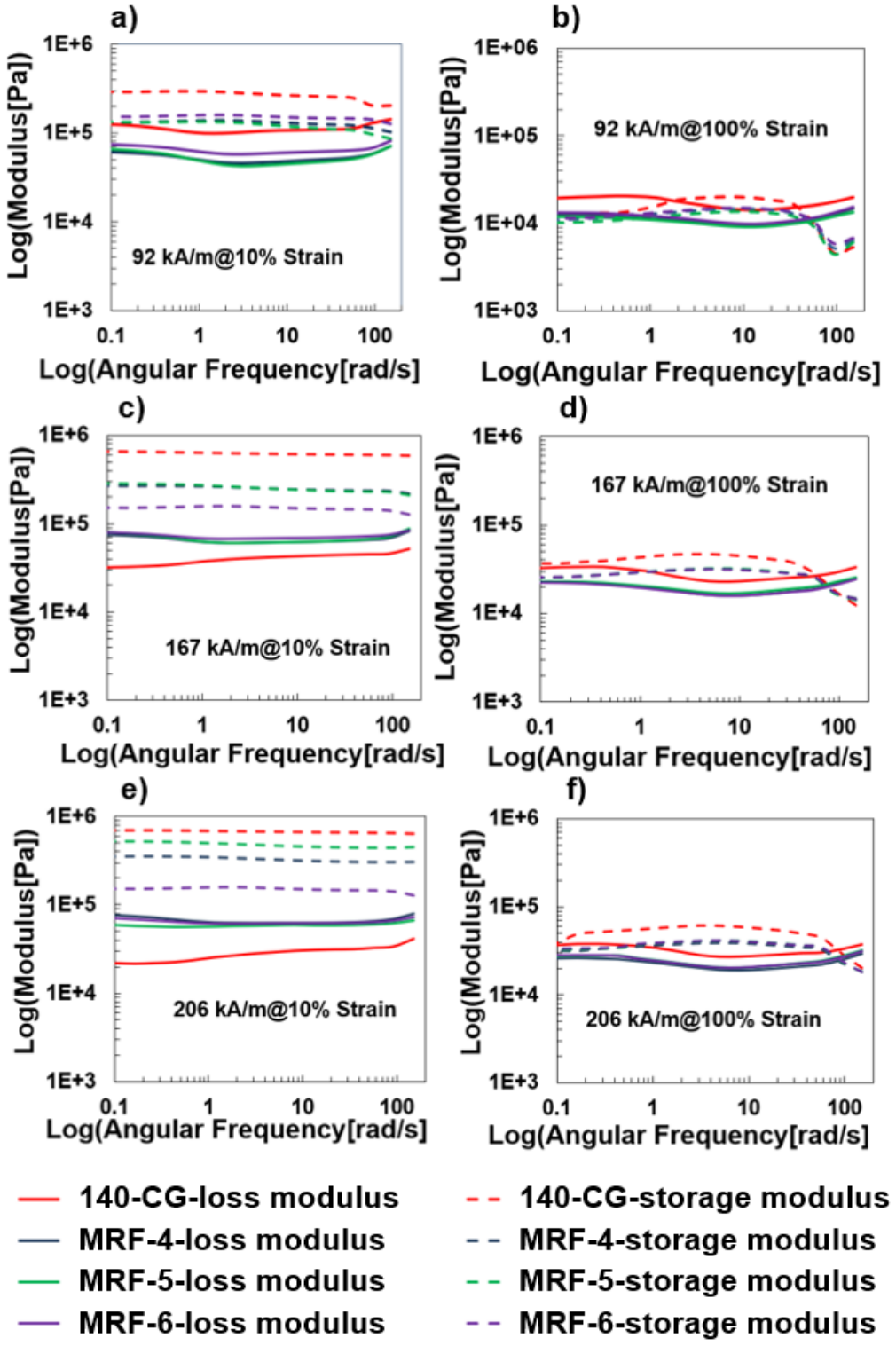

Figure 3.15: Storage (dashed lines) modulus and loss (solid lines) modulus versus applied angular frequency under different magnetic field strength: a) 92 kA/m and 10 % strain, b) 92 kA/m and 100 % strain, c) 167 kA/m and 10 % strain, d) 167 kA/m and 100 % strain, e) 206 kA/m and 10 % strain and f) 206 kA/m and 100 % strain.

Table 3.2: The angular frequency at yield point [rad/s] under 100% strain.

Magnetic Field Strength [kA/m]	140-CG [rad/s]	MRF-4 [rad/s]	MRF-5 [rad/s]	MRF-6 [rad/s]
92	40	50	50	50
167	60	76	76	76
206	85	85	85	85

3.2.5 Use of bidisperse MRFs in a magnetorheological (MR) damper

After studying the magnetorheological behavior of each synthesized bidisperse MRFs, samples with the best magnetorheological response and good stability were chosen to be tested on the MR damper of washing machines designed by the Manufacturing and Automation Research Center at KOÇ University. Table 3.3 gives the axial force on the MR damper using different MRFs and under five different applied currents. Also, the same tests were done by using 140-CG MRF LORD® as a benchmark.

Overall, these MRFs performed as good as the commercial one in damping but overwhelmingly better shelf-life and lifetime in use.

Table 3.3: Axial force on the MR damper in different currents by using different bidisperse MRFs.

Sample	Current (A)				
	0	0.3	0.4	0.5	0.6
MRF-3	14.03 N	155.2 N	165.6 N	166.17 N	175.8 N
MRF-4	20 N	170.3 N	195.11 N	206.43 N	222.16 N
MRF-5	21.01 N	150.51 N	183.92 N	195.24 N	215.05 N
LORD-140 CG	17.61 N	186.3 N	207.5 N	212.65 N	226.98 N

3.3 Conclusion

In this work, different bidisperse MRF using CI and SPIONs were synthesized. Performances of the new MRFs were compared with the commercial 140-CG® from Lord Corp.

Initially, the influence of carrier fluids was studied using bare CI between 75-85

wt% particle loading. Among different carrier fluids studied, namely mineral oil, silicone oil, glycerol, and hydraulic oil, silicon oil and glycerol seemed promising in stabilizing particles but at 75 wt%. CI based MRFs in hydraulic oil at 80-85 wt% loading, similar to the commercial one, did not provide good stability which was solved with the addition of SPION-PAA (MRF-3). This provided stability by interacting with CI surface possibly due to carboxylic acid adsorption on the CI surface and preventing interaction of micron-sized particles with each other and forming a less dense coating around them, however since the content of the CI decreased, magnetorheological properties such as viscosity, shear stress and yield strength fall below the commercial one. Then, a new set of bidisperse MRF were prepared using LA coated CI for better dispersion and with 3 wt% PVA which allowed an increase in the CI content to 71-72 wt% along with 9-12 wt% SPION-PAA. Among these MRF 4-6 with 12 wt% SPION-PAA showed excellent stability coupled with magnetorheological performance similar and even better than the commercial one. The best formulation which consists of 71-72 wt% CI-LA, 12 wt% SPION-PAA and 3 wt% PVA in hydraulic oil, showed stability for 4 months at rest.

The performance of this new bidisperse MRF was confirmed in a real MR damper by the group of Prof. İsmail Lazoğlu. Superb MR performance with ease of use due to the superb stability of the bidisperse MRF was reported.

Chapter 4

SIDE PROJECTS AND PUBLICATIONS

4.1 Other projects

During my four years in Polymers and Nanomaterials Research Laboratory, I have also contributed to other projects which enriched me significantly. Here are the projects that I had participated in.

Bidisperse MRF project was a collaboration with MARC team under the supervision of Prof. Dr. İsmail Lazoğlu. They evaluated the performance of the bidisperse MRFs that I have developed in real MR dampers designed by MARC for washing machines.

Mostafa Khalil Abdou Saleh also adopted these bidisperse MRFs in the development of *Magnetorheological Damper for Chatter Stability of Boring Tools*.

Nanoparticles developed here were also tested as magnetic inks for 3D printing of plastic parts in collaboration with Shahryar Atta Khan from MARC.

I worked with Prof. Dr. Alper Kiraz's group from the Physics Department as well to develop magnetically controllable membranes from magnetic particles dispersed in silicon.

I was also responsible for preparing SPION-LA and SPION-PAA solution for Prof. Dr. Ali Koşar's projects.

I have also prepared SPIONs for Prof. Dr. Metin Sitti to be evaluated as two photon photopolymerization initiator, which is in a way continuation of the SPION-based photoinitiation project.

Aqueous SPION-PAA has been investigated as a radical photoinitiator for the polymerization of hydrophilic vinyl monomers in aqueous solutions. Dimethylaminoethyl methacrylate (DEMAEMA), hydroxyethylmethacrylate (HEMA), poly(ethyleneglycol) diacrylate (PEGDA) and N-isopropylacrylamide (NIPA) were used as medically relevant hydrophilic monomers. Solution polymerizations of these monomers were tested using different amounts of SPION-PAA (5,10,20 wt.% of

monomers) and irradiation at 360 nm. Homogenous magnetic hydrogels were obtained. Such magnetic biocompatible hydrogels have several biomedical applications such as drug delivery, hyperthermia, biosensors, biorobots, etc. Polymerization kinetics of all solutions were studied by photo-DSC at 380-460 nm and 400-500 nm, at 40mW- 60mW powers by Mehmet Berk Bilgin (MS candidate). These hydrogels were also tested for photon-to-heat conversion at 808 nm IR irradiation to demonstrate that these gels are not only magnetically but also optically addressable and may be exploited in a broad application area, wherein especially temperature sensitivity is useful.

4.2 Publications

Published Paper:

Sadaghiani, A., Rajabnia, H., Çelik, S., Noh, H., Kwak, H., & Nejatpour, M. et al. (2020). Pool boiling heat transfer of ferrofluids on structured hydrophilic and hydrophobic surfaces: The effect of magnetic field. International Journal Of Thermal Sciences, 155, 106420. doi: 10.1016/j.ijthermalsci.2020.106420.

Accepted Paper:

M. Nejatpour, U. Unal , H. Yağcı Acar. Entitled: Bidisperse magneto rheological fluids consisting of functional SPIONs added to commercial MRF , Journal of Industrial and Engineering Chemistry.

Accepted Paper:

Mostafa K.A. Saleh, Mona Nejatpour, Havva Yagci Acar, Ismail Lazoglu. Entitled: A New Magnetorheological Damper for Chatter Stability of Boring Tools. Journal of Materials Processing Technology.

Under Preparation Papers:

M. Nejatpour, M. K. A. Saleh, A. Ulasyar, U. Unal, İ. Lazoğlu, H. Yağcı Acar, Bidisperse

Magnetorheological Fluids with Strong Magnetorheological Response and Long Term Stability.

M. Nejatpour, B. Bilgin, A. Muti , A Sennaroğlul , H. Yağcı Acar , SPION-PAA Based Magnetic Hydrogels.

4.3 Presentations

Poster presentation in NanoTR13: Bidisperse Magnetorheological Fluids, 22-25 September 2018, Çeşme, İzmir-Turkey

Oral presentation in Magnetism and Magnetic Materials Conference: Bidisperse Magnetorheological Fluids, 8-12 July 2019, Paris- France

Chapter 5

DISCUSSION AND CONCLUSION

The major problem that this thesis work aimed to solve was the sedimentation of MRFs without losing good magnetorheological properties. As a solution bidisperse MRFs consisting of micron-sized Fe particles and nano-sized SPIONs with surface functionalities that would aid interaction between the two types of particles were suggested.

The hypothesis was first tested on a commercial MRF with high particle loading and a known good magnetorheological response. Hence, bidisperse MRFs were prepared by adding either LA or PAA coated SPIONs to the diluted commercial 140-CG LORD® MRF, using MOBIL 27 hydraulic oil at different amounts to improve the stability of commercial MRFs without sacrificing the magnetorheological properties. Total particle loading was kept above 80 wt% and SPION content was tested as 6 and 12 wt%. Interestingly, both nanoparticles adsorb on the surface of fatty acid coated micron sized Fe-particles of the commercial MRF. We suggest that the hydrophobic interaction between the fatty acid coatings of SPION-LA and Fe-particles, and carboxylic acid binding to Fe-particle`s surface is responsible for such interaction.

Bidisperse MRFs have 175emu/g saturation magnetization, which is slightly lower than 140-CG LORD®. Rheological properties of commercial MRF and prepared bidisperse MRFs were measured in both rotational and frequency modes. Shear stress of 140-CG LORD® under high magnetic field strength was higher than bidisperse MRFs. In addition, under low shear rates (0.01-2 s^{-1}) 140-CG LORD® had a higher viscosity than the bidisperse MRFs. But under shear rates higher than $2s^{-1}$ there was no viscosity difference between the commercial and bidisperse MRFs with 12 wt% SPION loading. Also, high NP loading improved the magnetorheological response of the bidisperse MRFs and the addition of SPION-PAA showed better results than SPION-LA. Bidispersed MRFs with yields stress comparable to the commercial MRF up to 110 kA/m magnetic field strength were achieved. At higher magnetic field strengths 140-CG reaches its yield

point sooner with higher yield stress than the bidisperse ones. In frequency sweep mode, selected bidisperse MRFs with 12 wt% loaded SPION-PAA reached their yield point at a higher angular frequency than the commercial MRF.

The addition of nanoparticles to the commercial MRF with particle loading above 80wt%, improved the stability of dispersions and ability to re-suspend. This was better with 12 wt% SPION-PAA loading. Considering the magnetorheological performance and resistance to sedimentation and re-suspension efficiency, 12wt % SPION-PAA loaded bidisperse MRFs are quite promising.

Here, it is important to point out that all bidisperse MRFs that were cited from the literature have used bare CI or Fe-particles, yet the commercial MRF that we have used here consists of fatty acid coated Fe-particles, and hence has much higher particle loading. Overall, at even quite high particle loadings, the addition of SPION-PAA, which is suggested to interact with micron-sized particles electrostatically, provides a better chaining property and resistance to agglomeration and sedimentation, and improve re-suspension by preventing hard sediments.

In the second phase of the study, different MRFs and bidisperse MRFs were prepared with the most widely used carbonyl iron (CI). Here, surface modification of CI, as well as the effect of different carrier fluids and additives, were studied. The surface of the CI was coated with lauric acid for good dispersibility in hydrophobic carrier fluids. SPION-LA and SPION-PAA were added to uncoated or coated CI in a carrier fluid. Stability and magnetorheological properties of different CI and CI-LA based MRF and bidisperse MRFs in different carrier fluids were studied. Amongst silicon oil, hydraulic oil, paraffin and glycerol, the best performance was obtained with hydraulic oil for bidisperse MRFs. Results showed that unmodified CI based MRFs (75-85 wt%) with good magnetorheological response were not stable for a long time while CI-LA based bidisperse MRFs using SPION-PAA in hydraulic oil demonstrated a good stability along with a good magnetorheological response. Prepared bidisperse MRFs were stable even after 4 months. Specifically, the bidisperse MRF composed of 71wt% CI-LA, 12wt% SPION-PAA and 3wt% PVA in hydraulic oil have rheological properties similar to 140-CG LORD® but with no sedimentation in 4 months. Besides, yield stress was measured for the CI-LA based bidisperse MRFs at three different temperatures (20℃, 45℃, 60℃)

and no significant change was observed, suggesting consistent performance at these temperatures, as well.

These bidisperse MRFs with long-lasting stability and high magnetorheological properties discussed in chapters 2 and 3 can be suggested for use in MR devices instead of commercial MRFs. The most stable bidisperse MRF was tested in a designed washing machine MR damper by Abasin Ulasyar and Mostafa Khalil Abdou Saleh in Manufacturing and Automation Center at Koç University under the supervision of Prof. Dr. Ismail Lazoğlu. Mechanical tests indicated that comparable damping performance between the commercial MRF and the bidisperse one. But, the exceptional stability of the bidisperse one made it the choice of the users.

Overall, along with the new MR damper designed by MARC group, these bidisperse MRFs provided an enhanced vibration damping for the washing machines of Arçelik.

The critical contribution of this thesis work to the literature lies in the investigation of interacting particles rather than the prevention of particle interactions. In the view of the collected data it can be accepted that a favourable interaction between coated magnetic nanoparticles and coated micron-sized magnetic particles dispersed in hydrophobic carrier fluid does stabilize the MRFs without sacrificing the good magnetorheological response and also enhance redispersibility. The mentioned interaction between particles can be electrostatic or hydrophobic, related to the functional groups of the organic surface coatings of magnetic particles. However, electrostatic interaction, which is stronger, is also more successful in the stabilization of the MRFs. Electrostatic interaction between the nano and micron sized particles provide kind of a charged nanoparticle coating around the micron sized particles, which provides void filling with magnetic nanoparticles during the formation of columns/chains under magnetic field but also resist micron sized particles from aggregating during rest due to charge repulsion.

Since the interaction between the particles is strong, properties were maintained at high temperatures (up to 60°C) as well, which is critical in industrial applications.
It is also found out that although SPION-PAA does interact with bare CI, it is essential to stability to use the coated CI as well, to prevent intrinsic, inevitable aggregation of the bare particles.

Coating CI with an organic material and the loss from the micron sized magnetic

particles, which are the main contributors to high viscosity under magnetic fields, by the use of magnetic nanoparticles with much lower saturation magnetization, may seem like actions sacrificing the magnetorheological response. However, coated CI and the use of interacting SPIONs, especially SPION-PAA, allows preparation of bidisperse MRFs with high particle loadings (above 80%) with overwhelmingly better stability. Therefore, at the end a new generation, industrially valuable, bidisperse MRFs now can be achieved.

BIBLIOGRAPHY

[1] Hasan S. Review on nanoparticles: their synthesis and types. Research Journal of Recent Sciences, 2014, 4, 1-3.

[2] Akbarzadeh, A., Samiei, M., & Davaran, S. (2012). Magnetic nanoparticles: preparation, physical properties, and applications in biomedicine. *Nanoscale Research Letters*, *7*(1), 144. doi: 10.1186/1556-276x-7-144.

[3] Mahmoudi, M., Sahraian, M., Shokrgozar, M., & Laurent, S. (2011). Superparamagnetic Iron Oxide Nanoparticles: Promises for Diagnosis and Treatment of Multiple Sclerosis. *ACS Chemical Neuroscience*, *2*(3), 118-140. doi: 10.1021/cn100100e.

[4] Pokropivny, V. (2007). Introduction to Nanomaterials and Nanotechnology: Tartu University Press.

[5] Skomski, R. (2003). Nanomagnetics. *Journal Of Physics: Condensed Matter*, *15*(20), R841-R896. doi: 10.1088/0953-8984/15/20/202.

[6] T K, Indira & Lakshmi, P. (2009). Magnetic Nanoparticles – A Review. Int. J. Pharm. Sci. Nanotechnol. 3.

[7] Bazylinski D.A., Lefèvre C.T., Schüler D. (2013) Magnetotactic Bacteria. In: Rosenberg E., DeLong E.F., Lory S., Stackebrandt E., Thompson F. (eds) The Prokaryotes. Springer, Berlin, Heidelberg. https://doi.org/10.1007/978-3-642-30141-4_74.

[8] Morello, A., Angenent, W., Frossati, G., & de Jongh, L. (2005). Automated and versatile SQUID magnetometer for the measurement of materials properties at millikelvin temperatures. Review Of Scientific Instruments, 76(2), 023902. doi: 10.1063/1.1841831.

[9] Butt, H., Cappella, B., & Kappl, M. (2005). Force measurements with the atomic force microscope: Technique, interpretation and applications. Surface Science Reports, 59(1-6), 1-152. doi: 10.1016/j.surfrep.2005.08.003.

[10] Lisjak, D., & Mertelj, A. (2018). Anisotropic magnetic nanoparticles: A review of their properties, syntheses and potential applications. Progress in Materials Science, 95, 286-328. doi:10.1016/j.pmatsci.2018.03.003.

[11] Majetich, S., Scott, J., Kirkpatrick, E., Chowdary, K., Gallagher, K., & McHenry, M. (1997). Magnetic nanoparticles and magnetocrystalline anisotropy. Nanostructured Materials, 9(1-8), 291-300. doi: 10.1016/s0965-9773(97)90069-6.

[12] Kolhatkar, A. G., Jamison, A. C., Litvinov, D., Willson, R. C., & Lee, T. R. (2013). Tuning the magnetic properties of nanoparticles. Int J Mol Sci, 14(8), 15977-16009. doi:10.3390/ijms140815977.

[13] Özgür, Ü., Alivov, Y., & Morkoç, H. (2009). Microwave ferrites, part 1: fundamental properties. Journal Of Materials Science: Materials In Electronics, 20(9), 789-834. https://doi.org/10.1007/s10854-009-9923-2.

[14] Das, P., Colombo, M., & Prosperi, D. (2019). Recent advances in magnetic fluid hyperthermia for cancer therapy. Colloids Surf B Biointerfaces, 174, 42-55. doi:10.1016/j.colsurfb.2018.10.051.

[15] Teja, A., & Koh, P. (2009). Synthesis, properties, and applications of magnetic iron oxide nanoparticles. Progress In Crystal Growth And Characterization Of Materials, 55(1-2), 22-45. https://doi.org/10.1016/j.pcrysgrow.2008.08.003.

[16] Liu, Y., Sellmyer, D., & Shindo, D. (2006). Handbook of advanced magnetic materials. Berlin: Springer.

[17] Jeong, U., Teng, X., Wang, Y., Yang, H., & Xia, Y. (2007). Superparamagnetic Colloids: Controlled Synthesis and Niche Applications. Advanced Materials, 19(1), 33-60. doi:10.1002/adma.200600674.

[18] Majetich*, S. A., Wen, T., & Mefford*, O. T. (2013). Magnetic nanoparticles. *MRS Bulletin*, *38*(11), 899-903. doi:10.1557/mrs.2013.230.

[19] Reeves, D., & Weaver, J. (2014). Approaches for Modeling Magnetic Nanoparticle Dynamics. *Critical Reviews In Biomedical Engineering*, *42*(1), 85-93. doi: 10.1615/critrevbiomedeng.2014010845.

[20] Osaci, M., Abrudean, C., & Berdie, A. (2007). Relaxation Times in Magnetic Nanoparticles System and Memory Effects. *Acta Physica Polonica A*, *112*(6), 1203-1212. doi: 10.12693/aphyspola.112.1203.

[21] Deissler, R. J., Wu, Y., & Martens, M. A. (2014). Dependence of Brownian and Neel relaxation times on magnetic field strength. *Med Phys, 41*(1), 012301. doi:10.1118/1.4837216.

[22] Kötitz, R., Weitschies, W., Trahms, L., & Semmler, W. (1999). Investigation of Brownian and Néel relaxation in magnetic fluids. *Journal Of Magnetism And Magnetic Materials*, *201*(1-3), 102-104. doi: 10.1016/s0304-8853(99)00065-7.

[23] Shah, S. A., Reeves, D. B., Ferguson, R. M., Weaver, J. B., & Krishnan, K. M. (2015). Mixed Brownian alignment and Neel rotations in superparamagnetic iron oxide nanoparticle suspensions driven by an ac field. *Phys Rev B Condens Matter Mater Phys, 92*(9). doi:10.1103/PhysRevB.92.094438.

[24] Ota, S., & Takemura, Y. (2019). Characterization of Néel and Brownian Relaxations Isolated from Complex Dynamics Influenced by Dipole Interactions in Magnetic Nanoparticles. *The Journal of Physical Chemistry C, 123*(47), 28859-28866. doi:10.1021/acs.jpcc.9b06790.

[25] Bedanta, S., Barman, A., Kleemann, W., Petracic, O., & Seki, T. (2013). Magnetic Nanoparticles: A Subject for Both Fundamental Research and Applications. *Journal of Nanomaterials, 2013*, 1-22. doi:10.1155/2013/952540.

[26] Betancourt, I.. (2002). Nanocrystalline hard magnetic alloys. Revista Mexicana De Fisica - REV MEX FIS. 48. 283-289.

[27] Fujisaki, K. (2020). *Magnetic Material for Motor Drive Systems*. Singapore: Springer.

[28] Wu, W., He, Q., & Jiang, C. (2008). Magnetic iron oxide nanoparticles: synthesis and surface functionalization strategies. Nanoscale Res Lett, 3(11), 397-415. doi:10.1007/s11671-008-9174-9.

[29] Redl, F., Black, C., Papaefthymiou, G., Sandstrom, R., Yin, M., & Zeng, H. et al. (2004). Magnetic, Electronic, and Structural Characterization of Nonstoichiometric Iron Oxides at the Nanoscale. Journal Of The American Chemical Society, 126(44), 14583-14599. doi: 10.1021/ja046808r.

[30] Liu, X.-D., Chen, H., Liu, S.-S., Ye, L.-Q., & Li, Y.-P. (2015). Hydrothermal synthesis of superparamagnetic Fe3O4 nanoparticles with ionic liquids as stabilizer. Materials Research Bulletin, 62, 217-221. doi:10.1016/j.materresbull.2014.11.022.

[31] Hu, L., Percheron, A., Chaumont, D., & Brachais, C. (2011). Microwave-assisted one-step hydrothermal synthesis of pure iron oxide nanoparticles: magnetite, maghemite and hematite. Journal Of Sol-Gel Science And Technology, 60(2), 198-205. doi: 10.1007/s10971-011-2579-4.

[32] Marciello, M. et al. Iron Oxide Nanoparticles For Cancer Diagnosis And Therapy. 2020.

[33] Wallyn et al. "Synthesis, Principles, And Properties Of Magnetite Nanoparticles For In Vivo Imaging Applications—A Review". Pharmaceutics, vol 11, no. 11, 2019, p. 601. MDPI AG, doi:10.3390/pharmaceutics11110601.

[34] Rashdan, S. et al. "Nanoparticles For Biomedical Applications: Current Status, Trends And Future Challenges". Biomaterials And Medical Tribology, 2013, pp. 1-132. Elsevier, doi:10.1533/9780857092205.1. Accessed 15 Nov 2020.

[35] F. Hasany, S., Ahmed, I., J, R., & Rehman, A. (2013). Systematic Review of the Preparation Techniques of Iron Oxide Magnetic Nanoparticles. *Nanoscience and Nanotechnology, 2*(6), 148-158. doi:10.5923/j.nn.20120206.01.

[36] Palanisamy, S., & Wang, Y. M. (2019). Superparamagnetic iron oxide nanoparticulate system: synthesis, targeting, drug delivery and therapy in cancer. *Dalton Trans, 48*(26), 9490-9515. doi:10.1039/c9dt00459a.

[37] Majidi, S., Sehrig, F. Z., Farkhani, S. M., Goloujeh, M. S., & Akbarzadeh, A. (2016). Current methods for synthesis of magnetic nanoparticles. *Artif Cells Nanomed Biotechnol, 44*(2), 722-734. doi:10.3109/21691401.2014.982802.

[38] Yadollahpour, A. (2015). Magnetic Nanoparticles in Medicine: A Review of Synthesis Methods and Important Characteristics. *Oriental Journal of Chemistry, 31*(Special Issue 1(2015)), 271-277. doi: 10.13005/ojc/31.Special-Issue1.33.

[39] Malik, M. A., Wani, M. Y., & Hashim, M. A. (2012). Microemulsion method: A novel route to synthesize organic and inorganic nanomaterials. *Arabian Journal of Chemistry, 5*(4), 397-417. doi: 10.1016/j.arabjc.2010.09.027.

[40] Okoli, C., Sanchez-Dominguez, M., Boutonnet, M., Jaras, S., Civera, C., Solans, C., & Kuttuva, G. R. (2012). Comparison and functionalization study of microemulsion-prepared magnetic iron oxide nanoparticles. *Langmuir, 28*(22), 8479-8485. doi:10.1021/la300599q.

[41] Gul, S., Khan, S. B., Rehman, I. U., Khan, M. A., & Khan, M. I. (2019). A Comprehensive Review of Magnetic Nanomaterials Modern Day Theranostics. *Frontiers in Materials, 6*. doi:10.3389/fmats.2019.00179.

[42] Drmota, A., Drofenik, M., Koselj, J., & nidari, A. (2012). Microemulsion Method for Synthesis of Magnetic Oxide Nanoparticles. In *Microemulsions - An Introduction to Properties and Applications*.

[43] Maity, D., Ding, J., & Xue, J. (2008). Synthesis of magnetite nanoparticles by thermal decomposition: time, temperature, surfactant and solvent effects. *Functional Materials Letters*, *01*(03), 189-193. doi: 10.1142/s1793604708000381.

[44] Mahmoudi, M., Simchi, A., & Imani, M. (2010). ChemInform Abstract: Recent Advances in Surface Engineering of Superparamagnetic Iron Oxide Nanoparticles for Biomedical Applications. *Cheminform*, *42*(2), no-no. doi: 10.1002/chin.201102270.

[45] Kievit, F., & Zhang, M. (2011). Surface Engineering of Iron Oxide Nanoparticles for Targeted Cancer Therapy. Accounts Of Chemical Research, 44(10), 853-862. doi: 10.1021/ar2000277.

[46] Talluri, S., & Malla, R. R. (2019). Superparamagnetic Iron Oxide Nanoparticles (SPIONs) for Diagnosis and Treatment of Breast, Ovarian and Cervical Cancers. *Curr Drug Metab, 20*(12), 942-945. doi:10.2174/1389200220666191016124958.

[47] Shabestari Khiabani, S., Farshbaf, M., Akbarzadeh, A., & Davaran, S. (2017). Magnetic nanoparticles: preparation methods, applications in cancer diagnosis and cancer therapy. *Artif Cells Nanomed Biotechnol, 45*(1), 6-17. doi:10.3109/21691401.2016.1167704.

[48] Shokrollahi, H., Khorramdin, A., & Isapour, G. (2014). Magnetic resonance imaging by using nano-magnetic particles. *Journal of Magnetism and Magnetic Materials, 369*, 176-183. doi:10.1016/j.jmmm.2014.06.023.

[49] Azhdarzadeh, M., Atyabi, F., Saei, A. A., Varnamkhasti, B. S., Omidi, Y., Fateh, M., Dinarvand, R. (2016). Theranostic MUC-1 aptamer targeted gold coated superparamagnetic iron oxide nanoparticles for magnetic resonance imaging and photothermal therapy of colon cancer. *Colloids Surf B Biointerfaces, 143*, 224-232. doi:10.1016/j.colsurfb.2016.02.058.

[50] Sharifi, S., Seyednejad, H., Laurent, S., Atyabi, F., Saei, A. A., & Mahmoudi, M. (2015). Superparamagnetic iron oxide nanoparticles for in vivo molecular and cellular imaging. *Contrast Media Mol Imaging*, *10*(5), 329-355. doi:10.1002/cmmi.1638.

[51] Wahajuddin, & Arora, S. (2012). Superparamagnetic iron oxide nanoparticles: magnetic nanoplatforms as drug carriers. *Int J Nanomedicine, 7*, 3445-3471. doi:10.2147/IJN.S30320.

[52] Huang, X., Li, L., Liu, T., Hao, N., Liu, H., Chen, D., & Tang, F. (2011). The Shape Effect of Mesoporous Silica Nanoparticles on Biodistribution, Clearance, and Biocompatibility in Vivo. ACS Nano, 5(7), 5390-5399. doi: 10.1021/nn200365a.

[53] Chouly, C., Pouliquen, D., Lucet, I., Jeune, J., & Jallet, P. (1996). Development of superparamagnetic nanoparticles for MRI: effect of particle size, charge and surface nature on biodistribution. Journal Of Microencapsulation, 13(3), 245-255. doi: 10.3109/02652049609026013.

[54] Gupta, A. K., & Wells, S. (2004). Surface-modified superparamagnetic nanoparticles for drug delivery: preparation, characterization, and cytotoxicity studies. IEEE Trans Nanobioscience, 3(1), 66-73. doi:10.1109/tnb.2003.820277

[55] Mahmoudi, M., Sant, S., Wang, B., Laurent, S., & Sen, T. (2011). Superparamagnetic iron oxide nanoparticles (SPIONs): development, surface modification and applications in chemotherapy. Adv Drug Deliv Rev, 63(1-2), 24-46. doi: 10.1016/j.addr.2010.05.006.

[56] Prosen, L., Prijic, S., Music, B., Lavrencak, J., Cemazar, M., & Sersa, G. (2013). Magnetofection: a reproducible method for gene delivery to melanoma cells. Biomed Res Int, 2013, 209452. doi:10.1155/2013/209452.

[57] Lin, M. M., Kim, D. K., El Haj, A. J., & Dobson, J. (2008). Development of superparamagnetic iron oxide nanoparticles (SPIONS) for translation to clinical applications. IEEE Trans Nanobioscience, 7(4), 298-305. doi:10.1109/TNB.2008.2011864.

[58] Dulinska-Litewka, J., Lazarczyk, A., Halubiec, P., Szafranski, O., Karnas, K., & Karewicz, A. (2019). Superparamagnetic Iron Oxide Nanoparticles-Current and

Prospective Medical Applications. Materials (Basel), 12(4). doi:10.3390/ma12040617.

[59] Albarqi, H. A., Wong, L. H., Schumann, C., Sabei, F. Y., Korzun, T., Li, X., . . . Taratula, O. (2019). Biocompatible Nanoclusters with High Heating Efficiency for Systemically Delivered Magnetic Hyperthermia. *ACS Nano, 13*(6), 6383-6395. doi:10.1021/acsnano.8b06542.

[60] Kim, J., Oh, J., Kang, H. W., Feldman, M. D., & Milner, T. E. (2008). Photothermal response of superparamagnetic iron oxide nanoparticles. *Lasers Surg Med, 40*(6), 415-421. doi:10.1002/lsm.20650.

[61] Yang, R. M., Fu, C. P., Fang, J. Z., Xu, X. D., Wei, X. H., Tang, W. J., . . . Zhang, L. M. (2017). Hyaluronan-modified superparamagnetic iron oxide nanoparticles for bimodal breast cancer imaging and photothermal therapy. *Int J Nanomedicine, 12*, 197-206. doi:10.2147/IJN.S121249.

[62] Amirshaghaghi, A., Yan, L., Miller, J., Daniel, Y., Stein, J. M., Busch, T. M., Tsourkas, A. (2019). Chlorin e6-Coated Superparamagnetic Iron Oxide Nanoparticle (SPION) Nanoclusters as a Theranostic Agent for Dual-Mode Imaging and Photodynamic Therapy. *Sci Rep, 9*(1), 2613. doi:10.1038/s41598-019-39036-1.

[63] Fakayode, O. J., Kruger, C. A., Songca, S. P., Abrahamse, H., & Oluwafemi, O. S. (2018). Photodynamic therapy evaluation of methoxypolyethyleneglycol-thiol-SPIONs-gold-meso-tetrakis(4-hydroxyphenyl)porphyr in conjugate against breast cancer cells. *Mater Sci Eng C Mater Biol Appl, 92*, 737-744. doi:10.1016/j.msec.2018.07.026.

[64] Xu, P., Zeng, G. M., Huang, D. L., Feng, C. L., Hu, S., Zhao, M. H., . . . Liu, Z. F. (2012). Use of iron oxide nanomaterials in wastewater treatment: a review. *Sci Total Environ, 424*, 1-10. doi:10.1016/j.scitotenv.2012.02.023.

[65] Dave, P. N., & Chopda, L. V. (2014). Application of Iron Oxide Nanomaterials for the Removal of Heavy Metals. *Journal of Nanotechnology, 2014*, 1-14. doi:10.1155/2014/398569.

[66] Morillas, J., Bombard, A., & de Vicente, J. (2015). Preparation and characterization of magnetorheological fluids by dispersion of carbonyl iron

microparticles in PAO/1-octanol. Smart Materials And Structures, 25(1), 015023. doi: 10.1088/0964-1726/25/1/015023.

[67] Tang, X., Zhang, X., Tao, R., & Rong, Y. (2000). Structure-enhanced yield stress of magnetorheological fluids. Journal Of Applied Physics, 87(5), 2634-2638. doi: 10.1063/1.372229.

[68] Laun, H., & Gabriel, C. (2007). Measurement modes of the response time of a magneto-rheological fluid (MRF) for changing magnetic flux density. Rheologica Acta, 46(5), 665-676. doi: 10.1007/s00397-006-0155-6.

[69] Phulé, P. (1998). Synthesis of Novel Magnetorheological Fluids. MRS Bulletin, 23(8), 23-25. doi: 10.1557/s0883769400030773.

[70] de Vicente, J., Klingenberg, D., & Hidalgo-Alvarez, R. (2011). Magnetorheological fluids: a review. Soft Matter, 7(8), 3701. doi: 10.1039/c0sm01221a.

[71] Olabi, A. G., & Grunwald, A. (2007). Design and application of magneto-rheological fluid. *Materials & Design, 28*(10), 2658-2664. doi:10.1016/j.matdes.2006.10.009.

[72] Sapiński, B., & Horak, W. (2013). Rheological Properties of Mr Fluids Recommended for Use in Shock Absorbers. *Acta Mechanica et Automatica, 7*(2), 107-110. doi:10.2478/ama-2013-0019.

[73] Muhammad, A., Yao, X., & Deng, Z. (2006). Review of magnetorheological (MR) fluids and its applications in vibration control. Journal Of Marine Science And Application, 5(3), 17-29. doi: 10.1007/s11804-006-0010-2.

[74] Jönkkäri, I. (2018). Rheological Characterization of Magnetorheological Fluids. (Tampere University of Technology. Publication; Vol. 1566). Tampere University of Technology.

[75] Mezger, T., Sprinz, C., & Green, A. Applied rheology.

[76] Ashtiani, M., Hashemabadi, S. H., & Ghaffari, A. (2015). A review on the magnetorheological fluid preparation and stabilization. *Journal of Magnetism and Magnetic Materials*, *374*, 716-730. doi:10.1016/j.jmmm.2014.09.020.

[77] Sankar, N.R. (2016). Characterization of Magnetorheological Fluids and Its Application in Semi-active Vibration Control System in Automobiles.

[78] Carlson, J., & Jolly, M. (2000). MR fluid, foam and elastomer devices. Mechatronics, 10(4-5), 555-569. doi: 10.1016/s0957-4158(99)00064-1.

[79] Chand, M., Shankar, A., Ali, N., Jain, K., & Pant, R. (2014). An improved properties of bidispersed magneto-rheological fluids. RSC Adv.. doi: 10.1039/c4ra07431a.

[80] Hato, M., Choi, H., Sim, H., Park, B., & Ray, S. (2011). Magnetic carbonyl iron suspension with organoclay additive and its magnetorheological properties. Colloids And Surfaces A: Physicochemical And Engineering Aspects, 377(1-3), 103-109. doi: 10.1016/j.colsurfa.2010.12.029.

[81] Mezger, T. The rheology handbook.

[82] Bonnecaze, R., & Brady, J. (1992). Yield stresses in electrorheological fluids. Journal Of Rheology, 36(1), 73-115. doi: 10.1122/1.550343.

[83] Liu, C., Xie, J., & Cai, D. (2020). Analysis and Experimental Study on Rheological Performances of Magnetorheological Fluids. *Mechanics*, *26*(1), 31-34. doi:10.5755/j01.mech.26.1.25244.

[84] Gabriel, C., & Laun, H. M. (2009). Combined slit and plate–plate magnetorheometry of a magnetorheological fluid (MRF) and parameterization using the Casson model. *Rheologica Acta*, *48*(7), 755-768. doi:10.1007/s00397-009-0369-5.

[85] Wang, G., Zhao, D., Li, N., Zeng, Y., Han, S., Ma, Y., . . . Yu, R. (2019). Facile synthesis of hierarchically structured flower-like Fe3O4 microspheres for high-performance magnetorheological fluids. *Journal of Industrial and Engineering Chemistry*, *79*, 217-225. doi:10.1016/j.jiec.2019.06.040.

[86] Wang, G., Zhao, D., Ma, Y., Zhang, Z., Che, H., Mu, J., . . . Dong, X. (2017). Synthesis of calcium ferrite nanocrystal clusters for magnetorheological fluid with enhanced sedimentation stability. *Powder Technology*, *322*, 47-53. doi:10.1016/j.powtec.2017.08.065.

[87] Spaggiari, A. (2012). Properties and applications of Magnetorheological fluids. Frattura Ed Integrità Strutturale, 7(23), 48-61. doi: 10.3221/igf-esis.23.06.

[88] Zhu, X., Jing, X., & Cheng, L. (2012). Magnetorheological fluid dampers: A review on structure design and analysis. Journal of Intelligent Material Systems and Structures, 23(8), 839-873. doi:10.1177/1045389x12436735.

[89] Ahamed, R., Ferdaus, M. M., & Li, Y. (2016). Advancement in energy harvesting magneto-rheological fluid damper: A review. Korea-Australia Rheology Journal, 28(4), 355-379. doi:10.1007/s13367-016-0035-2.

[90] Ahamed, R., Choi, S., & Ferdaus, M. (2018). A state of art on magneto-rheological materials and their potential applications. Journal Of Intelligent Material Systems And Structures, 29(10), 2051-2095. doi: 10.1177/1045389x18754350.

[91] Obaid, Salwan & Khafaji, Salwan & Manring, Noah & Al-Mudhafar, Muhammed. (2019). Optimal Design Of A Conventional And Magnetorheological Fluid Brakes Using Sensitivity Analysis And Taguchi Method.

[92] Kavlicoglu, B., Gordaninejad, F., & Wang, X. (2013). Study of a magnetorheological grease clutch. Smart Materials And Structures, 22(12), 125030. https://doi.org/10.1088/0964-1726/22/12/125030.

[93] Lee, U., Kim, D., Hur, N., & Jeon, D. (1999). Design Analysis and Experimental Evaluation of an MR Fluid Clutch. Journal Of Intelligent Material Systems And Structures, 10(9), 701-707. https://doi.org/10.1106/ex6x-y4qq-xq5l-8jjv.

[94] Zhang, P., Dong, Y., Choi, H., Lee, C., & Gao, Y. (2020). Reciprocating magnetorheological polishing method for borosilicate glass surface smoothness. Journal Of Industrial And Engineering Chemistry, 84, 243-251. doi: 10.1016/j.jiec.2020.01.004.

[95] Weber, F., & Distl, H. (2014). Amplitude and frequency independent cable damping of Sutong Bridge and Russky Bridge by magnetorheological dampers. Structural Control And Health Monitoring, 22(2), 237-254. doi: 10.1002/stc.1671.

[96] Mrlík, Miroslav, Markéta Ilčíková, Vladimír Pavlínek, Jaroslav Mosnáček, Petra Peer, and Petr Filip. 2013. "Improved Thermooxidation And Sedimentation Stability Of Covalently-Coated Carbonyl Iron Particles With Cholesteryl Groups And Their Influence On Magnetorheology". Journal Of Colloid And Interface Science 396: 146-151. doi:10.1016/j.jcis.2013.01.027.

[97] Jun, Jung-Bae, Seong-Yong Uhm, Jee-Hyun Ryu, and Kyung-Do Suh. 2005. "Synthesis And Characterization Of Monodisperse Magnetic Composite

Particles For Magnetorheological Fluid Materials". Colloids And Surfaces A: Physicochemical And Engineering Aspects 260 (1-3): 157-164. doi:10.1016/j.colsurfa.2005.03.020.

[98] Zhang, Hansong, Hua Yan, Jianjian Yang, Zhide Hu, and Xuemei Wang. 2017. "The Properties Of Mrfs Based On Carbonyl Iron Particles Modified By Nano-Sized Silica And Phosphate Coating Layer". Arabian Journal For Science And Engineering 42 (11): 4713-4723. doi:10.1007/s13369-017-2639-3.

[99] Sedlacik, M, V Pavlinek, R Vyroubal, P Peer, and P Filip. 2013. "A Dimorphic Magnetorheological Fluid With Improved Oxidation And Chemical Stability Under Oscillatory Shear". Smart Materials And Structures 22 (3): 035011. doi:10.1088/0964-1726/22/3/035011.

[100] López-López, M.T., J. de Vicente, G. Bossis, F. González-Caballero, and J.D.G. Durán. 2005. "Preparation Of Stable Magnetorheological Fluids Based On Extremely Bimodal Iron–Magnetite Suspensions". Journal Of Materials Research 20 (4): 874-881. doi:10.1557/jmr.2005.0108.

[101] López-López, M T, P Kuzhir, S Lacis, G Bossis, F González-Caballero, and J D G Durán. 2006. "Magnetorheology For Suspensions Of Solid Particles Dispersed In Ferrofluids". Journal Of Physics: Condensed Matter 18 (38): S2803-S2813. doi:10.1088/0953-8984/18/38/s18.

[102] Iglesias, G.R., M.T. López-López, J.D.G. Durán, F. González-Caballero, and A.V. Delgado. 2012. "Dynamic Characterization Of Extremely Bidisperse Magnetorheological Fluids". Journal Of Colloid And Interface Science 377 (1): 153-159. doi:10.1016/j.jcis.2012.03.077.

[103] Wereley, N. M., A. Chaudhuri, J. -H. Yoo, S. John, S. Kotha, A. Suggs, R. Radhakrishnan, B. J. Love, and T. S. Sudarshan. 2006. "Bidisperse Magnetorheological Fluids Using Fe Particles At Nanometer And Micron Scale". Journal Of Intelligent Material Systems And Structures 17 (5): 393-401. doi:10.1177/1045389x06056953.

[104] Ashtiani, Mahshid, and Seyed Hassan Hashemabadi. 2015. "The Effect Of Nano-Silica And Nano-Magnetite On The Magnetorheological Fluid Stabilization And Magnetorheological Effect". Journal Of Intelligent Material Systems And Structures 26 (14): 1887-1892. doi:10.1177/1045389x15580659.

[105] Anupama, A.V., V. Kumaran, and B. Sahoo. 2018. "Application Of Monodisperse Fe3o4 Submicrospheres In Magnetorheological Fluids". Journal Of Industrial And Engineering Chemistry 67: 347-357. doi:10.1016/j.jiec.2018.07.006.

[106] Leong, Siti Asma' Nikmat, Pakharuddin Mohd Samin, Ani Idris, Saiful Amri Mazlan, and Azura Hanis A Rahman. 2016. "Synthesis, Characterization And Magnetorheological Properties Of Carbonyl Iron Suspension With Superparamagnetic Nanoparticles As An Additive". Smart Materials And Structures 25 (2): 025025. doi:10.1088/0964-1726/25/2/025025.

[107] de Vicente, J., M. T. López-López, F. González-Caballero, and J. D. G. Durán. 2003. "Rheological Study Of The Stabilization Of Magnetizable Colloidal Suspensions By Addition Of Silica Nanoparticles". Journal Of Rheology 47 (5): 1093-1109. doi:10.1122/1.1595094.

[108] Kim, Min Wook, Wen Jiao Han, Yu Hyun Kim, and Hyoung Jin Choi. 2016. "Effect Of A Hard Magnetic Particle Additive On Rheological Characteristics Of Microspherical Carbonyl Iron-Based Magnetorheological Fluid". Colloids And Surfaces A: Physicochemical And Engineering Aspects 506: 812-820. doi: 10.1016/j.colsurfa.2016.07.070.

[109] Shah, Kruti, and Seung-Bok Choi. 2014. "The Field-Dependent Rheological Properties Of Magnetorheological Fluids Featuring Plate-Like Iron Particles". Frontiers In Materials 1. doi:10.3389/fmats.2014.00021.

[110] Cvek, Martin, Miroslav Mrlik, Marketa Ilcikova, Tomas Plachy, Michal Sedlacik, Jaroslav Mosnacek, and Vladimir Pavlinek. 2015. "A Facile Controllable Coating Of Carbonyl Iron Particles With Poly(Glycidyl Methacrylate): A Tool For Adjusting MR Response And Stability Properties". Journal Of Materials Chemistry C 3 (18): 4646-4656. doi:10.1039/c5tc00319a.

[111] Jang, I. B., H. B. Kim, J. Y. Lee, J. L. You, H. J. Choi, and M. S. Jhon. 2005. "Role Of Organic Coating On Carbonyl Iron Suspended Particles In Magnetorheological Fluids". Journal Of Applied Physics 97 (10): 10Q912. doi:10.1063/1.1853835.

[112] Choi, H.J., B.J. Park, M.S. Cho, and J.L. You. 2007. "Core-Shell Structured Poly(Methyl Methacrylate) Coated Carbonyl Iron Particles And Their

Magnetorheological Characteristics". Journal Of Magnetism And Magnetic Materials 310 (2): 2835-2837. doi:10.1016/j.jmmm.2006.11.061.

[113] Liu, Ying Dan, and Hyoung Jin Choi. 2015. "Magnetorheology Of Core–Shell Typed Dual-Coated Carbonyl Iron Particle Fabricated By A Sol–Gel And Self-Assembly Process". Materials Research Bulletin 69: 92-97. doi:10.1016/j.materresbull.2015.01.028.

[114] Arias, J.L., V. Gallardo, F. Linares-Molinero, and A.V. Delgado. 2006. "Preparation And Characterization Of Carbonyl Iron/Poly (Butylcyanoacrylate) Core/Shell Nanoparticles". Journal Of Colloid And Interface Science 299 (2): 599-607. doi:10.1016/j.jcis.2006.03.005.

[115] Mrlik, Miroslav, and Vladimir Pavlinek. 2016. "Magnetorheological Suspensions Based On Modified Carbonyl Iron Particles With An Extremely Thin Poly(N-Butyl Acrylate) Layer And Their Enhanced Stability Properties". Smart Materials And Structures 25 (8): 085011. doi:10.1088/0964-1726/25/8/085011.

[116] Min, Tae Hong, Hyoung Jin Choi, Nam-Hui Kim, Kwonjin Park, and Chun-Yeol You. 2017. "Effects Of Surface Treatment On Magnetic Carbonyl Iron/Polyaniline Microspheres And Their Magnetorheological Study". Colloids And Surfaces A: Physicochemical And Engineering Aspects 531: 48-55. doi:10.1016/j.colsurfa.2017.07.070.

[117] Liu, Jianrong, Xianjun Wang, Xia Tang, Ruoyu Hong, Yaqiong Wang, and Wenguo Feng. 2015. "Preparation And Characterization Of Carbonyl Iron/Strontium Hexaferrite Magnetorheological Fluids". Particuology 22: 134-144. doi:10.1016/j.partic.2014.04.021.

[118] Bombard, Antonio J F, Laís S Antunes, and Douglas Gouvêa. 2009. "Redispersibility In Magnetorheological Fluids: Surface Interactions Between Iron Powder And Wetting Additives". Journal Of Physics: Conference Series 149: 012038. doi:10.1088/1742-6596/149/1/012038.

[119] Elizabeth Premalatha, S., R. Chokkalingam, and M. Mahendran. 2012. "Magneto Mechanical Properties Of Iron Based MR Fluids". American Journal Of Polymer Science 2 (4): 50-55. doi:10.5923/j.ajps.20120204.01.

[120] Yang, Jianjian, Hua Yan, Xuemei Wang, and Zhide Hu. 2016. "Enhanced Yield Stress Of Magnetorheological Fluids With Dimer Acid". Materials Letters 167: 27-29. doi:10.1016/j.matlet.2015.12.098.

[121] Huang, Yuehua, Yuhuan Jiang, Xiongbo Yang, and Ruizhen Xu. 2015. "Influence Of Oleic And Lauric Acid On The Stability Of Magnetorheological Fluids". Journal Of Magnetics 20 (3): 317-321. doi:10.4283/jmag.2015.20.3.317.

[122] Bae, Dong Hun, Hyoung Jin Choi, Kisuk Choi, Jae Do Nam, Md. Sakinul Islam, and Nhol Kao. 2017. "Microcrystalline Cellulose Added Carbonyl Iron Suspension And Its Magnetorheology". Colloids And Surfaces A: Physicochemical And Engineering Aspects 514: 161-167. doi:10.1016/j.colsurfa.2016.11.052.

[123] Ashtiani, M., and S.H. Hashemabadi. 2015. "An Experimental Study On The Effect Of Fatty Acid Chain Length On The Magnetorheological Fluid Stabilization And Rheological Properties". Colloids And Surfaces A: Physicochemical And Engineering Aspects 469: 29-35. doi:10.1016/j.colsurfa.2014.12.046.

[124] Jönkkäri, Ilari, Matti Isakov, and Seppo Syrjälä. 2014. "Sedimentation Stability And Rheological Properties Of Ionic Liquid–Based Bidisperse Magnetorheological Fluids". Journal Of Intelligent Material Systems And Structures 26 (16): 2256-2265. doi:10.1177/1045389x14551436.

[125] Guerrero-Sanchez, C., T. Lara-Ceniceros, E. Jimenez-Regalado, M. Raşa, and U. S. Schubert. 2007. "Magnetorheological Fluids Based On Ionic Liquids". Advanced Materials 19 (13): 1740-1747. doi:10.1002/adma.200700302.

[126] Zhang, Hansong, Hua Yan, Zhide Hu, Jianjian Yang, and Fanghao Niu. 2018. "Magnetorheological Fluid Based On Thixotropic PTFE-Oil Organogel". Journal Of Magnetism And Magnetic Materials 451: 102-109. doi:10.1016/j.jmmm.2017.11.005.

[127] Mohamad, N, S A Mazlan, Ubaidillah, Seung-Bok Choi, and M F M Nordin. 2016. "The Field-Dependent Rheological Properties Of Magnetorheological Grease Based On Carbonyl-Iron-Particles". Smart Materials And Structures 25 (9): 095043. doi:10.1088/0964-1726/25/9/095043.

[128] Kim, Min Su, Ying Dan Liu, Bong Jun Park, Chun-Yeol You, and Hyoung Jin Choi. 2012. "Carbonyl Iron Particles Dispersed In A Polymer Solution And Their Rheological Characteristics Under Applied Magnetic Field". Journal Of Industrial And Engineering Chemistry 18 (2): 664-667. doi:10.1016/j.jiec.2011.11.062.

[129] Yang, Jianjian, Hua Yan, Jun Dai, Zhide Hu, and Hansong Zhang. 2017. "The Rheological Response Of Carbonyl Iron Particles Suspended In Mineral Oil Solution Of 12-Hydroxy Stearic Acid". Journal Of Rheology 61 (3): 515-524. doi:10.1122/1.4980044.

[130] Carlson, (2002). United States Patent. No.: US 6,475,404 B1. Retrieved from https://worldwide.espacenet.com. Appl. No.: 09/564,169.

[131] Ngatu, Grum T., and Norman M. Wereley. 2007. "Viscometric And Sedimentation Characterization Of Bidisperse Magnetorheological Fluids". IEEE Transactions On Magnetics 43 (6): 2474-2476. doi:10.1109/tmag.2007.893867.

[132] Plachy, Tomas et al. "The Enhanced MR Performance Of Dimorphic MR Suspensions Containing Either Magnetic Rods Or Their Non-Magnetic Analogs". Smart Materials And Structures, vol 26, no. 2, 2017, p. 025026. IOP Publishing, doi:10.1088/1361-665x/aa56ef.

[133] Cvek, Martin et al. "A Systematical Study Of The Overall Influence Of Carbon Allotrope Additives On Performance, Stability And Redispersibility Of Magnetorheological Fluids". Colloids And Surfaces A: Physicochemical And Engineering Aspects, vol 543, 2018, pp. 83-92. Elsevier BV, doi:10.1016/j.colsurfa.2018.01.046.

[134] Anupama, A. V., V. Kumaran, and B. Sahoo. 2019. "Effect Of Magnetic Dipolar Interactions And Size Dispersity On The Origin Of Steady State Magnetomechanical Response In Bidisperse Mn–Zn Ferrite Spherical Particle Based Magnetorheological Fluids". New Journal Of Chemistry 43 (25): 9969-9979. doi:10.1039/c9nj00947g.

[135] Susan-Resiga, Daniela, V Socoliuc, A Bunge, Rodica Turcu, and L Vékás. 2019. "From High Colloidal Stability Ferrofluids To Magnetorheological Fluids:

Tuning The Flow Behavior By Magnetite Nanoclusters". Smart Materials And Structures 28 (11): 115014. doi:10.1088/1361-665x/ab3ba5.

[136] Zhang, Peizhi, Mitsuhiro Kamezaki, Kenshiro Otsuki, Zhuoyi He, Hiroyuki Sakamoto, and Shigeki Sugano. 2019. "Development Of Anti-Sedimentation Magnetorheological Fluids And Its Implementation To MR Damper". 2019 IEEE/ASME International Conference On Advanced Intelligent Mechatronics (AIM). doi:10.1109/aim.2019.8868739.

[137] Ngatu, G T, N M Wereley, J O Karli, and R C Bell. 2008. "Dimorphic Magnetorheological Fluids: Exploiting Partial Substitution Of Microspheres By Nanowires". Smart Materials And Structures 17 (4): 045022. doi:10.1088/0964-1726/17/4/045022.

[138] Zhu, Wanning, Xufeng Dong, Hao Huang, and Min Qi. 2019. "Iron Nanoparticles-Based Magnetorheological Fluids: A Balance Between MR Effect And Sedimentation Stability". Journal Of Magnetism And Magnetic Materials 491: 165556. doi:10.1016/j.jmmm.2019.165556.

[139] Zhu, Wanning, Xufeng Dong, Hao Huang, and Min Qi. 2020. "Enhanced Magnetorheological Effect And Sedimentation Stability Of Bimodal Magnetorheological Fluids Doped With Iron Nanoparticles". Journal Of Intelligent Material Systems And Structures, 1045389X2092483. doi:10.1177/1045389x20924831.

[140] Dorosti, A.H., M. Ghatee, and M. Norouzi. 2020. "Preparation And Characterization Of Water-Based Magnetorheological Fluid Using Wormlike Surfactant Micelles". Journal Of Magnetism And Magnetic Materials 498: 166193. doi:10.1016/j.jmmm.2019.166193.

[141] Acar, Havva Yagci, Rachel S. Garaas, Faisal Syud, Peter Bonitatebus, and Amit M. Kulkarni. 2005. "Superparamagnetic Nanoparticles Stabilized By Polymerized Pegylated Coatings". Journal Of Magnetism And Magnetic Materials 293 (1): 1-7. doi:10.1016/j.jmmm.2005.01.035.

[142] Bilici, K., A. Muti, F. Demir Duman, A. Sennaroğlu, and H. Yağcı Acar. 2018. "Investigation Of The Factors Affecting The Photothermal Therapy Potential Of Small Iron Oxide Nanoparticles Over The 730–840 Nm Spectral Region".

Photochemical & Photobiological Sciences 17 (11): 1787-1793. doi:10.1039/c8pp00203g.

[143] Leong, S. A. N., S. A. Mazlan, P. M. Samin, A. Idris, and Ubaidillah. 2016. "Performance Of Bidisperse Magnetorheological Fluids Utilizing Superparamagnetic Maghemite Nanoparticles". doi:10.1063/1.4941516.

[144] de Vicente, J., J. P. Segovia-Gutiérrez, E. Andablo-Reyes, F. Vereda, and R. Hidalgo-Álvarez. 2009. "Dynamic Rheology Of Sphere- And Rod-Based Magnetorheological Fluids". The Journal Of Chemical Physics 131 (19): 194902. doi:10.1063/1.3259358.

[145] Zubieta, M, S Eceolaza, M J Elejabarrieta, and M M Bou-Ali. 2009."Magnetorheological Fluids: Characterization And Modeling Of Magnetization". Smart Materials And Structures 18 (9): 095019. doi:10.1088/0964-1726/18/9/095019.

[146] Wang, Guangshuo, Yingying Ma, Yu Tong, and Xufeng Dong. 2017. "Development Of Manganese Ferrite/Graphene Oxide Nanocomposites For Magnetorheological Fluid With Enhanced Sedimentation Stability". Journal Of Industrial And Engineering Chemistry 48: 142-150. doi:10.1016/j.jiec.2016.12.032.

[147] Gutiérrez, Lucía, Leonor de la Cueva, María Moros, Eva Mazarío, Sara de Bernardo, Jesús M de la Fuente, M Puerto Morales, and Gorka Salas. 2019. "Aggregation Effects On The Magnetic Properties Of Iron Oxide Colloids". Nanotechnology 30 (11): 112001. doi:10.1088/1361-6528/aafbff.

[148] Shen, Lifen, Agnieszka Stachowiak, T. Alan Hatton, and Paul E. Laibinis. 2000. "Polymerization Of Olefin-Terminated Surfactant Bilayers On Magnetic Fluid Nanoparticles". Langmuir 16 (25): 9907-9911. doi:10.1021/la0005412.

[149] Kas, Recep, Esra Sevinc, Ugur Topal, and Havva Yagci Acar. 2010. "A Universal Method For The Preparation Of Magnetic And Luminescent Hybrid Nanoparticles". The Journal Of Physical Chemistry C 114 (17): 7758-7766. doi:10.1021/jp100312e.

[150] Sanchez, Laura M. et al. "Polyacrylic Acid-Coated Iron Oxide Magnetic Nanoparticles: The Polymer Molecular Weight Influence". Colloids And

Surfaces A: Physicochemical And Engineering Aspects, vol 543, 2018, pp. 28-37. Elsevier BV, doi:10.1016/j.colsurfa.2018.01.050.

[151] Sahin, Huseyin, Xiaojie Wang, and Faramarz Gordaninejad. 2009. "Temperature Dependence Of Magneto-Rheological Materials". Journal Of Intelligent Material Systems And Structures 20 (18): 2215-2222. doi:10.1177/1045389x09351608.

[152] Rabbani, Yahya, Mahshid Ashtiani, and Seyed Hassan Hashemabadi. 2015. "An Experimental Study On The Effects Of Temperature And Magnetic Field Strength On The Magnetorheological Fluid Stability And MR Effect". Soft Matter 11 (22): 4453-4460. doi:10.1039/c5sm00625b.

[153] Sherman, Stephen G., Louise A. Powell, Andrew C. Becnel, and Norman M. Wereley. 2015. "Scaling Temperature Dependent Rheology Of Magnetorheological Fluids". Journal Of Applied Physics 117 (17): 17C751. doi:10.1063/1.4918628.

[154] Guo, Xinlu, Zhengjun Yao, Haiyan Lin, Jintang Zhou, Yuxin Zuo, Xiangyu Xu, Bo Wei, Wenjing Chen, and Kun Qian. 2019. "Epoxy Resin Addition On The Microstructure, Thermal Stability And Microwave Absorption Properties Of Core-Shell Carbonyl Iron@Epoxy Composites". Journal Of Magnetism And Magnetic Materials 485: 244-250. doi:10.1016/j.jmmm.2019.04.059.

[155] Hajalilou, Abdollah, Abbas Kianvash, Kamyar Shameli, and Hossein Lavvafi. 2017. "Carbonyl Iron Based Magnetorheological Effects With Silver Nanoparticles Via Green-Assisted Coating". Applied Physics Letters 110 (26): 261902. doi:10.1063/1.4990679.

[156] Sheline, R., & Pitzer, K. (1950). The Infrared Spectra and Structures of the Iron Carbonyls1. Journal Of The American Chemical Society, 72(3), 1107-1112. doi: 10.1021/ja01159a012.

[157] Fang, Fei Fei, Hyoung Jin Choi, and Yongsok Seo. 2009. "Sequential Coating Of Magnetic Carbonyliron Particles With Polystyrene And Multiwalled Carbon Nanotubes And Its Effect On Their Magnetorheology". ACS Applied Materials & Interfaces 2 (1): 54-60. doi:10.1021/am900577w.

[158] Chen, Song, Jin Huang, Hongyu Shu, Tiger Sun, and Kailin Jian. 2013. "Analysis And Testing Of Chain Characteristics And Rheological Properties For

Magnetorheological Fluid". Advances In Materials Science And Engineering 2013: 1-6. doi:10.1155/2013/290691.